November 2015

Modeling the Self-Assembly of Ordered Nanoporous Materials

Szu-Chia Chien
University of Massachusetts Amherst

MODELING THE SELF-ASSEMBLY OF ORDERED NANOPOROUS MATERIALS

A Dissertation Presented

by

SZU-CHIA CHIEN

Submitted to the Graduate School of the
University of Massachusetts Amherst in partial fulfillment
of the requirements for the degree of

DOCTOR OF PHILOSOPHY

September 2015

Department of Chemical Engineering

MODELING THE SELF-ASSEMBLY OF ORDERED NANOPOROUS MATERIALS

A Dissertation Presented

by

SZU-CHIA CHIEN

Approved as to style and content by:

Scott M. Auerbach, Co-chair

Peter A. Monson, Co-chair

Wei Fan, Member

Jonathan Machta, Member

John Collura, Interim Department Head
Department of Chemical Engineering

DEDICATION

To my dearest Mom and loving husband.

ACKNOWLEDGMENTS

I would like to thank my two advisors, Professor Peter Monson and Professor Scott Auerbach, for giving me the opportunity to work with them. Their great advising, mentorship, patience, encouragement, and support helped me throughout my work. I would like to thank my committee members, Professor Jonathan Machta and Professor Wei Fan, for their critical and valuable suggestions regarding this work.

My thanks also go to Dr. Miguel Jorge and Dr. Germán Pérez-Sánchez, for working on the project together. I really enjoyed working with them, and I have learned a lot from both of them. In addition, I would like to thank Professor David Ford, Professor Bret Jackson, and Dr. Justin Fermann for their valuable suggestions on my research projects. I would also like to thank the members in Monson group, Crunch group and Ford group, Vaitheeswaran, Angela Migues, Mohammad Navaid Khan, Hongbo Shi, Qinfang Sun, Anish Desouza, Kiran Iyer, Raghuram Thyagarajan, Ashutosh Rathi, and Pranav Mashanka. I really enjoyed those research discussions and all the fun time we had together.

I am grateful to my friends who, through their love and support made this possible. Especially En-Hsin Lee and Chia-Jung Lee, for being my roommates and sharing everything together in the past five years. I would also like to thank my peer mentoring group members, Whitney Stoppel, Elizabeth Drellich, Cathy Walker, Jess McIver, and Dana Algaier. Their support and encouragement helped me overcome many difficulties I encountered and stimulated me to reach my goal.

A special gratitude goes to my family. I am grateful for the support and the love from my family and family-in-law. I would especially like to thank my mom, for

everything she has done for me. Her constant love and encouragement give me the motivation to pursue my goals. Finally and most importantly, I would like express appreciation to my beloved husband, Li-Chiang Lin, for always being there for me. I am really grateful to have him in my life. Without his love, support, encouragement, patience, and wise advice, I would not have been able to complete this work.

ABSTRACT

MODELING THE SELF-ASSEMBLY OF ORDERED NANOPOROUS MATERIALS

SEPTEMBER 2015

SZU-CHIA CHIEN

B.S. Ch.E., NATIONAL TAIWAN UNIVERSITY

M.S. Ch.E., NATIONAL TAIWAN UNIVERSITY

Ph.D., UNIVERSITY OF MASSACHUSETTS AMHERST

Directed by: Professor Scott M. Auerbach and Professor Peter A. Monson

Porous materials are of great importance in many fields due to their wide applications. An ongoing theme in this area is the tailoring of materials for specific applications. With a better understanding of the formation mechanisms, tailoring and controlling the pore structure may be achieved. The objective of this research is acquiring further understanding of the fundamental physics that govern the formation of these materials using molecular simulations.

We are aiming to unravel the assembly process of silica porous materials using a semi-rigid silica tetrahedral model. This model together with reaction ensemble Monte Carlo simulations allows us to study the formation of silica nanoparticles, the initial stages of microporous material formation. A two-step formation mechanism was found to be crucial for generating the nanoparticles.

A replica-exchange reaction ensemble Monte Carlo sampling together with the silica tetrahedral model is developed and applied to cross the energy barrier between

amorphous silica to crystalline silica materials for searching for the ground state structure of this model. The technique involves simulating several system copies with different equilibrium constants controlling silica condensation/hydrolysis reactions, which are essential for building higher-order network structures and eventually crystals, was preformed. Different silica polymorphs including all-silica zeolite frameworks were obtained. This model shows a great potential to study the crystallization of microporous materials.

We also study the formation of mesoporous materials using molecular dynamics simulations. We investigate the interplay of silica molecules and surfactants, and different mesophases such as micellar rods, hexagonal, bicontinuous and lamellar phases were obtained. Multiple charges on silicate oligomers were found to play an important role in the formation of hexagonal phases.

To study the later stages of MCM-41 formation, a hybrid molecular dynamics and Monte Carlo approach is proposed. The cooperation between the physical interaction and chemical reaction can be taken into account simultaneously. Preliminary study shows that the ratio of silicate to surfactant higher than 4 is essential to the growth of MCM-41. With a further enhancement on the model, this hybrid approach will be a powerful tool to simulate the formation of MCM-41 in a large system and at a long time scale.

TABLE OF CONTENTS

LIST OF TABLES

Table **Page**

LIST OF FIGURES

Figure **Page**

CHAPTER 1

INTRODUCTION

Nanoporous materials such as zeolites are of great importance to the chemical industries because of wide applications in catalysis and separations.[29, 31, 32, 105, 133, 141, 150] The development of new applications in areas including drug delivery, shape-selective sensors, and nano-electronic depends on tailoring material properties such as pore sizes, crystallite size and shape, and crystallite surface structures.[5, 7, 10, 29, 98, 116, 125] Key to tailoring and controlling nanoporous materials is having a better understanding of their formation mechanisms. To date, over 200 different zeolite structures have been identified[8] and several million more have been hypothesized.[39, 46] However, due to limitations of characterization techniques in the critical 5-10 nm range of length scales, the characterization length limits between NMR and X-ray crystallography,[7] understanding of their formation mechanisms remains largely incomplete.[5, 34, 58, 117, 122] Nanoparticles containing both silica and organic structure directing agents (OSDAs) have been observed and implicated as important in the formation of all-silica zeolites.[17, 20, 34, 36, 37, 38, 71, 72, 73, 98, 104] Despite the importance of such nanoparticles, their atomic-level structures remain poorly understood because of the difficulty of isolating and characterizing such colloidal species. The objective of this research is to have a better understanding of the formation mechanism of ordered porous materials by utilizing various techniques in molecular simulations.

We are also interested in the formation process of periodic mesoporous silicas (PMS) such as MCM-41.[11, 12, 78] PMS materials have been extensively studied

since two decades ago because of their potential applications in catalysis and separations of species that are too large to fit into micropores.[29, 42, 97, 151] The materials have also been applied in biotechnology as bioadsorbents, biocatalysts[53], and drug delivery vehicles.[133, 139, 140] These materials differ from the aforementioned zeolites in that the atomic level structure is amorphous rather than crystalline.

In this thesis, two types of materials are considered: silica microporous materials and silica mesoporous materials. Silica microporous materials such as silicalite-1 are usually obtained via clear-solution synthesis involving silica-source and structural directing agents in an aqueous system.[34, 48, 82, 122] The fabrication method for silica mesoporous materials is similar but the surfactants are added as structural directing agents into the solution.[12, 78]

1.1 Microporous Materials

1.1.1 Formation of Microporous Materials

Silicalite-1 is an all-silica zeolite with the MFI framework. The clear-solution synthesis provides an approach for fabricating silicalite-1 at relatively low silica concentrations, avoiding the complexities of silica gel formation (e.g., several phenomena such as solvolysis, acid-base equilibrium, metastability, and phase separation).[61, 67] Experiments are usually carried out by adding tetra-ethylorthosilicate (TEOS) and a tetra-alkylammonium (TAA) species – usually tetra-propylammounium (TPA) – as the organic structure directing agents (OSDA) into a basic aqueous solution (i.e., pH above 9) to prepare silicalite-1.[34, 48, 49, 119] TEOS initially undergoes hydrolysis to yield silicic acids – monomers for silica polymerization. Such monomers subsequently undergo condensation and hydrolysis over time to yield the aforementioned silica-TAA nanoparticles. Small-angle X-ray scattering (SAXS) and small-angle neutron scattering (SANS) experiments have shown that the nanoparticles have a typical size of about 2-5 nm containing 250-400 Si atoms, and a core-shell structure with a silica-rich

core surrounded by an OSDA-rich shell.[34, 48, 82, 83] The core size of the obtained nanoparticles was found to decrease with pH, increase with temperature, and otherwise remain nearly independent of solution composition. No reproducible evidence of silicalite-1 structure has been observed in these silica-TAA nanoparticles.[82, 83]

These nanoparticles are believed to transform into silicalite-1 crystals at long times and/or elevated temperatures,[34] thus possibly holding the key to understanding the formation mechanisms of silica zeolites. Several hypotheses have been proposed to explain the transformation of nanoparticles to silicalite-1 crystals. Schoeman *et al.* suggested that nanoparticles simply serve as sacrificial nutrients to feed the nucleation and growth of silicalite-1 crystallization,[122] while others suggested a zeolite growth process via nanoparticle aggregation.[1, 82, 83, 87] More recently, Lupulescu *et al.* have applied in-situ atomic force microscopy (AFM) to study silicalite-1 growth.[90] The authors proposed a growth mechanism of silicalite-1, which is a combination of the direct attachment of nanoparticles and the nanoparticles acting as nutrients yielding smaller silica species that contribute to silicalite-1 formation. Tsapatsis and co-workers reported evidence for aggregative growth in a lengthy room-temperature study on 2-5 nm nanoparticles characterized by SAXS, atomic force microscopy (AFM), and transmission electron microscopy (TEM).[34] They observed after several hundred days of room-temperature aging the emergence of $\sim$10 nm aggregates with identifiable sub-domains, clearly showing aggregation. These aggregates were subsequently found to provide nucleation centers for silicalite-1 nano-crystallites. Despite this progress, atomic-level structural information on these nanoparticles and their transformations has remained elusive.

Based on the experimental findings, a mechanism for the evolution of precursor nanoparticles to silicalite-1 was proposed by Davis and co-workers.[34] The precursor nanoparticles were found at first without the evidence of zeolite crystal in it. Those particles then evolve through several intermediates to form silicalite-1 nuclei. In the

proposed mechanism, the precursor particles were found having a silica-core/TPA-shell structure. Meanwhile, precursor nanoparticles have formed the structure similar to zeolite particles gradually. The authors suggested that those intermediate particles, not yet form the silicalite-1 nuclei, can contribute to crystal growth by attachment. In this process, how TPA cations redistribute from the shell to the nanopores in silicalite-1 crystals is a challenging task for researchers to understand.

In pursuit of such structural insights, Lesthaeghe *et al.* performed a combined quantum chemistry and infrared (IR) spectroscopy study on these nanoparticles, suggesting that these silica-TPA nanoparticles exhibit a modified version of the "pentasil" IR vibrational signature ($\sim$550 cm^{-1}), observed from five-membered silica ring vibrations in silicalite-1.[87] They reported an IR peak for the nanoparticles that shifts from 650 cm^{-1} after one minute aging to $\sim$600 cm^{-1} after 46 minutes. Quantum chemistry calculations performed by these authors to interpret the IR data show that such blue shifts (from the signature $\sim$550 cm^{-1} feature) can arise from system size effects in the growing nanoparticles, and from the details of the connectivity between various five-membered silica rings. Lesthaeghe *et al.* conclude that the synergistic combination of silica and TPA in these nanoparticles leads to a significant population of five-membered silica rings, a key building unit of the silicalite-1 structure. Their interpretation of the IR data warrants further study, and exemplifies the difficulty in direct experimental determination of nanoparticle structure.[7]

1.1.2 Modeling on Microporous Materials

Several modeling techniques have been applied to investigate the formation mechanisms of microporous materials, with various levels of detail.[6, 7] The requirements of modeling relatively long length and time scales, and the interplay of physical and chemical interactions make this class of systems challenging to model. Mora-Fonz *et al.* applied density functional theory (DFT) with the COSMO approximation to sol-

vation energy to study the chemistry of oligomerization processes of silica.[102, 103] Detailed thermodynamic properties of very initial stages of silica polymerization process were obtained. The authors have found that the formation of cyclic fragments is favored and driven by the high pH, and they suggested that the zeolite growth is most likely to occur by condensation of relatively small units that lead to the ring formation.

McCormick *et al.* introduced a dynamic Monte Carlo simulation to model silicic acid polymerization, which is a key reaction during the formation of zeolites.[112] Their method is based on solving material balances together with reaction rate expressions. This modeling approach has successfully reproduced the initial behavior of the Q_n distribution, where Q_n is the mole fraction of silicon atoms connected to n bridging oxygens. Because a given Q_n distribution does not uniquely specify the atomic-level structure, Wu and Deem developed an atomistic model to investigate the nucleation process of pure silica in the absence of OSDA species.[149]

They applied specialized Monte Carlo (MC) simulations to sample equilibrium structures of silica particles, suggesting that critical nuclei for pure silica crystallization may contain as few as 50 Si atoms, but leaving the effects of OSDAs uncertain. Rao and Gelb studied early stages of silica polymerization using molecular dynamics (MD) simulations at high temperatures (1500-2500 K) over a wide range of silicic acid concentrations in water.[113] At high silicic acid concentration, monomers quickly react to form a large population of dimers, which later become depleted as larger clusters appear. At lower silicic acid concentrations, the polymerization is reaction-limited in the initial stages, which are dominated by the formation of dimers. They also estimated the activation energy of condensation to be 13-15 kcal/mol in excess water. In addition, continuum kinetic Monte Carlo simulations have been reported to model the very early stages of silica polymerization by van Santen and co-workers.[154, 155, 156] The silica condensation rate constants were computed using

DFT and *ab initio* molecular dynamics (AIMD) calculations[134, 135]. The model was further extended to study the silica oligomerization process by the lattice-gas kinetic Monte Carlo method. Their results suggest the gelation process proceeds from four-membered rings, while five-membered rings and six-membered rings share Si with four-membered rings and form during the later gelation stages. Because of the computational demands of such atomistic modeling, these MC and MD methods could not approach the length and time scales needed to simulate the self-assembly of silica nanoparticles that lead to zeolites.

Jorge and co-workers presented a lattice model using simple cubic lattice to describe the formation of silica nanoparticles in the early stages of a clear-solution synthesis of silicalite-1.[67] In addition to MC simulations in the canonical ensemble, parallel tempering MC was implemented to probe the existence of metastable states, as well as reactive ensemble MC to study reaction equilibrium. The spontaneous formation of silica nanoparticles with core-shell structure under conditions was experimentally observed. In the model, silica condensation/hydrolysis is modeled by a nearest-neighbor attraction, while the electrostatics is represented by an orientation-dependent, short-range interaction. The nanoparticles are identified as a metastable state, stabilized by electrostatic interactions between ionized silicates and organic cations. The size of a nanoparticle is controlled mainly by the solution pH, through nanoparticle surface charge. The increment in the pH increases the surface charge and, hence, leads to the formation of the TAA layer for smaller particle sizes. Increasing the temperature allows for further particle growth by Ostwald ripening, the mechanism may play a role in the growth of zeolite crystals.

Due to the coarse-graining of the model, quantitative comparisons with experimental data are difficult to make. Furthermore, the simplifications introduced herein preclude us from predicting the internal structure of the particles. This type of information can best be obtained from off-lattice atomistic simulations of silica-TAA

alkaline solutions. Such simulations may also help clarify the precise role of TAA in nanoparticle stabilization. On the other hand, there is scope for refining the present model; efforts in this direction may yield additional insights into the early stages of zeolite growth.

Recently, Lin *et al.* built an extension of the simple cubic lattice model developed by Jorge *et al.* of nanoparticle growth in the clear solution synthesis of silicalite-1.[62, 67] The model was implemented on a body-center cubic (bcc) lattice with second-neighbor repulsions to generate a four-coordinate network that mimics the tetrahedral structure of silica. With this low-coordination lattice model, it was found that the nanoparticles are metastable, possessing a core-shell structure with mostly silica in the core and templates forming a shell. The TPA cations tend to adsorb to silica anions near the nanoparticle surface, thus providing a barrier protecting the nanoparticles from further addition of silica monomers. This low-coordination feature makes it possible to model porosity in the silica core of nanoparticles. The most significant feature of the refined bcc lattice model is that templates can and do penetrate the interior of nanoparticles. It was found that template penetration is rare for bulky templates.

1.1.3 Questions

Elucidating the mechanisms by which ordered nanoporous materials form has remained challenging for experiment and theory alike. During the synthesis of silicalite-1, a suspension of silica nanoparticles with the particles size around 5 nm, has been observed prior to the appearance of zeolite crystals.[83] These nanoparticles are found to lead to the formation of silicalite-1 crystals at elevated temperatures, are believed as a key to understand zeolite formation. However, their structure and their precise role in zeolite synthesis remain the subject of debate. The techniques like ^{29}Si NMR, has proven to be a powerful, non-destructive method for providing distances

and chemical environments within 1-2 nm, whereas SAXS and SANS techniques can probe crystalline structure with long-range order about 50 nm above the nucleation length scale. Characterization techniques for experiments suffer from a nanoscale blind spot at length scales where zeolite nucleation is likely to occur.[7] The detailed information about the structure of silica during the polymerization is lacked.

One the other hand, molecular modeling has a potential to shed light on the problem. However, due to the requirements of relatively long length and time scales on the system, the interplay of physical and chemical interactions makes the system challenging to model. It is thus obvious why this problem has remained a grand challenge for several decades. Previous simulations either dynamics MC method or lattice model MC simulation study physical or chemical properties of the formation of zeolites, the key information of zeolites formation, SDA effects, remain incomplete. It is believed that SDA has great impact on the forming the porous materials from the experiments. Several key questions s listed below remain unclear and they need to be addressed.

- What are the structures of precursor nanoparticles form prior to the formation of the zeolite crystals?
- What is the role of silica nanoparticles in zeolite formation?
- How do OSDAs redistribute from their shell domain into the nanopores of silicalite-1?
- How do the nuclei form? What are the critical sizes and shapes of the nuclei lead the zeolites?
- What are the critical sizes and structure of the precursors of formation of silica microporous materials?

1.2 Mesoporous Materials

Periodic mesoporous silicas (PMSs) materials have attracted great interest since the first synthesis of MCM-41 in 1992.[12, 78] PMSs possess porous structure in a long-range order while exhibiting amorphous nature at the atomic scale. This kind of materials have been widely applied to many fields such as shape-selective catalysis, separation and adsorption-desorption processes, drug delivery, biocatalysis, optical and electronic devices, etc.[18, 41, 53, 54, 79, 100, 111, 131, 148, 157] PMSs are usually fabricated via a templated sol-gel synthesis route, in which the interplay of physical interaction and chemical reaction of surfactants, silica source, and water self-assemble into a liquid-crystal phase. M41S family, one of the most studied PMS materials, has different interesting morphologies: hexagonal arrays with ordered channels (MCM-41), the cubic structures (MCM-48) and the layered structure (MCM-50).[29, 132, 136]

1.2.1 Formation of Mesoporous Materials

MCM-41 has cylindrical pores in a hexagonal array with pore sizes ranging from 1.6 nm to 10 nm.[12, 78] The synthesis of MCM-41 usually starts from a solution using alkyltrimethylammonium surfactants $C_nH_{2n+1}(CH_3)_3NBr$ as structure directing agent, together with tetramethyl orthosilicate in a solution. Surfactant micelles form in the system, followed by addition of inorganic species (silica, silica-alumina).[78] The final products with pore sizes around 40 Å were obtained via calcination under 540°C.

Two MCM-41 formation pathways were proposed by Beck and co-workers.[12, 78] The two pathways: liquid-crystal templating (LCT) mechanism and silicate anion initiated mechanism. In the LCT mechanism (Pathway 1 in Figure 1.1), the authors proposed the structures were determined by the liquid-crystals of the water-surfactant, which servers as templates in the formation of MCM-41. The surfactants form the hexagonal arrays first, and silica condenses at the surface of inorganic walls

between the surfactant cylinders. The other mechanism, the silicate anion initiated mechanism (Pathway 2 in Figure 1.1), suggests that the addition of the incorporation between the inorganic silicates and surfactants results in the ordering of the subsequent silicate anions-encaged surfactant micelles.[11, 29, 78]

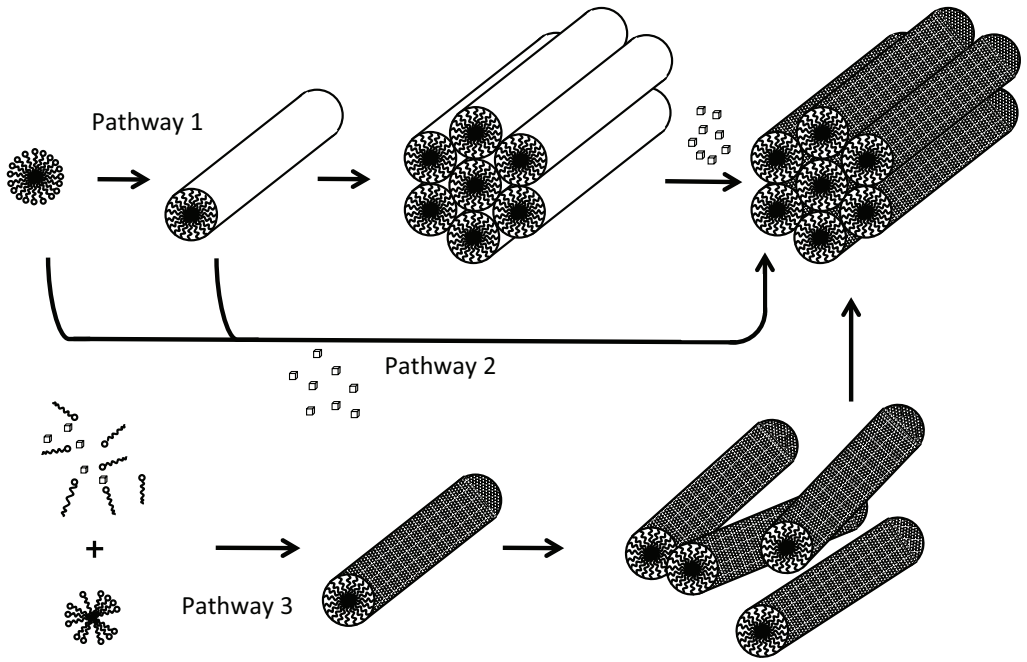

Figure 1.1. The proposed formation mechanisms of MCM-41.[51, 78]

Beck and co-workers also carried out a series of experiments with different alkyl chain length of $C_nH_{2n+1}(CH_3)_3NBr$ to form the porous materials.[11, 78] It was found that the amorphous or microporous zeolitic materials were obtained only if n is equal to 6. As increasing the alkyl chain length (i.e., n=8, 10, 12, 14, and 16), MCM-41 is formed with increasing pore sizes in a low temperature synthesis (100°C). These results showed that the structure of surfactants is the crucial key for determining the structure of the final products. The formed liquid crystal structure is extremely sensitive to the condition of solvents.[78]

Beside to the two proposed mechanisms by Beck and co-workers, a model to explain the formation and morphologies of surfactant-silicate mesostructures (Pathway 3 in Figure 1.1) was presented by Stucky and co-workers.[51, 59, 60, 101] The authors had successfully synthesized mesoporous materials under a wide range of conditions, and they proposed that the charge matching between the charged surfactant heads and inorganic components governs the assembly process. The formation mechanism is the so-called cooperative template mechanism (CTM). In the proposed model, three processes are identified: multidentate binding of silicate oligomers to the cationic surfactant, preferential silicate polymerization in the interface region, and charge density matching between the surfactant and the silicate. Furthermore, they proposed that the properties and structure of a particular system were governed by the dynamic interplay among ion-pair inorganic and organic species instead of the preorganized order of the organic array. Through a small change of synthesis parameters, e.g., the composition and temperature, different mesostructures can be obtained.[51] Surfactants and synthesis conditions can be chosen and controlled to obtain predicted silica-based mesophase products.

Different characterization techniques were performed to study the formation of MCM-41. Davis and co-workers carried out In situ ^{14}N nuclear magnetic resonance (NMR) spectroscopy, which revealed that the liquid crystal phase does not exist during the synthesis of MCM-41.[24] The authors suggested that randomly ordered rod-like organic micelles interact with silicate species to form two or three monolayers of silica encapsulation at the surfaces of the micelles. Then the composite species spontaneously assemble into the long-range ordered structure characteristic of MCM-41.

X-ray diffraction (XRD) was also performed to study the formation of ordered mesoporous silicate/surfactant composites.[14] The formation of the MCM-41 structure was found to be kinetically controlled by the silicate condensation rates. In situ

electron paramagnetic resonance (EPR) was used to monitor the formation of M41S materials.[153] The experimental evidence has shown that micelles serve as precursors for the mesoporous materials. EPR and XRD studies indicate that the MCM-41 forms in two stages: Hexagonal arrays form immediately after mixing the reagent, followed by a slow silica polymerization (1-1.5 h). The polymerization at the interface is a slow process while the long-range order is acquired almost immediately after the initiation of the reaction. The addition of TEOS first yields to rodlike, silicate anions-coated micelles, followed by the silica condensation at the interface to form the final MCM-41 product.

1.2.2 Modeling on Mesoporous Materials

Physical and chemical interplay of species in solutions at the initial synthesis stages of self-assembly process remains unclear due to limitations of characterization techniques. Whether micelle growth proceeds via successive micelle fusion or accretion of free surfactants around silica pre-polymers remains a question of debate. Therefor molecular simulations emerge as a powerful tool to address these issues. Due to the complexity and multiscales of mesophase formation processes, approximations need to be made to simulate the self-assembly process.

A kinetic Monte Carlo method was presented to simulate the hydrothermal synthesis of PMS.[123] The simulation was carried out by using simplified potentials and representations of templated micelles. The work focused mainly on the silica condensation, assuming the geometry of the mesostructure of templating micelles. The authors also simulated the adsorption properties of PMS using grand canonical Monte Carlo simulations. Reasonable agreement with experimental findings was obtained from the work. However, how the interplay between silica and the surfactant determines the mesoscale structure in this model was not addressed due to the rigid boundaries of the model. The possibility of considering variations in the pore size

and shape created by interfacial fluctuations during the self-assembly process was eliminated.

Siperstein and Gubbins[126] performed lattice Monte Carlo simulations to study the behavior of surfactant-inorganic oxides-solvent systems. The authors made use of a lattice surfactant model presented by Larson.[85] A phase separation was found: high silica/surfactant concentration and solvent-rich phases. Ordered liquid crystal phases are observed in the surfactant-rich region. Qualitative agreement with experimental data was obtained from the model. The phase transition of hexagonal to lamellar phases occurs while increasing silica/surfactant ratio. Reversible lamellar to hexagonal phase was observed with the increasing temperature, and the observation is in qualitative agreement with experimental results. However, the structure of inorganic species in the model was oversimplified.

Jin *et al.* recently made use a lattice Monte Carlo simulation to study the formation mechanism of MCM-41.[63] The authors took a surfactant lattice model built by Larson[85] with a silica tetrahedron lattice model to capture the self-assembly process of mesophase. A two-step synthesis was proposed: (i) simulating the mesostructure formation in a silica monomer-surfactant system at high pH and low temperature; (ii) performing irreversible silica condensation at lower pH and higher temperature. The author also found a reversible transformation between hexagonal and lamellar phases by changing temperature. Though the authors provide a feasible approach to probe the formation of mesoporous materials, an off-lattice model is necessary to gain profound insights and more realistic structure in a significant level.

All-atom MD simulations were also used to investigate the early stages of the formation of silica mesoporous materials by Jorge and co-workers.[68, 69] Significant level of details was obtained: anionic silicates adsorb strongly on the surface of micelles, displacing some of the bromide counterions and promoting the growth of small aggregates from micelles. The authors also found that as the degree of condensation

increases, the multiple charges on silicate oligomers interact with more than one micelle. However, the simulations were limited by the length and time scales of the PMS formation.

Recently a coarse-grained (CG) model was carried out to study the silica/surfactant mesostructures during the synthesis of periodic mesoporous silica.[108] The authors made a direct comparison of density profiles of preassembled micelles obtained from an all-atom (AA) simulation with those calculated using CG model to obtain the CG model parameters. The micelle formation and micelle fusion/fission processes revealed that the interaction between anionic silicates and cationic surfactants promotes a sphere-to-rod transition. Key components such as surfactant, water and silicate can be therefore all included into the system by applying this CG model, which gives a chance to investigate later stages of silica mesostructure formation.

1.2.3 Questions

Though several mesoporous materials have been fabricated, the cooperative templating mechanism during the formation of mesoporous materials is still not well understood. In general, there exists a broad agreement that silicate and surfactant species cooperate is the key during the formation of mesoscale structures. Moreover, the nature and extent of polymerization of these oligomers is unclear, and the overall scheme for mesoscale order formation in this hypothetical mechanism remains uncertain.

Here we focus on modeling the formation of PMSs. Several issues will be explored including modeling the effects of surfactant chain length on the cooperative templating of mesoporous structures. We will also investigate the interplay between silica polymerization and mesoscale surfactant assembly, to identify the most likely mechanism for cooperative structure formation in these materials. We strive to answer

the following questions through molecular modeling; these issues are crucial to the formation mechanism of these kinds of porous materials:

- How does silica oligomerization alter the nature of silica-surfactant interactions?
- How is mesoscale assembly influenced by these factors and by the surfactant chain length?
- Do silica particles condense around preformed surfactant liquid-crystal, or do silica species actually participate and promote the formation of liquid crystals?
- How does a structural directing agent influence the way zeolites and mesoporous materials form?
- Does polymerization process occur at the surface of preformed surfactants to form mesoporous materials?

1.3 Summary of the Project

To facilitate the future synthesis and design of micro- and mesoporous materials, there is a need to have a better understanding in the structural formation mechanism. There are several key questions remained in the area, and we aim to unravel these questions by using computational approaches. We also build a unified modeling perspective for both microporous and mesoporous silica materials – this has been lacking in the field. In particular, off-lattice models are adopted in this research project. Previous modeling results from lattice model elucidate the low coordination number model is feasible to model the formation of the porous materials. However, structures at the atomic level can not be explored. Off-lattice models herein provide a more realistic molecular representation to approach the problem. Moreover, infinite spatial configurations generated from this model can potentially mimic actual topologies of a huge variety of porous materials.

1.4 Dissertation Outline

In this dissertation, we will present our work in the followed manners: Chapter 2 investigates the formation process of silica nanoparticles using reaction ensemble Monte Carlo technique. Silica nanoparticle structure at an atomic level was obtained from the simulation. Detailed analysis is also presented. Chapter 3 describes an advanced sampling technique, replica-exchange reaction ensemble Monte Carlo, developed to overcome the energetic barrier between amorphous and crystalline silica materials. Different dense silica polymorphs and all-silica zeolite frameworks can be achieved using this simulation technique. In Chapter 4, molecular dynamics simulations applied to study the self-assembly process of the mesoporous materials, such as MCM-41 formation, in early stages is discussed. The coarse-graining of MARTINI force field allows us to study large systems within a feasible computational time. Phase diagram of a surfactant/silicates/water system was successfully obtained. Chapter 5 proposes a hybrid MD/MC simulation to study the later stages in the formation of MCM-41. Preliminary study has been launched, and several issues are discussed to facilitate the future development of the model. Chapter 6 concludes the summary and outlook of this work.

CHAPTER 2

MODELING THE SELF-ASSEMBLY OF SILICA-TEMPLATE NANOPARTICLES IN THE INITIAL STAGES OF ZEOLITE FORMATION

In the present work, we apply reaction ensemble Monte Carlo to simulate a detailed molecular model of silica-OSDA self-assembly, to reveal heretofore unknown structural properties of these nanoparticles found in the initial stages of the clear-solution synthesis of silicalite-1 zeolite. Such nanoparticles, which comprise both silica and organic structure directing agents (OSDAs), are believed to play a crucial role in the formation of silica nanoporous materials, yet very limited atomic-level structural information is available for these nanoparticles. We have modeled silica monomers as flexible tetrahedra with spring constants fitted in previous work to silica bulk moduli, and OSDAs as spheres attracted to anionic silica monomers. We have studied one-step and two-step formation mechanisms, the latter involving initial association of silica species and OSDAs driven by physical solution forces, followed by silica condensation/hydrolysis reactions simulated with reaction ensemble Monte Carlo. The two-step process with preassociation was found to be crucial for generating nearly spherical nanoparticles; otherwise without preassociation they exhibited jagged, ramified structures. The two-step nanoparticles were found to exhibit a core-shell structure, with mostly silica in the core surrounded by a diffuse shell of OSDAs, in agreement with SANS and SAXS data. The Q_n distribution, quantifying silicon atoms bound to n bridging oxygens, found in the simulated nanoparticles is in broad agreement with ^{29}Si solid-state NMR data on smaller, 2 nm nanoparticle populations. Ring-size distributions from the simulated nanoparticles show that five-membered

rings are prevalent when considering OSDA/silica mole fractions (~ 0.2) that lead to silicalite-1, in agreement with a previous IR and modeling study. Nanoparticles simulated with higher OSDA concentrations show ring-size distributions shifted to smaller rings, with three-membered silica rings dominating at an OSDA/silica mole fraction of 0.8. Our simulations show no evidence of long-range silicalite-1 order in these nanoparticles.

2.1 Introduction

Our group has reported lattice model Monte Carlo simulations to describe the formation of silica-OSDA nanoparticles in the early stages of clear-solution synthesis of silicalite-1.[67, 62] Such models dramatically reduce the space of allowed configurations, allowing the study of much larger system sizes. Our studies reproduced the core-shell structure found in SAXS and SANS measurements, and predicted the metastable nature of these nanoparticles found by Davis *et al.*[34] However, such lattice models cannot reveal the detailed structural information we seek herein.

To address this need, Malani it et al. reported an off-lattice MC simulation of silica polymerization using the reaction ensemble MC method with specialized MC moves.[91, 92] This approach has provided the best agreement to date with ^{29}Si NMR data on the evolution of the Q_n distribution,[40] as well as atomic-level structural information on the evolution of ring-size distributions during the process of silica polymerization. The work of Malani *et al.* was restricted to the iso-electric point of silica (pH $\sim$ 2), and in the absence of OSDA. We now generalize these off-lattice reaction ensemble MC simulations to a wide range of pH values, and in the presence of a simple model of an OSDA. We find below that reproducing known properties of these silica-OSDA nanoparticles such as size and shape requires a two-step process beginning with preassociation driven by physical solution forces, followed by silica polymerization with reaction ensemble MC. We also find that, when considering OSDA/silica

mole fractions that lead to silicalite-1, the resulting simulated nanoparticles exhibit ring-size distributions dominated by five-membered silica rings, corroborating the work of Lesthaeghe *et al.*[87]

The remainder of this Chapter is organized as follows: Sec. 2.2 describes the model and simulation methodology; Sec. 2.3 provides our results and discussion of nanoparticle structure; and Sec. 2.4 offers a summary and concluding remarks.

2.2 Model and Simulation Methodology

2.2.1 Molecular Model

This work makes use of a molecular model consisting of flexible, corner-sharing tetrahedra to represent silicic acid ($Si(OH)_4$) and silicate molecules ($Si(OH)_3O^-$) as neutral and anionic monomers for silica polymerization, respectively. (We do not consider species such as $[Si(OH)_2O_2]^{2-}$ in the present work because these are only important at very high pH, and we are interested here in more moderate alkaline conditions.) We also consider hard sphere particles with short-range attractions to represent OSDA molecules. The silica tetrahedron model was inspired by the "rigid unit mode" work of M. Dove [52] and was proposed in detail by Astala *et al.* for modeling the mechanical properties of crystalline silica solids.[4] OSDA molecules were taken to be spherical particles for simplicity; we will consider more complex OSDA structures in forthcoming work. Each silica tetrahedron is represented as a hard-sphere core in the center of each tetrahedron with four corners occupied by one of three possible oxygenic species: (*i*) hydroxyl groups (OH) represented as single particles, (*ii*) one oxide atom in the case of anionic silicate, and/or (*iii*) bridging oxygen atoms (BO) for condensed silica as shown in Figure 2.1. The structure of each flexible tetrahedron is maintained via harmonic springs between the various kinds of possible oxygen atoms according to:

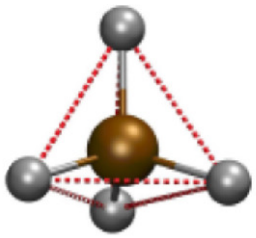

Figure 2.1. Tetrahedral unit of silicic acid. A silicon atom (brown) is centered and four hydroxyl groups (gray) are at the vertices. Dashed lines (red) connecting hydroxyl groups represent springs between them.[92]

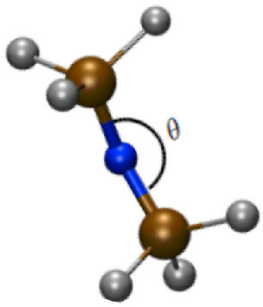

Figure 2.2. Silica dimer formed after a condensation reaction. Silicon atoms are connected through a bridging oxygen (blue) with a Si-O-Si angle (θ).[92]

$$U_1 = \sum_{i=1}^{3} \sum_{j=i+1}^{4} \frac{k_S}{2} (|r_i - r_j| - r_0)^2, \tag{2.1}$$

where U_1 is the internal potential energy of a tetrahedron, r_i is the position of the i^{th} BO/OH/O^- vertex, k_S is a spring constant, and r_0 is the equilibrium distance between two vertices (i.e., oxygen-oxygen distance). The value of k_S was determined in previous work to be 851 kJ mol^{-1}Å^{-2},[3] while r_0 is set at 2.61 Å based on the geometry of silica tetrahedra (Si-O bond length = 1.6 Å and O-Si-O angle = 109.47°).[91, 92]

In addition to specifying the energetics of each silica tetrahedron, it is also important to describe at a base case level the energetics of the silica network. A general condensation/hydrolysis reaction taking place during silica polymerization can be

written as:

$$\equiv Si - OH + HO - Si \equiv \rightleftharpoons \equiv Si - O - Si \equiv + H_2O \tag{2.2}$$

where the forward reaction is condensation and the reverse reaction is hydrolysis. The polymerization process is thus viewed as the assembly of $Si(OH)_4$ and $Si(OH)_3O^-$ tetrahedra via condensation reactions. Two tetrahedra are connected via a bridging oxygen (Si-O-Si) after a condensation reaction occurs (shown in Figure 2.2. In our previous lattice model work on silica polymerization at high pH,[63] we have assumed for simplicity that such condensations only occur between terminal hydroxyls (OH) and not between OH/O^- or O^-/O^- groups; we will implement herein the application of this assumption to the present off-lattice model of silica polymerization. We have modeled the Si-O-Si angle formed by the bridging oxygen in our present work using the following harmonic potential:

$$U_2 = \frac{k_A}{2}(\cos\theta - \cos\theta_0)^2, \tag{2.3}$$

where θ is the Si-O-Si angle formed by the bridging oxygen, θ_0 is a reference angle, and k_A is an angular force constant. The value of 155° was used for the reference Si-O-Si angle, and the value 226.74 kJ mol^{-1} was used for k_A. Those values were determined by optimizing infinite silica chains using periodic DFT calculations,[3] and were found to reproduce bulk moduli of silica polymorphs.[4] We note that the value of the reference angle falls roughly midway in the range of commonly observed Si-O-Si angles in silica materials (i.e., 130-180°).[44, 70]

We have simulated nanoparticle formation as one-step and two-step processes. The one-step process goes directly into reaction ensemble Monte Carlo to simulate polymerization. In contrast, the two-step procedure begins with a preassociation step involving several canonical MC moves to form silica-OSDA clusters held together by physical solution forces, followed by reaction ensemble MC to condense the physical clusters into silica networks. The rationale behind the two-step approach comes

from previous non-reactive simulations of Catlow and co-workers,[107] which found that silica species tend to cluster in aqueous solutions, even under dilute conditions, perhaps driven by a measure of hydrophobicity. The two-step process described above is also reminiscent of the two-step procedure for synthesizing silica mesoporous solids such as MCM-41,[63] involving an initial step to produce silica-surfactant mesoscale order, followed by silica network condensation at elevated temperatures.

To model the preassociation of silicic acids, we applied the Stillinger-Weber (SW) potential for the interaction between neutral and anionic silica monomers. This potential, which comprises two-body and three-body interactions, was first proposed to model solid and liquid forms of silicon.[129] The SW model has been also applied to water molecules, carbon, and germanium – all tetrahedrally coordinated units.[99] We apply SW herein as a smooth potential that mimics the anharmonicity of a square well, because such anharmonicity provides liquid-like flexibility important for facilitating subsequent silica polymerization.

In the SW potential, tetrahedral coordination is enforced by the three-body term. However, as introduced previously, our model already includes harmonic interactions (Eq. 2.3) to restrict Si-O-Si angles. In addition, calculating three body potentials can become computationally intensive. As such, we apply in this work only the two-body SW potential given by:

$$\varphi_2(r) = A\epsilon \left[B \left(\frac{\sigma}{r}\right)^p - \left(\frac{\sigma}{r}\right)^q \right] exp\left(\frac{\sigma}{r - a\sigma}\right), \tag{2.4}$$

where A is 7.05, B is 0.602, p is 4, q is 0, and the reduced cutoff a is 1.8 to ensure the potential and forces go to zero at a distance of $a\sigma$. These are the standard parameters of the Stillinger-Weber potential.[129]

The SW potential well depth, ϵ, was taken to be 6.0 kJ/mol and 12.0 kJ/mol for the neutral-neutral and anionic-neutral silica interactions, respectively. These well depths were chosen to be less than the energy scale of silica polymerization so that

in stage two of the simulation, where such polymerization takes place, our results will yield substantial and experimentally reasonable degrees of condensation. This model uses 4.5 Å for σ; the value has been shown to lead to a first shell at about 5 Å in the radial distribution function of silica solution, which is consistent with the one calculated by Pereira *et al.*[107] Note that there is no SW interaction between two chemically bound silica tetrahedra (i.e., two silica tetrahedra that are connected through a bridging oxygen).

In addition to the interaction between silica tetrahedra, an attraction between charged species – anionic silica and cationic OSDA – is also included. As a substantial amount of screening between charged species is expected in the solution phase, the electrostatic potential is modeled using short-range attractions with the simplified SW potential (i.e., only the two-body potential). This short-range interaction enforces local charge balancing, which likely plays a role in inorganic material growth. The same value of σ in the silica pairwise interaction was applied to the SW potential binding anionic silica and cationic OSDA, whereas the larger well depth of 36 kJ/mol was applied to describe the charge-balancing interaction between anionic silica and cationic OSDA. Previous MD simulations by Vlachos and co-workers [22] find that a free-energy well depth for silicate-TMA interactions is on the order of 20 kJ/mol. We apply a slightly larger well depth in our present simulations, 36 kJ/mol, which we find is necessary in the context of the present coarse-grained model to produce nanoparticles associated with OSDA species.

Various Stillinger-Weber potential wells for the neutral-anionic silica interaction and the $OSDA^+$-anionic silica interaction were tested in our simulations. With more favorable interactions between neutral and anionic silica (i.e., from of 6 to 10 kJ/mol), silica cluster size was found to increase. The cluster size, however, remains nearly constant when the neutral-anionic silica interaction is greater than 11 kJ/mol. Varying

$OSDA^+$-anionic silica interactions from 25 to 75 kJ/mol was found to leave nanoparticles size essentially unchanged.

2.2.2 Sampling and Methodologies

Each simulation started with a random configuration in a cubic box with dimensions 192 Å × 192 Å × 192 Å, giving sufficient volume to simulate the early stages of clear-solution zeolite synthesis. Specifically it needs to be large enough to accommodate several nanoparticles without their agglomerating to form a gel as occurred in our previous low pH studies.[91, 92] For both one-step and two-step processes, we studied compositions given by TEOS:OSDA = 1000:x including 1000 TEOS molecules and x = 0, 100, 200, 300, 400, 500, 600, 700, 800, or 900 OSDA molecules. In general we focus below on results from the TEOS:OSDA = 1000:200 composition, as this most closely resembles typical clear-solution zeolite synthesis conditions.[48, 49] We assumed that TEOS hydrolysis is rapid compared to all other processes, yielding 1000 silicic acid molecules randomly placed in the simulation box at the beginning of the simulation. We also assumed that the cationic OSDA is introduced as its hydroxide salt [$OSDA^+(OH^-)$], producing an equal number of anionic silicate monomers and cationic OSDA molecules assuming completion of the strong base (OH^-)/weak acid ($Si(OH)_4$) reaction. As such, each simulation began with x OSDA species, x anionic silicate monomers, and $1000 - x$ silicic acid monomers, all initially placed randomly in the simulation cell.

In each simulation, at least two million MC steps were performed to allow sufficiently complete structural assemblies. The MC moves included random translations performed on all species, including anionic-silicate-$OSDA^+$ pairs, and rotations performed on all silica tetrahedron (i.e., non-spherical species) in the canonical (NVT) ensemble to sample all possible spatial configurations. Furthermore, to sample reaction events in our simulations, the reaction ensemble MC (REMC) technique[65, 128]

was used to simulate silica polymerization. REMC provides a convenient way to study self-assembly arising from silica polymerization at ambient temperatures. REMC also eliminates the need for reactive force fields to bring about assembly of the polymerized silica network. Our choice for the REMC technique is further supported by the recent simulation study of Malani *et al.*, where they studied silica polymerization at a low pH value (∼2) corresponding to the iso-electric point of silica.[91, 92] The REMC was performed on the two OH groups only within a distance of 2 Å to mimic the real behavior of condensation reaction. In general our attempt probabilities for moves were chosen as 0.79 for translations on all species, 0.20 for tetrahedron rotations, and 0.01 for REMC moves.

In the REMC method, the probability for accepting reactive moves is given by

$$P_{rxn} = e^{-\beta \Delta U} V^{\bar{\nu}} \prod_{i=1}^{n_c} \frac{N_i!}{(N_i + \nu_i)!} q_i^{\nu_i} = e^{-\beta \Delta U} V^{\bar{\nu}} K_{\mathrm{eq}} \prod_{i=1}^{n_c} \frac{N_i!}{(N_i + \nu_i)!} \tag{2.5}$$

where ΔU is the change in potential energy arising from tetrahedral and network distortions; V is the volume, n_c is the total number of components, $\bar{\nu} = \sum_{i=1}^{n_c} \nu_i$, and q_i, N_i, ν_i are the molecular partition function, number of molecules, and stoichiometric coefficient of component i, respectively. The molecular partition functions q_i are related to the equilibrium constant and standard Gibbs free energy of reaction via $K_{\mathrm{eq}} = \mathrm{e}^{-\Delta G_0 / k_B T} = \prod_{i=1}^{n_c} q_i^{\nu_i}$. We simplify the calculations by using the standard Gibbs energy of reaction as an input parameter to the calculation. In our study, all reaction types are assumed for simplicity to have the same value of standard Gibbs free energy. We have used K_{eq} of 500 in this work and our previous studies, corresponding to a condensation free energy at $T = 300$ K of -15.5 kJ/mol $= -3.7$ kcal/mol. This number, 500, is in a reasonable agreement with the electronic energy change of -3.2 kcal/mol obtained from a DFT calculation on silicic acid dimerization in water.[23] More detailed information on our simulation methods and MC sampling moves can be found in the previously published paper from our group.[91, 92] As described above,

we considered one-step (polymerization) and two-step (preassociation followed by polymerization) silica self-assembly processes. In the two-step process, we generally carried out two million preassociation MC steps (translations and rotations), followed by two million polymerization steps (translations, rotations, and REMC steps).

2.3 Results and Discussion

In this section, we discuss the simulation results on the formation and structural characteristics of the silica-OSDA nanoparticles. We begin by briefly discussing the one-step process, followed by a more thorough description of results for the two-step process.

2.3.1 One-Step Process

We begin by discussing the one-step simulation with the TEOS:OSDA = 1000:200 composition system. This simulation proceeds directly into silica polymerization from a random initial condition without any preassociation. Figure 2.3 shows that this produces relatively small nanoparticles with highly non-spherical shapes, in contrast to the roughly spherical particles observed from experiments.[48] In particular, the one-step simulations produce nanoparticles with diameters consistently less than 1.5 nm and with ∼20 Si tetrahedra, in comparison with the 2-5 nm nanoparticles found in experiments containing several hundred Si tetrahedra.[34] This result suggests that silica polymerization in the earliest stages of nanoparticle formation may substantially suppress further nanoparticle growth, presumably because hydrolysis of Si-O-Si linkages releases too few silica tetrahedra for mass transport among nanoparticles. This finding also suggests that non-reactive silica preassociation may be important for nanoparticle formation,[107] which we discuss in the next section.

To track silica polymerization during the one-step process, the Q_n distribution was computed as the reaction proceeded. The evolution of the Q_n distribution for

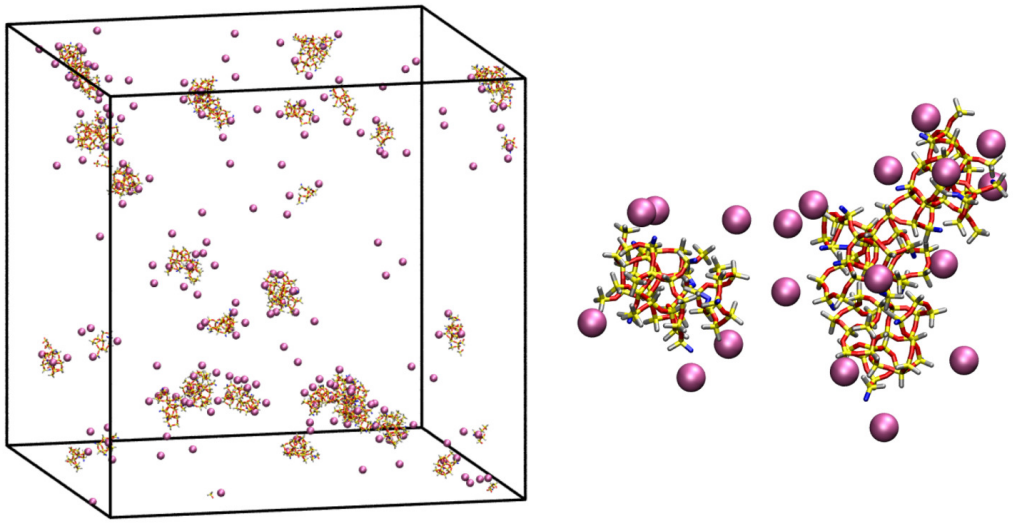

Figure 2.3. Ramified, highly non-spherical, and relatively small clusters of silica and OSDA obtained from the one-step formation process. Color code: Si (yellow), Oxide (blue), Bridging Oxygen (red), Hydroxyl (gray), and OSDA (purple).

the TEOS:OSDA = 1000:200 system is shown in Figure 2.4. It can be seen that Q_0 and Q_1 cross at a mole fraction of ∼0.4, while the mole fraction at the Q_0/Q_2 crossing is around 0.2, and that for Q_0/Q_3 is at around 0.1. In principle, the pattern of crossing points and maxima in the Q_n distribution provides a signature describing the polymerization process; we find that the evolution of the Q_n distribution for silica gel formation simulated previously by Malani *et al.*,[92] the one-step nanoparticle formation shown in Figure 2.4, and the two-step nanoparticle formation shown in Figure 2.5 show substantially similar patterns suggesting similar polymerization mechanisms. One difference pertains to the overall degree of polymerization, which is given by:

$$c = (1/f)\Sigma_{n=0}^{f} n q_n \tag{2.6}$$

where q_n is the mole fraction of Q_n silicon atoms and f is the coordination number of the network (normally $f = 4$ in this case).

In our previous simulations of gel formation,[92] the degree of polymerization was found to reach a value of around 0.8 after 10^5 MC steps, indicating that 80% of the terminal oxygens transformed into bridging oxygens. Figure 2.4 shows a final degree of polymerization of around 0.6 after 2 million MC steps; a similar degree of polymerization was found for the two-step process applied to the TEOS:OSDA = 1000:200 system. This decrease of 0.2 in the degree of polymerization is consistent with 20% of the silica tetrahedra being anionic silicate with a maximum allowed coordination number of 3. This finding may explain why we see so little Q_4 silica in our nanoparticles, with Q_4 mole fractions reaching values little more than 0.1, whereas in the gel we found Q_4 mole fractions of 0.3. We compare Q_n mole fractions to experiment in the next section on the two-step process, finding good overall agreement with NMR data.

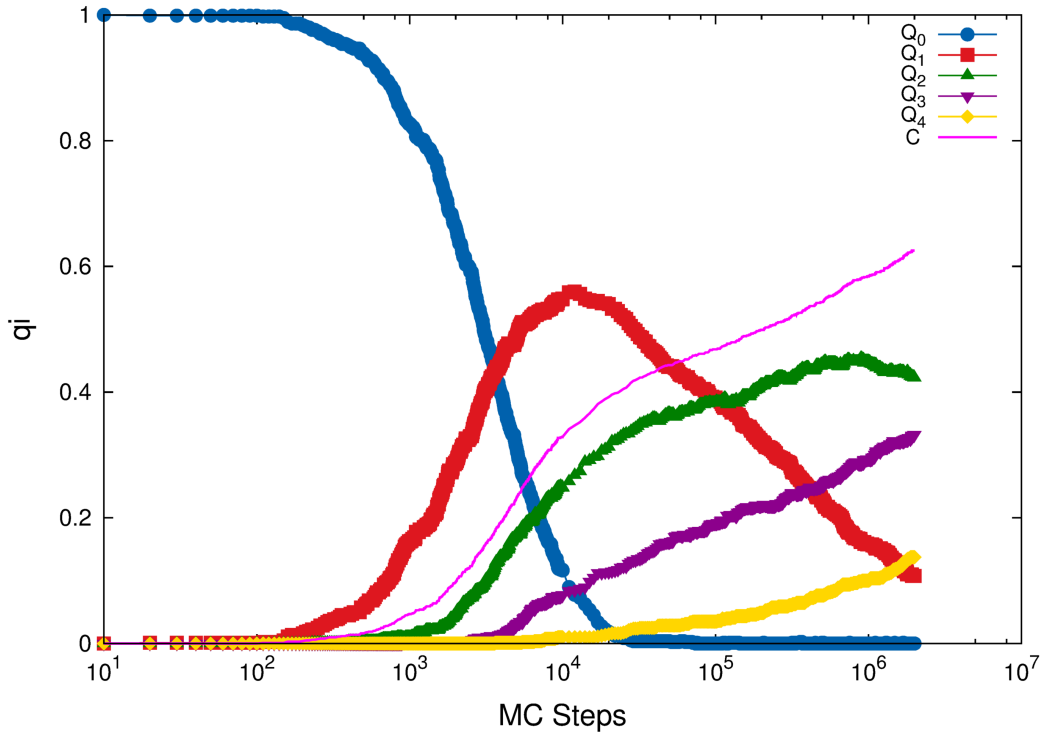

Figure 2.4. Evolution of the Q_n distribution during polymerization obtained from the $one - step$ formation process.

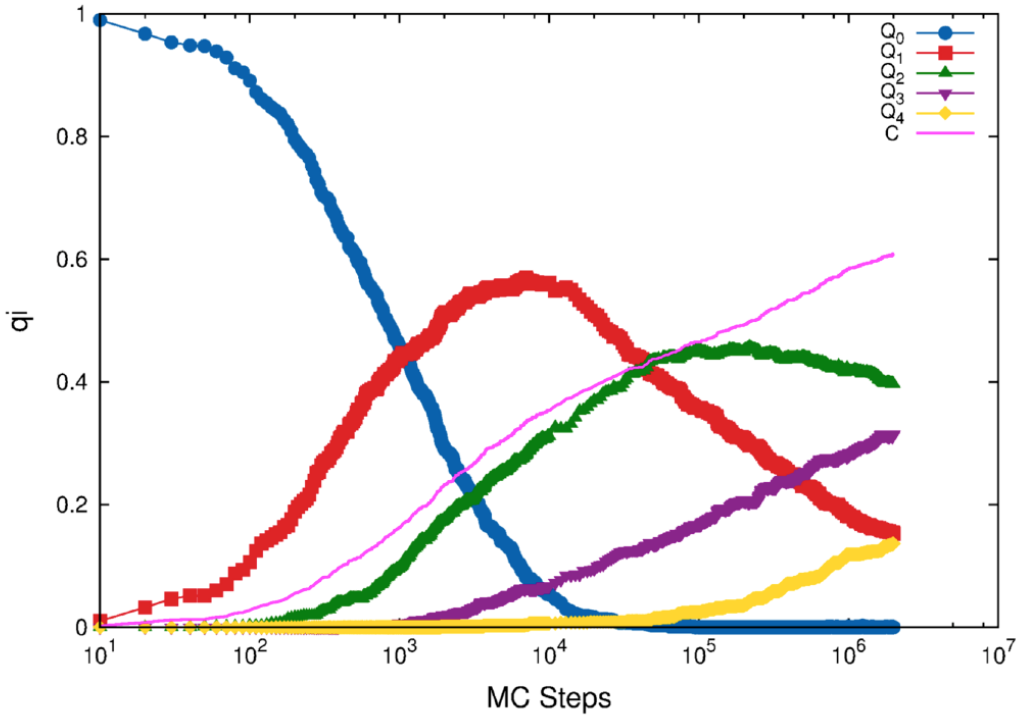

Figure 2.5. Evolution of the Q_n distribution during polymerization obtained from the $two - step$ formation process.

2.3.2 Two-Step Process

Here we show results for the two-step process involving non-reactive preassociation MC driven by the SW potential, followed by silica polymerization simulated with REMC. The resulting nanoparticles were found to exhibit a core-shell structure with most of the silica in the core and OSDA molecules at the surface of the nanoparticles, as shown in Figure 2.6.

Such core-shell structure was observed experimentally via SAXS and SANS characterization techniques.[48, 49] Pair-distance distribution functions (PDDFs) can be extracted from the SAXS and SANS data. PDDFs from SAXS are more sensitive to the relatively high electron density of the silicon atoms in the silica core, while PDDFs from SANS tend to reveal the structure of the entire nanoparticle, receiving signal from both lighter and heavier elements. For comparison with PDDFs from

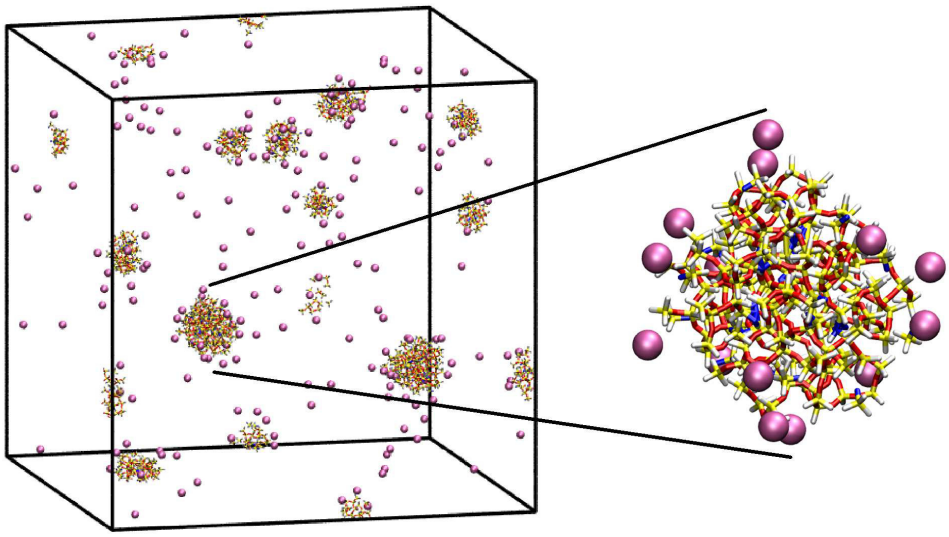

Figure 2.6. Snapshots of nanoparticles obtained from the two-step formation process in the system with TEOS:OSDA = 1000:200. Color code: Si (yellow), Oxide (blue), Bridging Oxygen (red), Hydroxyl (gray), and OSDA (purple).

SAXS and SANS, we have computed PDDFs among silica tetrahedra and among all particles, respectively. We have also computed PDDFs among OSDA molecules; all these and experimental results[48] are shown in Figure 2.7. The silica-silica PDDF has a peak around 1.5 nm, indicating a particle core size of around 3.0 nm, in good agreement with experiments which find silica-OSDA nanoparticles in the 2-5 nm range.[48, 49, 34] The All-All PDDF in Figure 2.7 is essentially the same as the silica-silica PDDF, because the number of silica tetrahedra significantly exceeds that of the OSDAs, making the statistical effect of the OSDAs to be minimal in the all-all graph. This is a consequence of the coarse-graining of the OSDA from 41 atoms, in the case of TPA, to one lumped particle. The simulated OSDA-OSDA PDDF reveals that OSDAs exist in a shell about 1 nm larger than the silica core, which makes sense given the 4.5 Å Stillinger-Weber length scale multiplied by two because distal OSDAs are on opposite sides of a given nanoparticle. In contrast, PDDFs from experimental SAXS and SANS data reveal a 3.5 nm difference between silica core and TPA shell,

which likely arises from the details of Debye screening in solution not accounted for by our model. In future work we will consider more complex models of OSDA structure and OSDA-silicate interactions, to build on the insights gained from base case model presented herein.

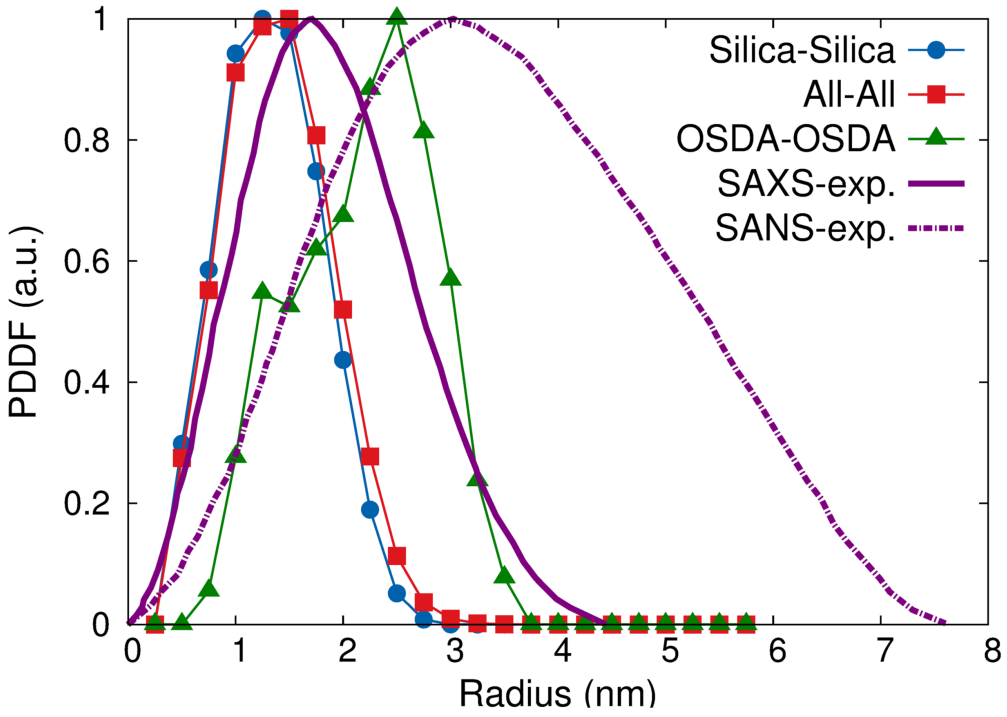

Figure 2.7. Core-shell structure shown by pair-distance distribution functions (PDDFs) among silica tetrahedra, all particles, and OSDAs; from simulations with composition TEOS:OSDA = 1000:200; and experimental PDDFs of SAXS and SANS patterns of a nanoparticle solution (40 SiO_2:9 TPAOH:9500 H_2O:320 TEOS) from literature.[48]

Detailed visualizations of nanoparticles from a single simulation with a range of sizes were obtained as shown in Figure 2.3.2(a). The numbers of OSDAs at the surfaces of these nanoparticles are 15, 12, and 9 for nanoparticles composed of 208, 148, and 108 silica tetrahedra, respectively, corresponding to a mean OSDA:Silica ratio of 0.09, well in excess of the ratio in as-made TPA-silicalite of 4 TPA:92 SiO_2 per unit cell. The PDDFs for distances among silica tetrahedra for these particles is shown

in Figure 2.3.2(b). These PDDFs reveal that these particles have sizes ranging roughly from 2-3.5 nm, which is in good agreement with experimental observations.[48, 49] In addition, the densities of the simulated nanoparticles shown in Figure 2.3.2(a) were calculated from the number of atoms and the particle sizes extracted from PDDFs. It was found that the density is in the range of 1.68-1.83 g/cm^3, which is in good agreement with the experimental value of 1.75 g/cm^3 reported by Rimer *et al.*[118]

Now we consider the effect of varying the initial composition according to TEOS: OSDA = 1000:x, where x varies from 0, 100, 200, ..., 900. We have found that the number of OSDA molecules has a substantial effect on the topology of the resulting nanoparticles. For example, Figure 2.10 shows a simulated nanoparticle (front and side views) from a simulation with composition TEOS:OSDA = 1000:500 (on the left-hand side) and TESO:OSDA = 1000:800 (on the right-hand side), showing an ordered arrangement of neutral silicate and anionic silicate. We note that only few bridging oxygens form in the particles. However, such ordered arrangement of nanoparticles were found to exhibit lower degrees of polymerization, and hence may be too unstable to survive in experiments at longer observation times.

We have found that the number of OSDA molecules plays an important role in determining the sizes of clusters in the preassociation step. Figure 2.11 shows the average maximum cluster size as a function of the number of OSDA molecules obtained from 20 independent simulations. When considering no OSDA, the system evolves to a single cluster consisting of almost all available silicic acids. With the addition of 100 OSDA molecules into the system, the interplay between OSDA and silica leads to smaller clusters. Considering systems with $\geq$200 OSDA molecules produces cluster sizes that are roughly constant with respect to the number of OSDAs. We have also observed in our simulations that as the silica preassociation process proceeds, the dissolution of smaller clusters contributes to the growth of larger clusters, following Ostwald ripening.[67] We have also extracted OSDA surface coverages by defining

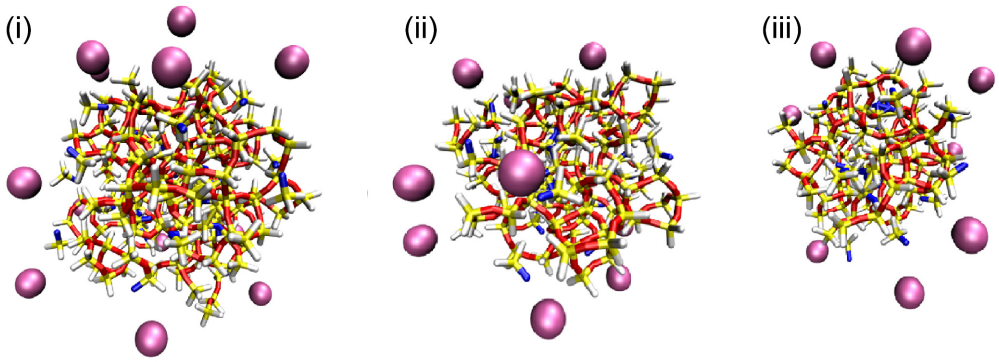

Figure 2.8. Snapshots of nanoparticles with number of silica tetrahedra of (i) 208, (ii) 148, and (iii) 108. Color code: Si (yellow), Oxide (blue), Bridging Oxygen (red), Hydroxyl (gray), and OSDA (purple).

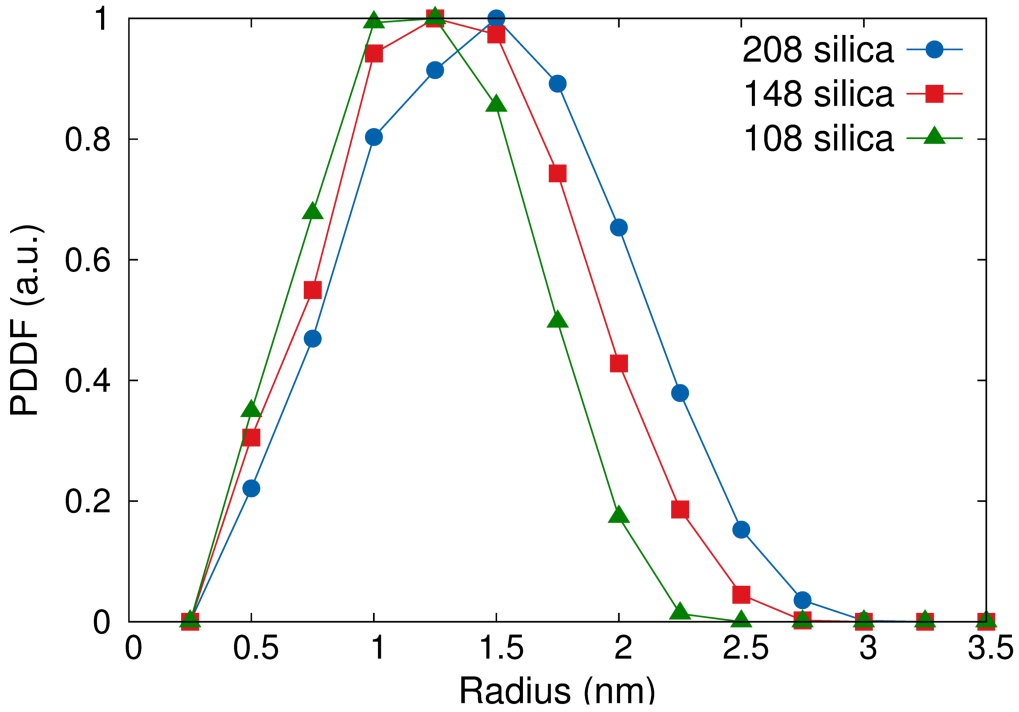

Figure 2.9. PDDFs (silica-silica) of nanoparticles corresponding to the snapshots in Figure 2.8

an OSDA-Si distance criterion corresponding to half the Stillinger-Weber well depth. After analysis, we have found that OSDA surface coatings depend on the number of

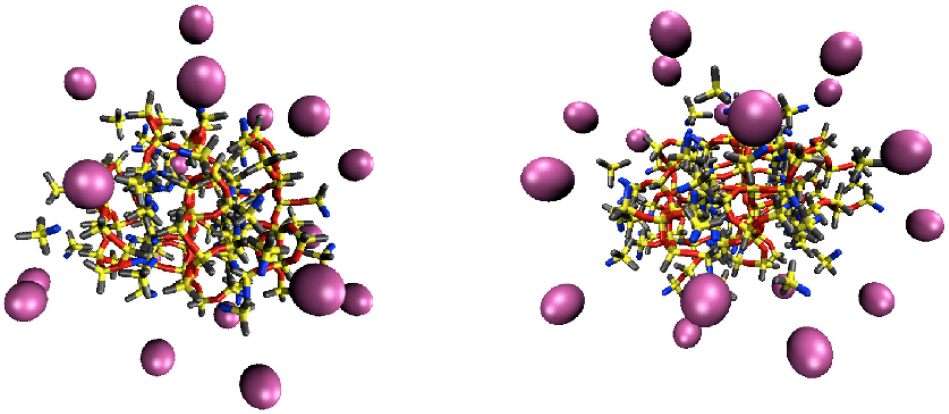

Figure 2.10. Snapshot of particles with ordered arrangement of neutral silica and anionic silica. Color code: Si (yellow), Oxide (blue), Bridging Oxygen (red), Hydroxyl (gray), and OSDA (purple).

OSDAs in the simulation, and on nanoparticle size, as shown in Figure 2.12. Surface coverages were obtained for TEOS:OSDA = 1000:x where x=100-900. We have found a plateau effect for x > 300, and a log(OSDA)-log(Si) slope of 0.61± 0.15, indicating a surface coverage scaling (expected exponent of 2/3). In the plateau range, the mole fractions for small clusters are around 1:4 OSDA:Si, while those for large clusters are around 1:12 OSDA:Si. For comparison, silicalite-1 with TPA in each intersection corresponds to 1:24, indicating by this standard that these nanoparticles are generally rich in OSDA.

Table 2.1 shows the Q_n distribution of the final configuration of nanoparticles simulated for TEOS:OSDA = 1000:200, compared to several experimental Q_n distributions. The experimental data in Table 2.1 include Q_n distributions from two studies on 3-5 nm nanoparticles,[115, 77] and from a study on smaller, 2 nm nanoparticles.[1] The simulated Q_n distribution was computed from nanoparticles consisting of more than 100 silica tetrahedra, to eliminate spurious statistics from small clusters. Table 2.1 indicates that the simulated Q_n distribution is in much better agreement with

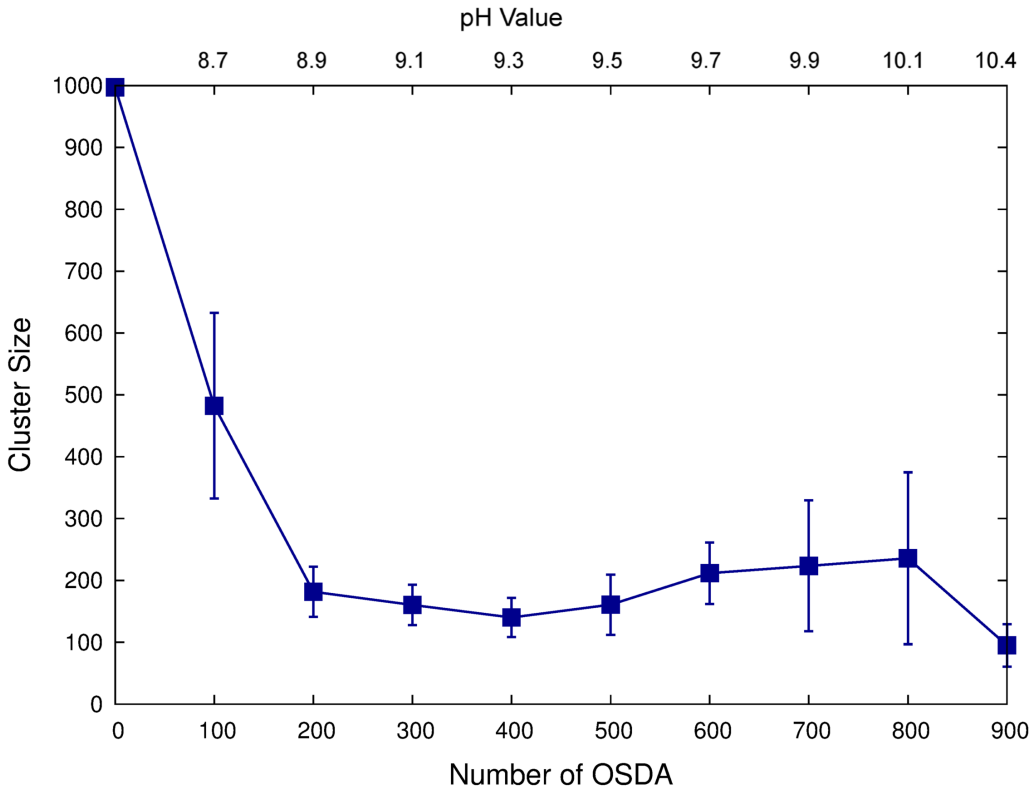

Figure 2.11. Maximal cluster size obtained from preassociation process after performing two million MC steps.

experimental data on the 2 nm nanoparticle population, showing high Q_2 and Q_3 fractions and low Q_4 fractions. Larger nanoparticles, especially aggregates of smaller nanoparticles, have been hypothesized to lead to silicalite-1 crystallization.[34] This is consistent with the notion that larger nanoparticles should exhibit higher Q_4 fractions, considering that crystalline silica consists almost exclusively of Q_4 silicon species. The nanoparticles formed during our simulations are in the smaller range of 2-3.5 nm, and condensation processes have not yet plateaued by the end of our simulations as evidenced by the non-zero slope in the degree of condensation (see, e.g., Figure 2.4), suggesting that the population of nanoparticles that self-assemble in our simulations represents the nascent nanoparticles isolated by Aerts *et al.*[1] Despite the advances

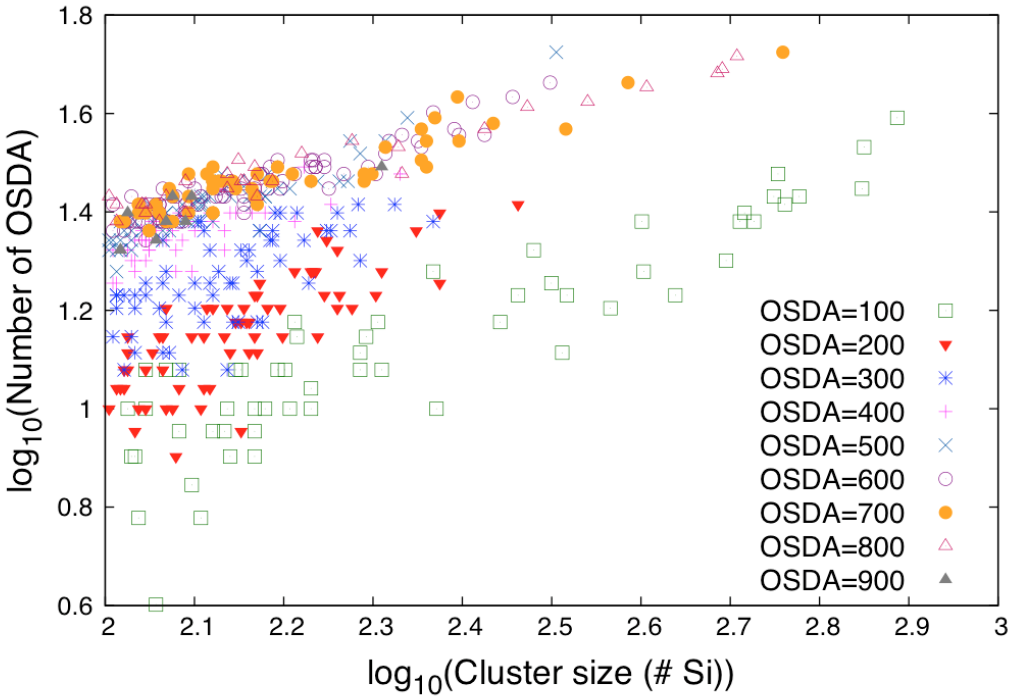

Figure 2.12. Surface coverage of OSDA on the obtained silica clusters for TEOS:OSDA = 1000:x, where x=100-900.

in model development and Monte Carlo simulation reported in this work, it remains computationally challenging to simulate the self-assembly of larger (>4 nm) silica-OSDA nanoparticles.

Our simulations allow a detailed structural analysis of early-stage precursor nanoparticles. The simulated nanoparticles exhibit no discernable short- or medium-range order. In the absence of such order, we focus on ring-size distributions as a structural descriptor of disordered silica. Figure 2.13 shows the computed ring-size distribution for the TEOS:OSDA = 1000:200 system, using an algorithm that counts primitive rings in disordered networks.[152] These results were obtained by averaging ring-size distributions from nanoparticles with more than 100 silica tetrahedra, consistent with the Q_n analysis above. The ring-size distribution in Figure 2.13 is slightly different from that of silica gels, which was shown by Malani *et al.*[92] to be dominated by four-

mole fraction of Q_n silicon	Q_0	Q_1	Q_2	Q_3	Q_4
our simulation	0	12.9	35.2	37.8	14.1
experiment a (2 nm) [1]	0	<10	40-50	40-50	0
experiment b (3-5 nm) [115]	0	0	8.3	40.6	51.1
experiment c (3-5 nm) [77]	0	0	6.4	43.5	50.1

Table 2.1. Comparison Q_n distributions for silica-OSDA nanoparticle populations of various sizes obtained from our simulation and from experiments.

membered rings (involving four alternating, adjacent silicon and oxygen atoms). In contrast, the ring-size distribution in Figure 2.13 exhibits a plurality of five-membered rings, a key component of the silicalite-1 framework structure.[8] A detailed investigation of the simulated nanoparticles shows no evidence for the presence of pentasil units, higher-order building units of the silicalite-1 structure involving chains of five-membered rings.[8] As such, our simulations predict that the atomic structures of these nanoparticles show no evidence of MFI structure other than the predominance of five-membered silica rings. Our results nonetheless support the experiments and quantum chemistry calculations of Lesthaeghe *et al.*,[87] who report IR spectroscopy evidence for the importance of five-membered rings in silica-OSDA precursor nanoparticles.

We also calculated the radius of gyration of each nanoparticle, the center-of-mass of all four-membered rings and five-membered rings, and the distance distribution of each of these rings relative to the center-of-mass of a given nanoparticle, for a system of TEOS:OSDA = 1000:200. The relative position of rings in the nanoparticles is defined as:

$$relative\ position = \frac{D_{rings}}{R_g} \tag{2.7}$$

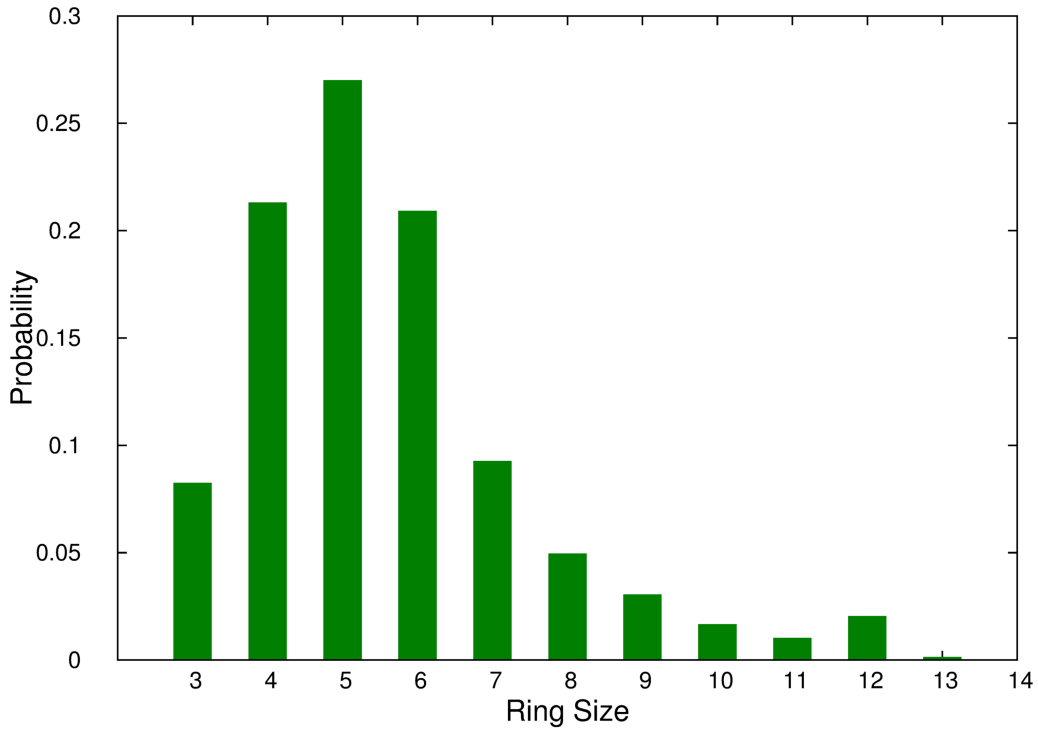

Figure 2.13. Computed ring-size distribution from the TEOS:OSDA = 1000:200 system.

where D_{rings} is the distance of the center-of-mass of a given four-membered ring or five-membered ring to the center-of-mass of a given nanoparticle, and R_g is the radius of gyration of the corresponding nanoparticle. A histogram of the probability of the relative position is shown in Figure 2.14. Figure 2.14 shows that five-membered rings are closer to the surface of nanoparticles than are four-membered rings.

Computed ring-size distributions for systems with various TEOS:OSDA ratios are shown in Figure 2.15. For the simulations without OSDA there is a roughly equal population of five- and six-membered rings, in contrast to the situation in the simulated gel,[92] which is dominated by four-membered rings. Simulations with 200 and 400 OSDA molecules show plurality of five-membered rings, while 600 and 800 OSDA molecules are dominated by four-membered rings and three-membered rings, respectively. The trend predicted in our simulations of the predominance of smaller rings

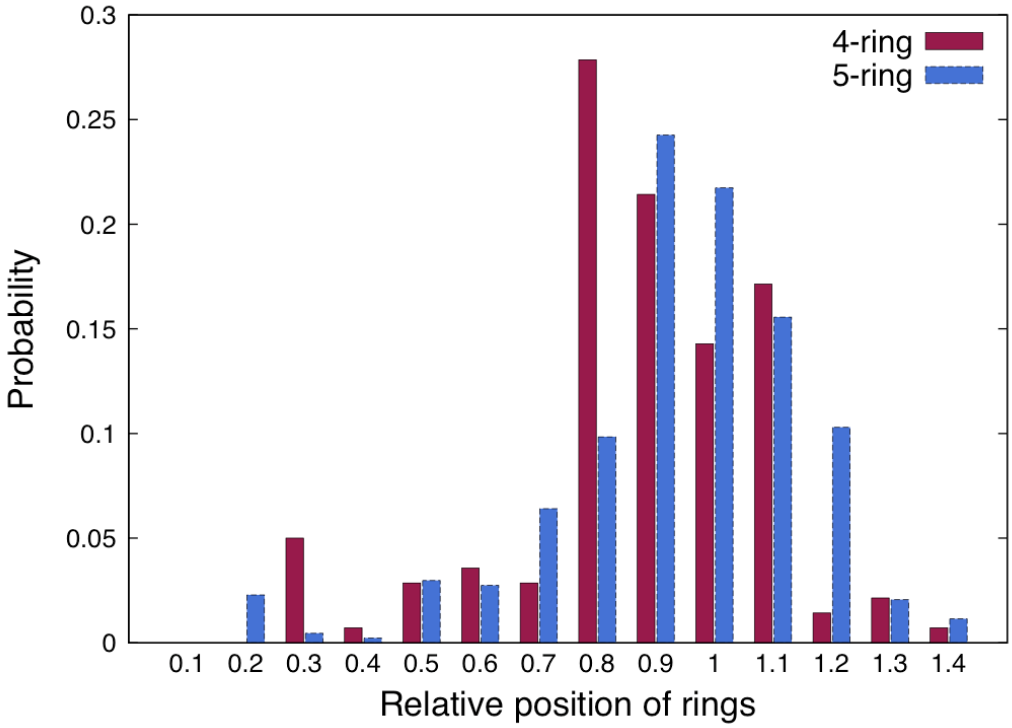

Figure 2.14. The relative position of four-membered rings and five-membered rings in the obtained nanoparticles with TEOS:OSDA=1000:200.

arising from higher OSDA content is interesting and worthy of experimental testing, perhaps with Raman spectroscopy, which is a powerful tool for probing collective vibrations in silica networks.[74] It is also important to consider more accurate representations of OSDAs such as TPA, to determine the extent to which the predicted trend in Figure 10 is influenced by the assumed representation of OSDAs. These results predict that the silica:OSDA composition may not only influence nanoparticle shape but also impact ring formation in the early stages of precursor nanoparticle self-assembly. It is interesting to consider whether the rings formed during these early stages may be important in determining which zeolites crystallize from a sample of precursor nanoparticles.

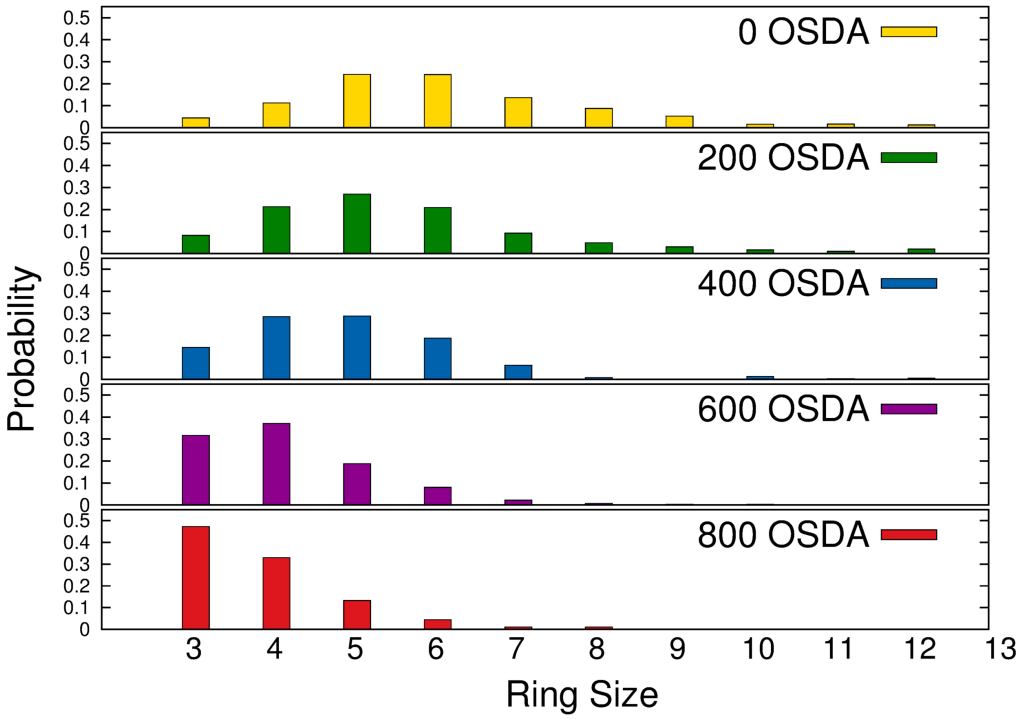

Figure 2.15. Ring-size distributions as a function of OSDA content.

2.4 Conclusions

We have applied the reaction ensemble Monte Carlo method to sample an off-lattice model of silica association and polymerization to investigate structures of nanoparticles formed from silica and organic structure directing agents (OSDAs) used for zeolite fabrication. We are particularly interested in modeling silica-OSDA nanoparticles that have been studied extensively when using tetrapropyl ammonium (TPA) as the OSDA in the clear-solution synthesis of silicalite-1. We have applied a previously-developed model of silica monomers as flexible tetrahedra with spring constants fitted in previous work to reproduce mechanical properties of silica. OSDAs were modeled in the present work as spheres attracted to anionic silica monomers. We have studied nanoparticle self-assembly by comparing one-step and two-step formation mechanisms. The one-step process goes directly into sampling silica poly-

merization via reaction ensemble Monte Carlo, whereas the two-step process begins with non-reactive preassociation of silica species and OSDAs driven by physical solution forces, followed by silica polymerization simulated with reaction ensemble Monte Carlo. We have characterized the resulting nanoparticles using particle size, shape, pair-distance distribution functions, Q_n distributions, and ring size distributions.

The two-step process with preassociation was found to be crucial for generating sufficiently large and nearly spherical nanoparticles; otherwise without preassociation the resulting nanoparticles were found to be rather small ($<$ 100 silica tetrahedra) and with jagged, ramified structures. The two-step nanoparticles exhibit a core-shell structure, with mostly silica in a core of size 2-4 nm, surrounded by a diffuse shell of OSDAs of thickness about 1 nm, in broad agreement with SANS and SAXS data. The computed Q_n distribution, quantifying silicon atoms bound to n bridging oxygens, is in good agreement with ^{29}Si solid-state NMR data on smaller, 2 nm nanoparticles. Ring-size distributions from the simulated nanoparticles for systems with TEOS:OSDA = 1000:200, i.e., for compositions that lead to silicalite-1, show that five-membered rings are prevalent, in agreement with a previous IR and quantum chemistry study. Nanoparticles simulated with higher OSDA concentrations show ring-size distributions shifted to four-membered silica rings. Our simulations show no evidence of medium-range silicalite-1 order in these nanoparticles, such as the presence of pentasil chains.

Our simulations include relatively simple, base-case representations of the OSDA and its interaction with silica, approximations that are crucial for our computational ability to simulate the self-assembly of nanoparticles in the 2-3.5 nm length scale. These initial approximations leave great scope for further refinements to the model, allowing future investigation into the role of OSDA molecular structure on nanoparticle formation and network structure, and the role of longer-range OSDA-silica interactions on the nature of core-shell structure in these nanoparticles. In particular,

in forthcoming work we will study how more accurate molecular representations of OSDAs such as TPA influence ring-size distributions in silica-OSDA nanoparticles. Despite the simplicity of the present model, this work represents the first atomic-level model of the self-assembly of precursor silica-OSDA nanoparticles, opening the door to unprecedented insights into the formation of ordered nanoporous materials.

CHAPTER 3

USING REPLICA-EXCHANGE REACTION ENSEMBLE MONTE CARLO SIMULATIONS TO SEARCH THE GROUND STATE STRUCTURES OF ALL-SILICA ZEOLITES

We have used replica-exchange reaction ensemble Monte Carlo simulations to search for the ground state structure of the reactive silica model. The study makes use of a model of silica polymerization based on the reactive assembly of semi-flexible tetrahedral units developed by us previously to reproduce silica bulk moduli as well as self-assembly of amorphous silica gels and nanoparticles. With a replica-exchange, the model involves simulating several system copies, each with its own value of the equilibrium constant controlling silica condensation/hydrolysis reactions, which are essential for building higher-order network structures and eventually crystals. Using this replica exchange approach, the simulations successfully cross the energy barrier between amorphous silica and crystalline silica, the dense silica polymorphs α-cristobalite, β-cristobalite, and keatite, as well as the porous silica materials SOD and EDI, and porous phosphates with DFT and ATT structures were found. Simulated crystal structures were confirmed by computing X-ray patterns for comparison with known XRD data. The presented result shows that this reactive model has a great potential to possibly simulate the zeolites crystallization in the future.

3.1 Introduction

Several molecular modeling studies have been reported to elucidate the process of zeolite formation.[121] However, relatively few of these simulations actually result in

microporous crystalline materials. Deem and co-workers have applied algorithms for predicting hypothetical zeolite structures, resulting in extensive libraries of energetically feasible framework topologies.[46, 47, 109] Their approach used a MC procedure to sample positions of Si atoms within a unit cell, followed by insertion of oxygens and energy minimization to yield reasonable structures. Despite this progress, such zeolite discovery algorithms do not follow the actual pathways of zeolite formation.

To address this issue, Jin *et al.* recently reported an atomic lattice model of silica polymerization on the body-centered cubic (bcc) lattice.[64] Canonical MC simulations of this model reproduce semi-quantitative NMR data on the evolution of silica gel formation. In addition, parallel tempering MC simulations of this bcc lattice model study a wide array of all-silica zeolite analogs, as well as layered materials and known chalcogenides. Although this lattice model approach shows promise for revealing qualitative aspects of zeolite nucleation and growth, the use of any lattice model fundamentally limits the possible structures that may form. In particular, no known zeolite topology in the IZA database (Database of zeolite structures: http://www.izastructure.org/databases/)[8] maps directly onto the bcc lattice. As such, there remains a need for off-lattice model- and algorithm-development to capture the early stages of zeolite formation.

Malani *et al.* applied reaction ensemble MC (REMC) to sample an off-lattice, spring-tetrahedron model of flexible silica to simulate silica polymerization yielding amorphous gels.[91, 92] This work has produced the best agreement to date of any molecular simulation with the evolution of the so-called Q_n distribution—the distribution of silica atoms bound to n bridging oxygens—measured by ^{29}Si solid-state NMR. These MC simulations accomplished such agreements through a collection of targeted moves that efficiently capture the fundamental condensation and hydrolysis fluctuations in the formation of silica networks. The same approach was recently ap-

plied to model the self-assembly and structures of silica-SDA nanoparticles thought to play a role in silicalite-1 formation.[27]

In this Chapter, we investigate the extent to which this reactive approach to silica polymerization can yield crystalline silica structures, including all-silica zeolite frameworks. Applying molecular simulations to model crystallization requires methods to surmount free energy barriers that separate disordered and crystalline phases. Replica exchange MC algorithms such as the parallel tempering method[45, 75, 76, 114, 130]—simulating several replicas with different temperatures and allowing for replica exchange between MC configurations at adjacent temperatures—have proven useful for equilibrating systems constrained by free energy barriers. Another replica exchange approach developed specifically for reaction ensemble MC was reported by Turner *et al.*,[138] involving simulations at various values of the appropriate standard free energies of reaction. This method can fit naturally within our present silica reaction ensemble model, by simulating system copies with different equilibrium constants controlling silica condensation/hydrolysis reactions. We show below that the replica exchange REMC (RE-REMC) approach promotes ample silica network fluctuations while keeping silica bond lengths and angles within ranges characteristic of a target temperature. As a result, RE-REMC efficiently generates the crystalline ground states of our off-lattice model, producing various dense silica and zeolite crystal structures as confirmed through X-ray pattern analysis.

The remainder of this Chapter is organized as follows: In Sec. 3.2, we describe the model, simulation, and characterization methods applied herein; in Sec. 3.3, we discuss the results of our replica-exchange reaction ensemble Monte Carlo simulations of dense and zeolite silica phases; and in Sec. 3.4, we offer a summary and concluding remarks on the prospects for future work.

3.2 Sampling and Methodologies

This work makes use of a molecular model consisting of a flexible, corner-sharing tetrahedron to represent a silicic acid ($Si(OH)_4$) for silica polymerization.[91, 92] Each silica tetrahedron is represented as a hard-sphere core in the center of each tetrahedron with four corners occupied by one of two possible oxygenic species: (i) hydroxyl groups (OH) represented as single particles, and/or (ii) bridging oxygen atoms (BO) connecting condensed silica. A detailed description of the model has been reported previously;[27, 91, 92] here we give a brief overview.

A general condensation/hydrolysis reaction taking place during silica polymerization can be written as:

$$\equiv Si - OH + HO - Si \equiv \leftrightharpoons \equiv Si - O - Si \equiv + H_2O, \tag{3.1}$$

where the forward and reverse reactions are condensation and hydrolysis, respectively. The polymerization process is thus viewed as the assembly of $Si(OH)_4$ tetrahedra via condensation reactions. Two tetrahedra are connected via a bridging oxygen (Si-O-Si) after a condensation reaction occurs. The equilibrium constant for a reverse (hydrolysis) reaction is denoted below as K_{inv}.

The MC moves included random translations performed on all silica tetrahedra and clusters. In addition, we attempted random translations on terminal hydroxyls (OH) and bridging oxygens (BO), hence producing vibrational excitations of tetrahedra, and eventually rotations from many such atomic translations. These moves were attempted in the canonical ensemble (NVT) to sample important spatial configurations. Furthermore, to sample reaction events in our simulations, REMC was used to simulate silica polymerization. REMC eliminates the need for reactive force fields to bring about assembly of the polymerized silica network. A detailed description of our implementation of REMC can be found in our recent simulation studies on silica polymerization by Malani *et al.*[91, 92] Monomer-monomer, monomer-cluster,

and cluster-cluster aggregation moves where attempted with acceptance probabilities controlled by cluster size through assumed diffusion limitations. Intra-molecular condensations were attempted via force-bias moves that relax strained ring structures. The attempt probabilities for moves were chosen as 0.97 for translations on all species mentioned above, and 0.03 for REMC moves equally split between cluster-cluster and intra-molecular reactions.

3.2.1 Replica-Exchange Reaction Ensemble Monte Carlo (RE-REMC)

To allow efficient sampling of the assembly of zeolite structures, we have used a replica exchange reaction ensemble MC (RE-REMC) simulation technique similar to that presented by Turner *et al.*[138] In the work of Turner *et al.* they used the standard Gibbs energy of reaction as a tempering variable, while in this work we use the inverse equilibrium constant, $K_{inv} = K_{eq}^{-1}$ as the tempering variable. Similar to the parallel-tempering MC (PTMC) technique,[45, 75, 76, 114, 130] RE-REMC was performed with a number (m) of replicas with each replica having a different inverse hydrolysis reaction equilibrium constant, K_{inv}, in which $K_{inv,1} < K_{inv,2} < K_{inv,3} < ... < K_{inv,m}$. As shown in Appendix, the probability of swapping adjacent replicas, m and n, is given by:

$$P_{mn} = min\left\{1,\ \left(\beta P^0 V\right)_m^{\bar{\nu}(\xi_n-\xi_m)} K_{inv,m}^{\xi_m-\xi_n} \cdot \left(\beta P^0 V\right)_n^{\bar{\nu}(\xi_m-\xi_n)} K_{inv,n}^{\xi_n-\xi_m}\right\}. \tag{3.2}$$

In Eq. (3.2), $\beta = 1/k_B T$ where k_B is Boltzmann's constant and T is absolute temperature; V is volume and P^0 is the reference pressure that connects an equilibrium constant to a reference free energy; $\bar{\nu} = \sum_i \nu_i$ is the net change in the total number of molecules; ξ_m and ξ_n are the extent of reaction in the current configuration (before performing a swapping move) in replica m and n, respectively. More detailed derivations can be found in the Appendix.

In the reaction system studied herein, $A + B \rightarrow C + D$, the value of the net stoichiometry $\bar{\nu}$ equals zero. Accordingly, the acceptance probability provided in Eq. (3.2) becomes

$$P_{mn} = min\left\{1, K_{inv,m}^{\xi_m - \xi_n} \cdot K_{inv,n}^{\xi_n - \xi_m}\right\}. \tag{3.3}$$

Furthermore, the quantities ξ_n-$\xi_m = N_{BOn} - N_{BOm}$, in which N_{BOm} and N_{BOn} are the numbers of bridging oxygens in replica m and n, respectively. The final form of the RE-REMC probability can be used herein:

$$P_{mn} = min\left\{1, \left(\frac{K_{inv,n}}{K_{inv,m}}\right)^{\xi_n - \xi_m}\right\} = min\left\{1, \left(\frac{K_{inv,n}}{K_{inv,m}}\right)^{N_{BOn} - N_{BOm}}\right\}. \tag{3.4}$$

An adequate number of replicas and the choice of $K_{inv,m}$ values are essential to the success of this RE-REMC approach. We have found that using 16 replicas is sufficient for generating silica crystals in our simulations. The grid of $K_{inv,m}$ values began with a minimum value of 10^{-6}, corresponding to a condensation equilibrium constant of 10^6, a value large enough to drive network formation. The rest of the $K_{inv,m}$ values were obtained through the relationship $K_{inv,m+1}/K_{inv,m} = 4$, producing a maximum $K_{inv,16}$ value of 537, sufficient to drive silica hydrolysis and hence network deconstruction and annealing.

For comparison with the RE-REMC results reported below, standard parallel tempering reaction ensemble MC (PT-REMC) was applied, involving the simultaneous simulation of several system replicas, each at a different temperature. The probability of a PT-REMC replica exchange move is given as:

$$P_{mn} = min\left\{1,\ exp\left[(\beta_m - \beta_n)(U_m - U_n)\right] \cdot (\beta_n P^0 V)_n^{\bar{\nu}(\xi_m - \xi_n)} K_{inv,n}^{\xi_n - \xi_m} \cdot (\beta_m P^0 V)_m^{\bar{\nu}(\xi_n - \xi_m)} {K_{inv,m}}^{\xi_m - \xi_n}\right\}. \tag{3.5}$$

In the case where $\beta_m = \beta_n$, the PT-REMC probability in Eq. (3.5) reverts back to the RE-REMC result in Eq. (3.2). The challenge in developing an appropriate,

Keq	temperature
1000000.000	74.796
250000.000	80.336
62500.000	86.763
15625.000	94.308
3906.250	103.289
976.563	114.162
244.141	127.593
61.035	144.605
15.259	166.852
3.815	197.189
0.954	241.008
0.238	309.868
0.060	433.777
0.015	723.025
0.004	2169.074
0.002	1504231.000

Table 3.1. Parameters used in this work for PT-REMC.

'apples-to-apples' comparison between RE-REMC and PT-REMC is generating a prescription for computing $K_{inv}(T_m)$ values in PT-REMC in agreement with the grid of $K_{inv,m}$ values in RE-REMC. To achieve this, we have assumed that the $K_{inv}(T)$ formula in PT-REMC follows the Arrhenius temperature dependence: $K_{inv}(T) = A \cdot e^{B/RT}$. We emphasize that, in the present context, these A and B values are posited only to provide a mapping between T_m values in PT-REMC, and $K_{inv,m}$ values in RE-REMC; i.e., they may or may not take physically meaningful values. In our mapping approach, we assumed that $A = 537 = K_{inv,max}$ and $B = 12.5$ kJ/mol, a physically reasonable reaction energy for silica hydrolysis.[102] Using these values we computed a grid of T_m values so that $K_{inv}(T_m)$ (PT-REMC) = $K_{inv,m}$ (RE-REMC), yielding T_m values ranging from 75 K to 150,000 K (see Table 3.1 for all T_m and $K_{inv,m}$ values).

In general for both PT-REMC and RE-REMC, replica exchanges were attempted in 10% of moves, with the other 90% of moves being the translations and reaction moves described above. Simulations were performed generally over 100 million MC steps, requiring in the range 1-7 CPU days on 16 2.2 GHz AMD Opteron 848 CPU-cores.

In addition to visualizing the obtained structures, simulated X-ray diffraction (XRD) patterns were computed to characterize the crystalline structures of the obtained materials. Theoretical XRD patterns were calculated using Debyer software (code.google.com/p/debyer/) on systems with 20 × 20 × 20 unit cells, to ensure sufficient system size to generate reasonably narrow diffraction peaks. Comparison XRD patterns were computed using coordinates obtained from the IZA database and American Mineralogist Crystal Structure Database.[8, 43]

3.2.2 Simulation Algorithm

To implement the RE-REMC, 16 replicas were used with different inverse equilibrium constants, K_{inv}, ranging from 10^{-6} to 536.87 with ratio of $K_{inv,m+1}$ to $K_{inv,m}$ of 4. Lower K_{inv} values facilitate the search for ground state structures, whereas higher K_{inv} values increase the likelihood of crossing energy barriers between local energy minima.

The probability for conventional Monte Carlo moves, P_{MC}, was set to 0.9, for sufficient sampling of possible configurations with a given equilibrium constant; while the probability for replica exchange moves, P_{RE}, was set to 0.1, for crossing energy barriers between replicas.

The simulation was implemented as follows: Pick a move between replica exchange and conventional Monte Carlo using a random number. If the random number is smaller than P_{MC}, conventional Monte Carlo move is performed in all replicas. If

Structures	Number of SiO_2	Box dimensions (Å)
α-cristobalite	16	9.9434 × 9.9434 × 6.922
β-cristobalite	8	7.16 × 7.16 × 7.16
keatite	12	7.46 × 7.46 × 8.61
SOD	12	8.9561 × 8.9561 × 8.9561
ATT	12	9.980 × 7.514 × 9.369
DFT	8	7.075 × 7.075 × 9.023
EDI	5	6.926 × 6.926 × 6.410

Table 3.2. System parameters of studied structures in this work.

the random number is greater than P_{MC}, the replica exchange move is carried out as following:

- Using random number to pick a replica, m (the inverse equilibrium constant is $K_{inv,m}$). And then $m+1$ replica (the inverse equilibrium constant is $K_{inv,m+1}$) is chosen for exchange.
- Determine the numbers of bridging oxygen generated from those two replicas, N_{BOm} in replica m, and N_{BOm+1} in replica $m+1$, respectively.
- Calculate the probability of replica exchange between replica m, and replica $m+1$ by using Eq. (3.5).

3.3 Results and Discussion

We now discuss results from RE-REMC simulations on systems with various densities corresponding to different silica polymorphs. Simulations yielding dense silica crystals as well as all-silica zeolite crystals are described below. All materials considered exhibit orthorhombic, tetragonal, or cubic unit cells; the system parameters of all the investigated structures are summarized in Table 3.2.[8, 43]

3.3.1 Formation of Dense Silica Polymorphs

To test the RE-REMC sampling technique, we started with an investigation of β-cristobalite formation. β-cristobalite is a high temperature and low pressure polymorph of silica. We initialized the RE-REMC simulations with random configurations; a fully condensed silica crystal was achieved in the first replica (with $K_{inv} = 10^{-6}$) after 4 million MC steps. The X-ray diffraction (XRD) patterns of RE-REMC-simulated and known β-cristobalite crystals[43] are shown to agree very well in Figure 3.1.

We then applied RE-REMC to study the ground state structure of the α-cristobalite polymorph. We note that the α-cristobalite system represents the largest simulation cell studied herein, with 4 unit cells containing a total of 16 silica tetrahedra in a box of dimension 9.9434 Å $\times$ 9.9434 Å $\times$ 6.922 Å. α-cristobalite crystals formed in RE-REMC after 55 million RE-REMC steps; the XRD patterns of simulated and known α-cristobalite structures are shown in Figure 3.2.

We also simulated the ground state structure of crystalline keatite, a silica polymorph with density higher than those of β-cristobalite and α-cristobalite, using the RE-REMC sampling technique. Crystalline keatite was found in the first replica (with $K_{inv} = 10^{-6}$) in 4.5 million MC steps; the XRD patterns of simulated and known keatite are shown in Figure 3.3. It is instructive to point out that the Monte Carlo simulations without replica exchange moves did not produce crystalline keatite, even after 26 million MC steps with K_{inv} of 10^{-6}. This suggests that configuration-exchange between adjacent replicas strongly increases the likelihood of overcoming energy barriers and generating crystalline silica.

Having established the utility of the RE-REMC approach for generating silica crystals, we now compare this with the PT-REMC method using the temperature mapping discussed above. Using the initial condition that generated β-cristobalite with the RE-REMC method, we applied PT-REMC with the temperature mapping

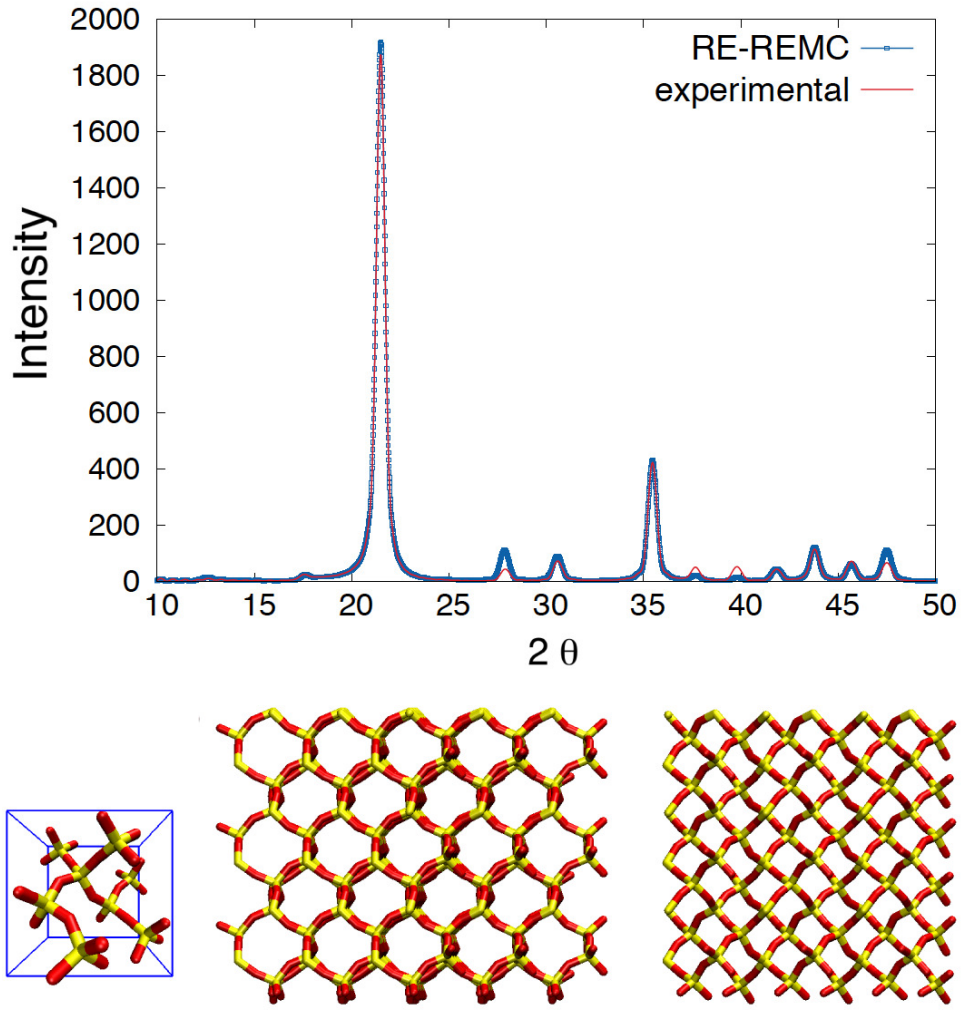

Figure 3.1. Calculated XRD patterns for β-cristobalite comparing RE-REMC structures and known coordinates from the experimental data.[43] Visualizations at the bottom show the obtained atomic structure in a system box (left) and that with the 3×3×3 extension (right).

involving temperatures in the range 75 – 150,000 K (see Table 3.1). We found that PT-REMC also produced crystalline β-cristobalite after 4 million MC steps. The PT-REMC replicas with the lowest three temperatures (75 K, 80 K, and 87 K) were found to produce crystalline β-cristobalite. For comparison, the RE-REMC replicas with the lowest *five* values of K_{inv} were found to crystallize β-cristobalite. In addition,

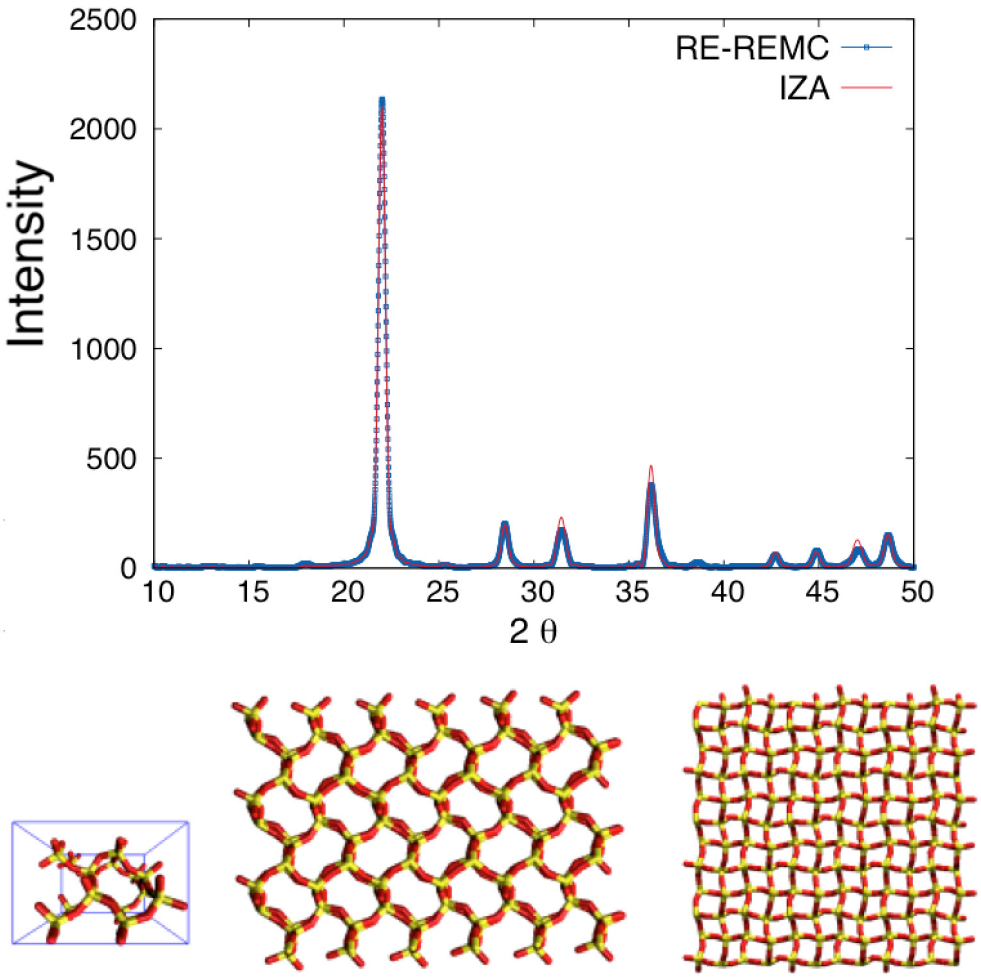

Figure 3.2. Calculated XRD patterns for α-cristobalite comparing RE-REMC structures and known coordinates from the IZA Database.

high temperature replicas in PT-REMC produced rather distorted silica tetrahedra that are not representative of structures found in silica materials. Finally, replica exchange probabilities were of order 10^{-2} in RE-REMC, but only of order 10^{-4} in PT-REMC, which indicates that RE-REMC can provide an efficient and effective sampling for crossing the energy barrier to produce zeolite materials.

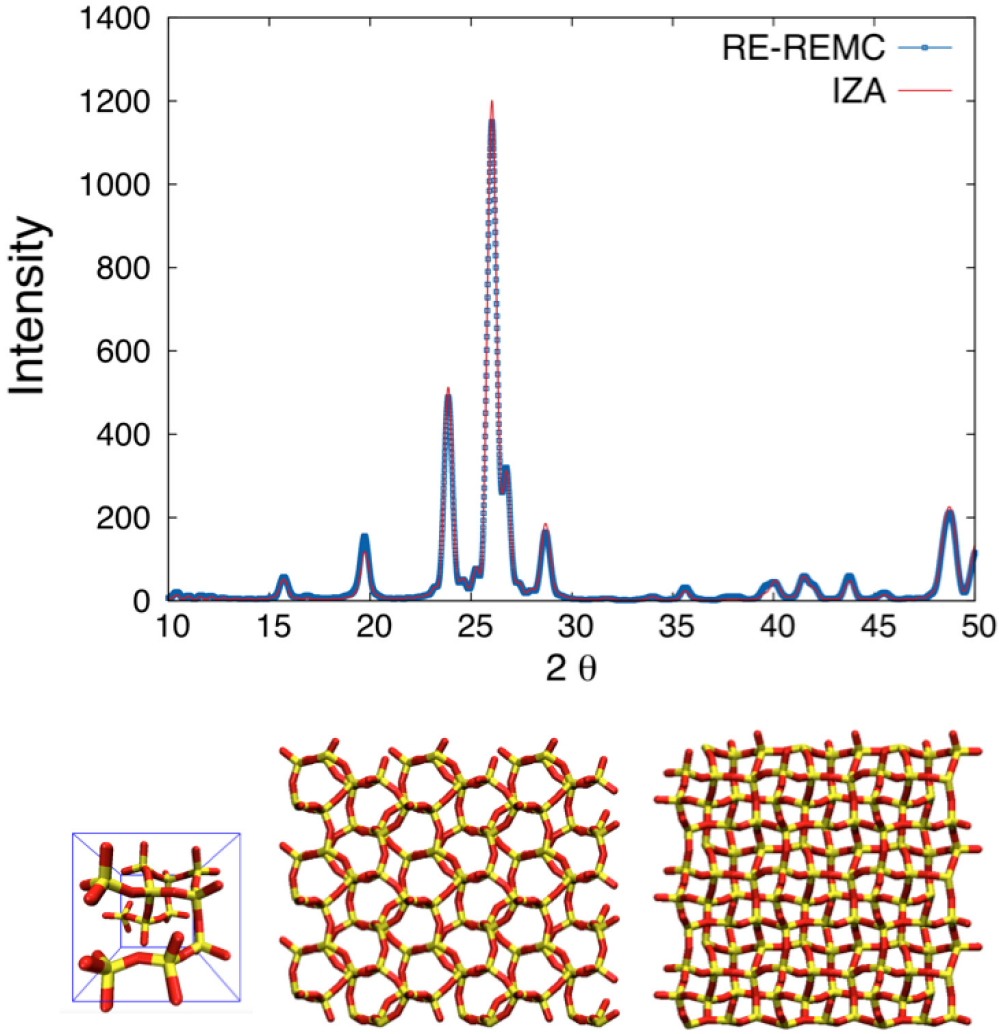

Figure 3.3. Calculated XRD patterns for keatite comparing RE-REMC structures and known coordinates from the IZA Database.

3.3.2 Formation of All-Silica Zeolites Frameworks

Sodalite (SOD) is a porous alumino-silicate material with ultra-small cages and windows accessible only to small molecules such as water. The all-silica version of sodalite was synthesized for the first time several decades ago.[15] We applied RE-REMC to study the ground state structure of all-silica SOD by beginning with an initially random collection of 12 silica tetrahedra in a box with dimensions shown in Table 3.2. A fully condensed crystal with the SOD framework structure was obtained

after 3.3 million RE-REMC steps. The initial and final configurations are shown in Figs. 3.4(a) and 3.4(b), respectively. Small sodalite cages and windows can also be seen in the 3×3×3 periodic extension of the final configuration, shown in Figs. 3.4(c) and 3.4(d).

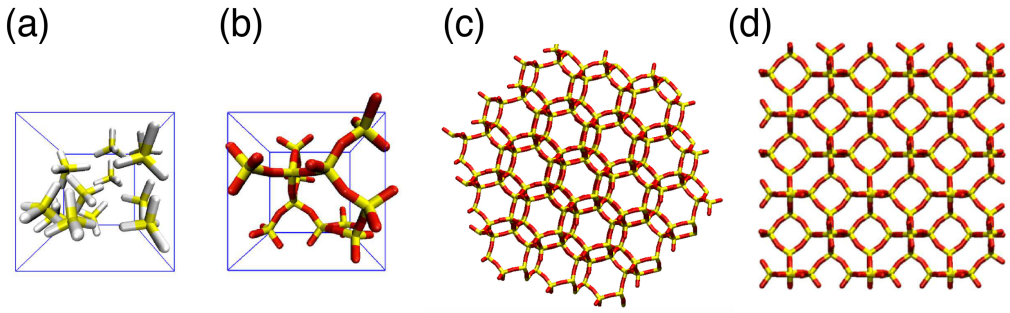

Figure 3.4. Snapshots of (a) initial configuration, (b) final structure, and (c, d) two orthographic views of a 3 × 3 × 3 extension of the final RE-REMC configuration. Color code: Si (yellow), Bridging Oxygen (red), Hydroxyl group (white).

Figure 3.5 shows the calculated XRD pattern of the simulated SOD crystal structure from RE-REMC, for comparison with the XRD pattern computed from the known SOD structure.[8] The striking agreement shown in Figure 3.5 shows the quantitative agreement in crystal structure arising from the RE-REMC simulation.

Next we simulated the ground state structure of an all-silica EDI zeolite – a small-pore zeolite whose tetragonal unit cell consists of five TO_2 (T = Al or Si) units. Despite the fact that, to our knowledge, an all-silica version of EDI zeolite has not yet been synthesized, EDI remains a promising target for our RE-REMC approach because of its relatively small unit cell. The RE-REMC simulation initiated with random configurations in each replica using the corresponding dimensions in Table 3.2, and formed EDI crystals after 3 million RE-REMC steps. The XRD patterns of simulated and known EDI, shown in Figure 3.6, demonstrate again quantitative agreement between known EDI structure and RE-REMC results.

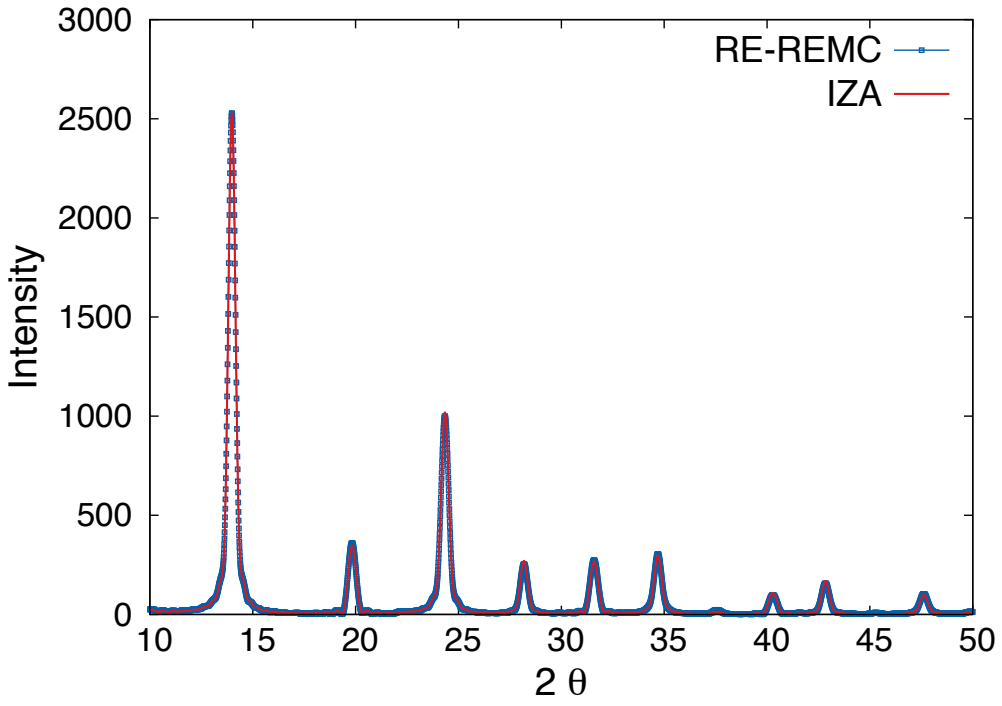

Figure 3.5. Calculated XRD patterns for SOD comparing RE-REMC structures and known coordinates from the IZA Database.

Non-silica based materials may also provide targets for our tetrahedral RE-REMC approach. The open-framework cobalt phosphate material with DFT structure[26] was studied with our RE-REMC approach. Crystals of DFT were obtained in our simulation after 4 million steps, giving rise to the XRD pattern shown in Figure 3.7, again in quantitative agreement with the IZA database. We find it most interesting that a model based on silica tetrahedra can produce crystals of a material composed of cobalt phosphate.

We then simulated ground state structure of the alumino-phosphate (AlPO) with ATT structure using our tetrahedral REMC approach. Fully-connected structures were obtained after 50 million RE-REMC steps in the first two replicas. Interestingly, in the case of the ATT study, these two replicas produced slightly different structures as shown in Figure 3.8.

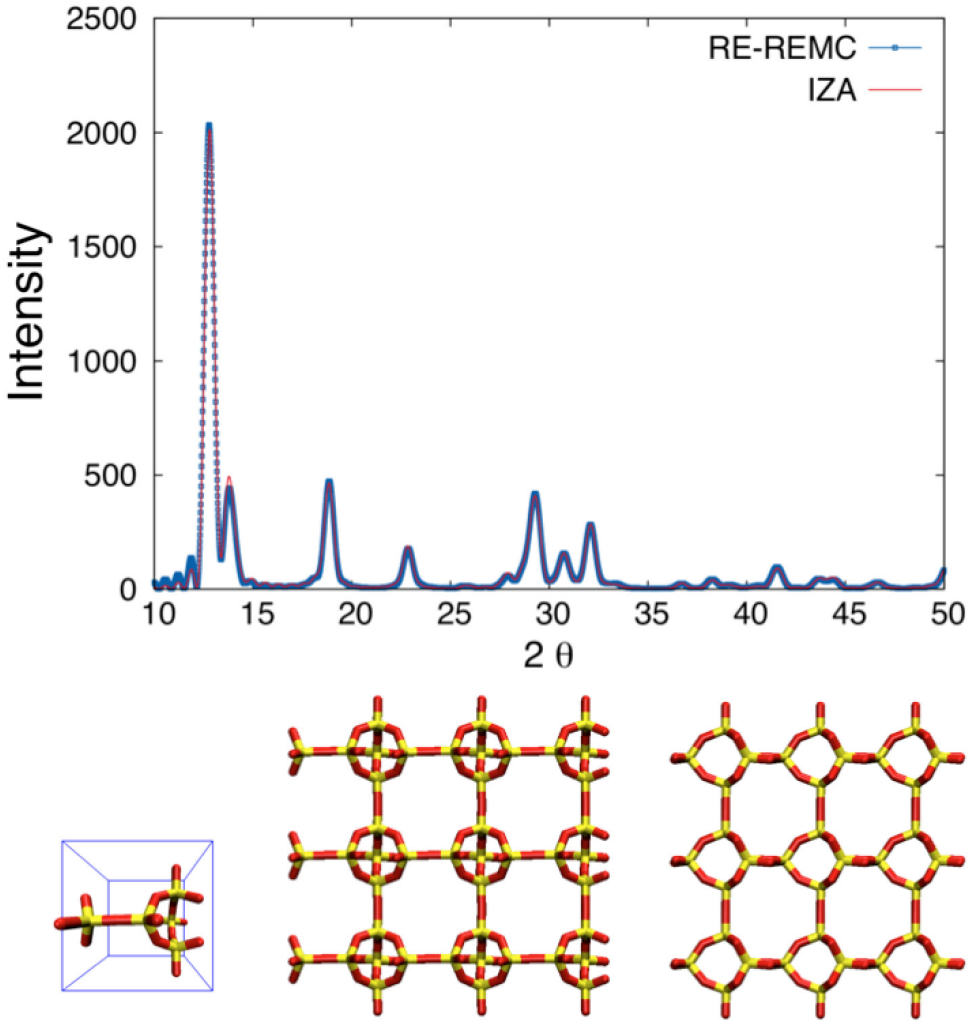

Figure 3.6. Calculated XRD patterns for EDI comparing RE-REMC structures and known coordinates from the IZA Database.

To examine these different crystal structures we computed their XRD patterns, shown in Figs. 3.9(a) and 3.9(b). Figure 3.9(a) shows that the structure obtained from the second replica exhibits the known ATT framework structure, whereas the structure obtained from the first replica does not. This shows how subtle changes in crystal structure manifest clearly in computed XRD patterns. However, Figure 3.9(b) shows that the structure from replica 1 agrees well with the predicted silica-

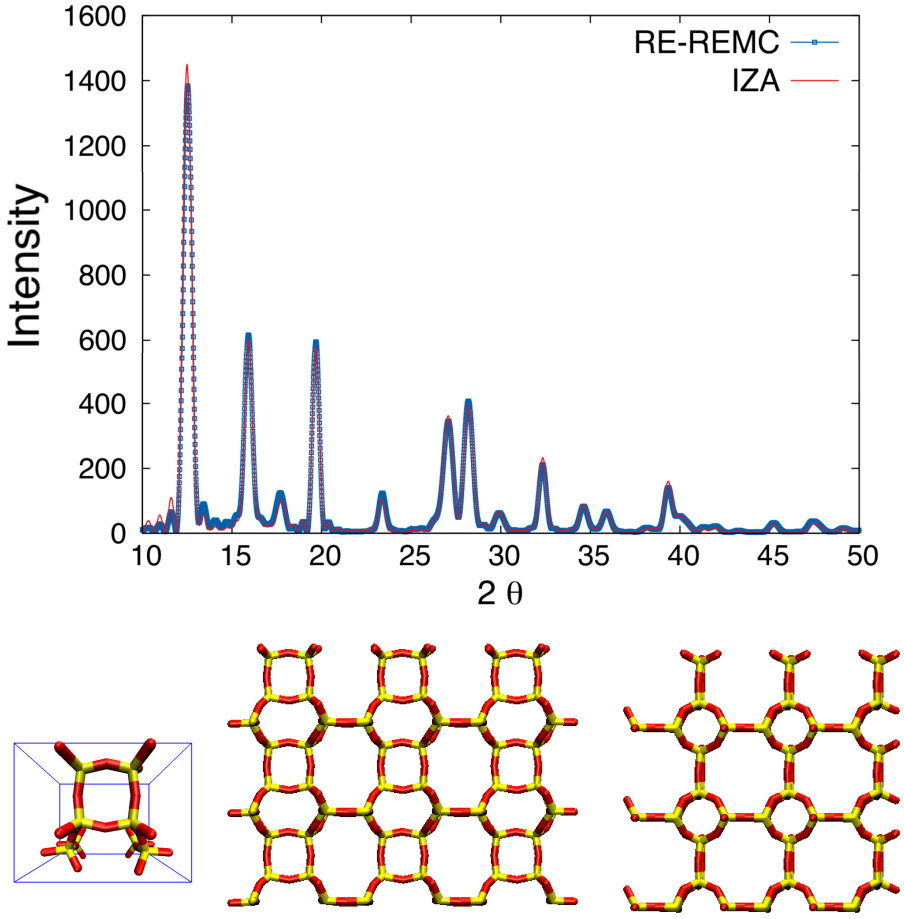

Figure 3.7. Calculated XRD patterns for DFT comparing RE-REMC structures and known coordinates from the IZA Database.

based structure PCOD 3102553 by Le Bail.[86] As shown in Figure 3.9(b), the major XRD peaks of these two structures are well aligned with only small shifts.

Given that RE-REMC approach with a tetrahedral model can successfully simulate an open framework cobalt phosphate, DFT, and an AlPO material, ATT zeolite, it is worthwhile to speculate about why this is the case. The two frameworks involve corner-sharing tetrahedra, in which Al-O bond lengths are in the range 1.70-1.75 Å, while P-O bond lengths are 1.50-1.58 Å.[127, 16, 84] Averaging these ranges yields 1.6 Å, close to the Si-O bond length in our model[4], which explains why this silica

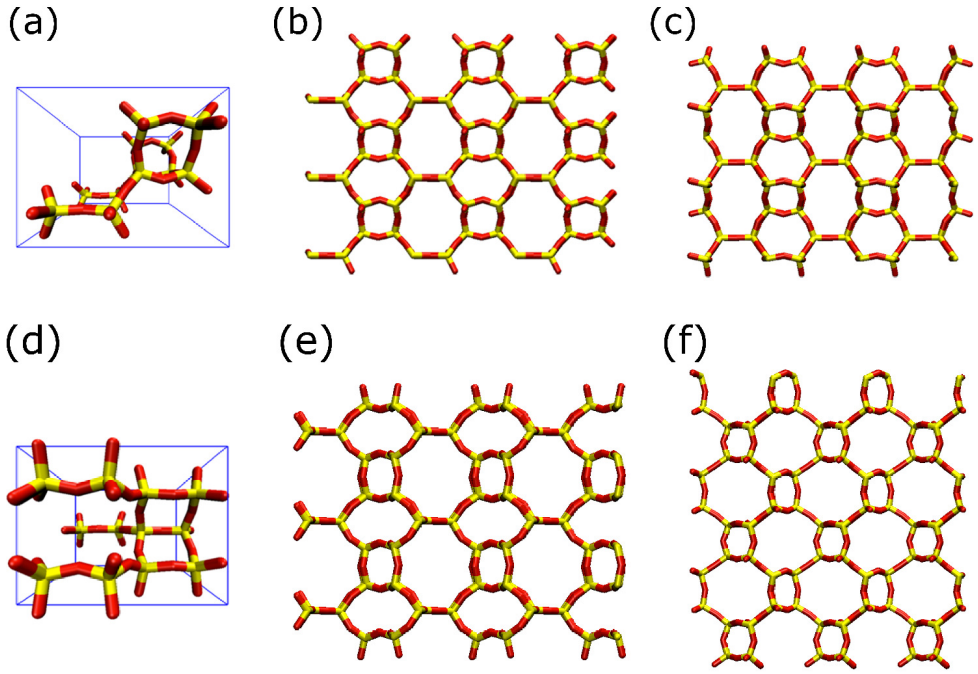

Figure 3.8. Snapshots of (a) final structure, and (b, c) two orthographic views of the final structure with 3 × 3 × 3 extension obtained in RE-REMC *replica 1* with the ATT lattice parameter; (d), (e), (f) same as (a), (b), (c) except from RE-REMC *replica 2*. Color code: Si (yellow), Bridging Oxygen (red).

tetrahedral model also fairly well reproduces XRD patterns for Co-phosphates and AlPOs.

3.4 Conclusions

In summary, we have applied a replica-exchange reaction ensemble MC (RE-REMC) approach to search for ground state structure of several open-framework materials, including all-silica zeolites and related cobalt phosphate and alumino-phosphate materials. Our approach is based on three-dimensional polymerization of semi-rigid tetrahedral units undergoing condensation/hydrolysis chemistry in the reaction ensemble. This reactive model was previously used to model the formation

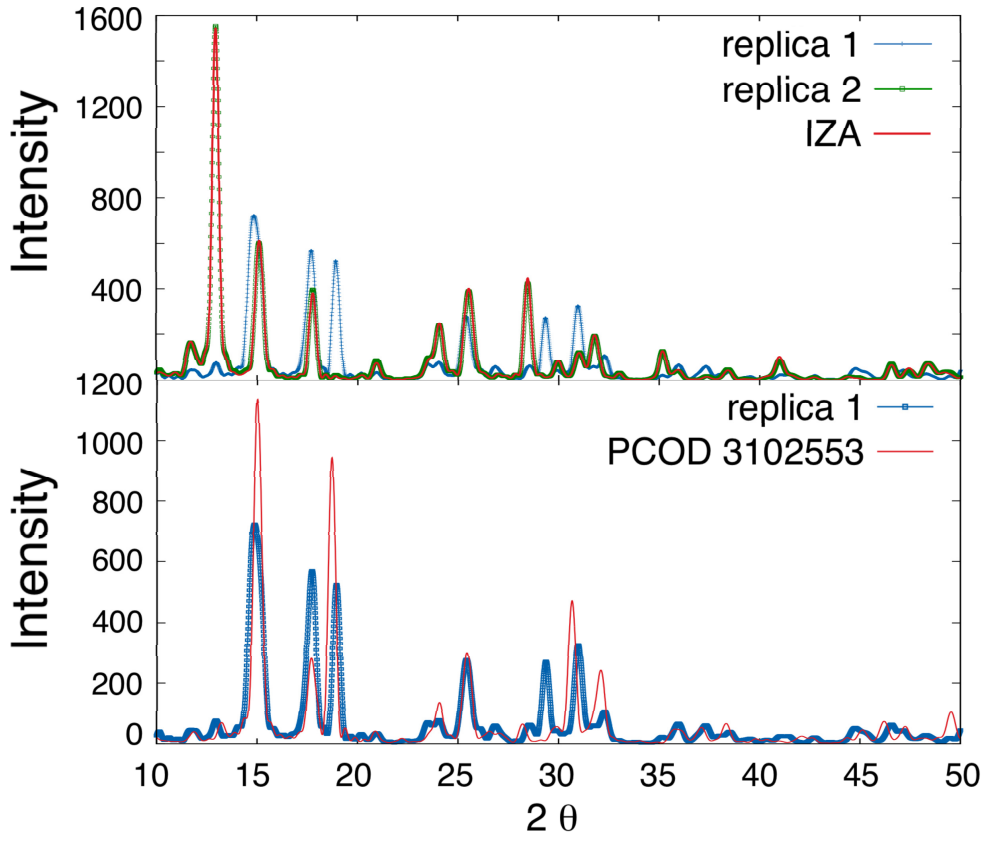

Figure 3.9. Calculated XRD patterns comparing ATT framework obtained from (a) IZA website and RE-REMC *replicas 1* and *2*, and (b) predicted structure from GRINSP 2.00 (Predicted Crystallography Open Database, PCOD 3102553)[86] and obtained from RE-REMC *replica 1*.

of amorphous silica gels and silica nanoparticles, and results shown very good agreement with the experimental observation. With the replica-exchange, this approach has produced crystals of dense silica polymorphs α-cristobalite, β-cristobalite, and keatite, as well as crystals of open-framework materials with SOD, EDI, DFT, and ATT structures, confirmed by computing XRD patterns for comparison with known coordinates. The reactive silica tetrahedron model can provide opportunities to study the crystallization of zeolites in the future. Our modeling approach opens the door to more detailed understanding of the kinetics and mechanisms of zeolite crystallization for both all-silica and non-silica-based open-framework materials.

CHAPTER 4

MOLECULAR DYNAMICS SIMULATION ON MCM-41 MATERIALS FORMATION

In this chapter, we use the MARTINI coarse-grained (CG) model[93, 94, 108] to simulate the phase diagram of a CTAB-H_2O system, and different mesophases including micellar rods, hexagonal, bicontinuous and lamellar phases of CTAB-H_2O system are obtained. The model shows good qualitative agreement with experimental observation in the phase behavior. We observe a phase transition between hexagonal, lamellar, and bicontinuous phases via changing the temperature. To study the silica oligomer-surfactant-water system, we further develop CG parameters for different silicate oligomers by comparing the density profiles in a spherical micelle obtained from AA and CG simulations. A substantial amount of silicate dimers is found to be crucial for generating an ordered hexagonal array due to the double charges on the silicates that may interact strongly with two adjacent micellar rods. We also find that multiple charges on silicate oligomers lead to a phase separation which is consistent to the experiments.[50] Different charges on D4R result in the formation of different mesophases: lamellar phase is observed in the system of D4R with charge of 8^-, whereas D4R with mild charges (4^- and 6^-) results in hexagonal phase, indicating that the D4R existed in solution are most likely remain averaged charges of no more than 6^- in the solutions.

4.1 Introduction

Several studies have been carried out to investigate various aspects of MCM-41 materials, one of most popular periodic mesoporous silicas (PMSs), including

their pore structure, pore properties, structural modification, and the formation mechanisms.[79, 80, 81, 120, 143] In order to tailor these mesoporous materials for specific applications, a full understanding of the formation process is necessary. However, limited knowledge has been gained so far because the synthesis process of PMSs involves complex interplay between different species in different phases (i.e., a multiphase and multi-component silica/surfactant/water system) and chemical reactions. Obtaining detailed understanding of the synthesis pathway by simulations at an atomic level is therefore restricted by this high complexity and large system size of the self-assembly process.

To address such limitations, a coarse-grained model has been applied within molecular dynamics (MD). In particular, we have applied the MARTINI CG approach[93, 94, 95], following previous work on the sphere-to-rod transition, which was created by micelle-micelle fusion processes and silicate was found to be a key to the process.[108] In this work, we extended the previous work for the investigation of the formation of mesoporous materials[108] to study the later stages of the formation in larger time and length scales. The results shown in this chapter enhance our understanding of the formation process of mesoporous materials.

4.2 Simulations Details and Model Description

All MD simulations were carried out with the Gromacs packages[13, 55, 88, 142], and the leapfrog algorithm[56] was adopted to integrate the equations of motion. The temperature was fixed through the velocity-rescaling thermostat[21] while the Berendsen pressure coupling method[21] and the Parrinello-Rahman barostat[106] were used to maintain a pressure of 1 bar in both CG and all-atom (AA) simulations. AA simulations were carried out in this work to validate the parameterization of CG models by comparing the computed density profiles of a spherical micelle obtained from CG and AA models. Periodic boundary conditions with isotropic pressure scaling were

used. Integration time steps of 2 fs and 30 fs were used in AA simulations and CG simulations, respectively.

Unless otherwise stated, all systems were prepared initially by randomly placing all the molecules using the PACKMOL package.[96] The following procedure was applied for all simulations carried out in this study: (1) use the steepest descent algorithm to minimize the total energy of the system to prevent short-range contacts between atoms; (2) perform a short (150 ps) simulation in the NVT ensemble to stabilize the kinetic energy under the chosen condition; and (3) carry out production runs in the NpT ensemble with a total simulation time ranging from a few to tens of microseconds.

The MARTINI 2.2 force field was adopted for CG models with a dielectric constant value of 15.[94] A 1.2 nm cutoff distance was applied in computing both Coulombic and van der Waals interactions with the standard Gromacs shift functions suggested by MARTINI model to mimic the distance-screening phenomena.[94] The shifting of the potential was from 0.9 to 1.2 and 0 to 1.2 nm for van der Waals and Coulomb, respectively. A 10 % fraction of CG water was using antifreeze particles[93] to avoid the freezing of the CG water at a higher temperature than that of real water, which is an unwanted phenomenon of CG model. Therefore anti-freeze particles were introduced to break the freezing process. This antifreeze particle is denoted as BP_4 particle whereas normal CG water is denoted as P_4. Larger σ value and greater potential well, ϵ, of the Lennard-Jones potential interaction between BP_4 and P_4 compared to that of P_4-P_4 were assigned to disturb the lattice generated by the uniform size of solvent particles and to avoid the phase separation of two different solvent particles.[94] The interaction of antifreeze particles to other type particles is the same as that of regular CG water particles.

Different concentrations of cetyltrimethylammonium bromide (CTAB) surfactant together with the silicic acid, $Si(OH)_4$ under high pH conditions ($\sim$ 14) and at rela-

tively low temperatures (from 300 to 430 K) were performed in our simulations. The silica inorganic source holds a full charge on each silica—in fact, at pH of 11, 95 % of silicic acids are deprotonated.[124] Therefore each silica on the dimers, trimers, and tetramers was assigned as a singly charged due to the high pH solution of the studied system. The amphiphilic CTA^+ surfactant is described by four C_1 CG beads for the hydrophobic tail groups with a charged Q_a CG bead for the hydrophilic head group. Each anionic silicate monomer is described by one Q_{SI} CG bead reported by Jorge and co-workers.[108]

In addition to the non-bonded interaction (i.e., Lennard-Jones and Coulombic terms) described above, bonded interactions including bond stretching, angle bending, and torsion are also taken into account. More details regarding the bond length, stretching force, bond angles, and torsion forces values can be found in previous work.[66, 68, 69, 108]

The CG parameters for CTA^+, water, bromide ions, and silicate monomers were taken from the previous work,[108] whereas the CG parameters for dimers were obtained through the comparison of CG and AA simulations carried out in this work. The detailed procedure to acquire the CG parameters can be also found in the previous work[108]: comparing the density profile of a spherical micelle obtained in both AA and CG simulations in the dimer-surfactant-water system. The density profile was measured from the center of mass (COM) of the micelle radially.[57] In the cluster-counting algorithm for the AA model, two surfactant molecules were considered to belong to the same cluster if any of their last four tail carbon atoms were separated within the distance of 0.64 nm[66], corresponding to the first minimum in the radial distribution function between tail carbon atoms. As for CG model, the two surfactants were considered to belong to the same aggregate if the last tail groups (CG bead) were located with a distance shorter than 1.2 nm. The density profiles measured from the center of mass (COM) of the micelle obtained from CG and AA

simulations were compared to parameterize the CG model. In the comparison, the AA parameters for surfactant and silica dimers were taken from the work of Jorge and co-workers,[69] and the standard MARTINI interaction matrix was the initial attempt for CG parameters.

4.3 Results and Discussion

In this section, we discuss the simulation results on the formation and structural characteristics of the surfactant-silicate-water systems in the following manner: Sec. 4.3.1 examines the surfactant-water phase diagram built by our model; Sec. 4.3.2 shows the parameterization of CG model for silicate oligomers; Sec. 4.3.3 discusses the mesophases form from the addition of dimers; Sec. 4.3.4 provides our results on simulating surfactant-silicate oligomer-water systems; Sec. 4.3.5 shows the addition of benzene on changing the mesostructures.

4.3.1 Water-surfactant Phase Diagram

To test the accuracy of the model, we first calculated the phase diagram of the ternary system of CTA^+-Br^--H_2O and compared the obtained phase diagrams with experimental results.

A series of simulations were performed with different surfactant concentrations at temperatures ranging from 300 to 430 K. These simulations were carried out with a total MD time span of more than 10 μs, sufficiently long to ensure that equilibrium conditions have been achieved. Micellar rods, hexagonal and lamellar phases were found as the surfactant concentration increases at a temperature of 390 K. A comparison of the simulation results with the phase diagram obtained from experiments[19] is shown in Figure 4.1. Qualitative agreement between simulations and experimental observation is obtained: different mesophases such as micellar rods, hexagonal structure, and lamellar phase were obtained as a function of the CTAB concentra-

tion. Surprisingly, the bicontinuous phase which is regarded as unstable and hard to observe was also found at the CTAB concentration of 65 wt%.[89]

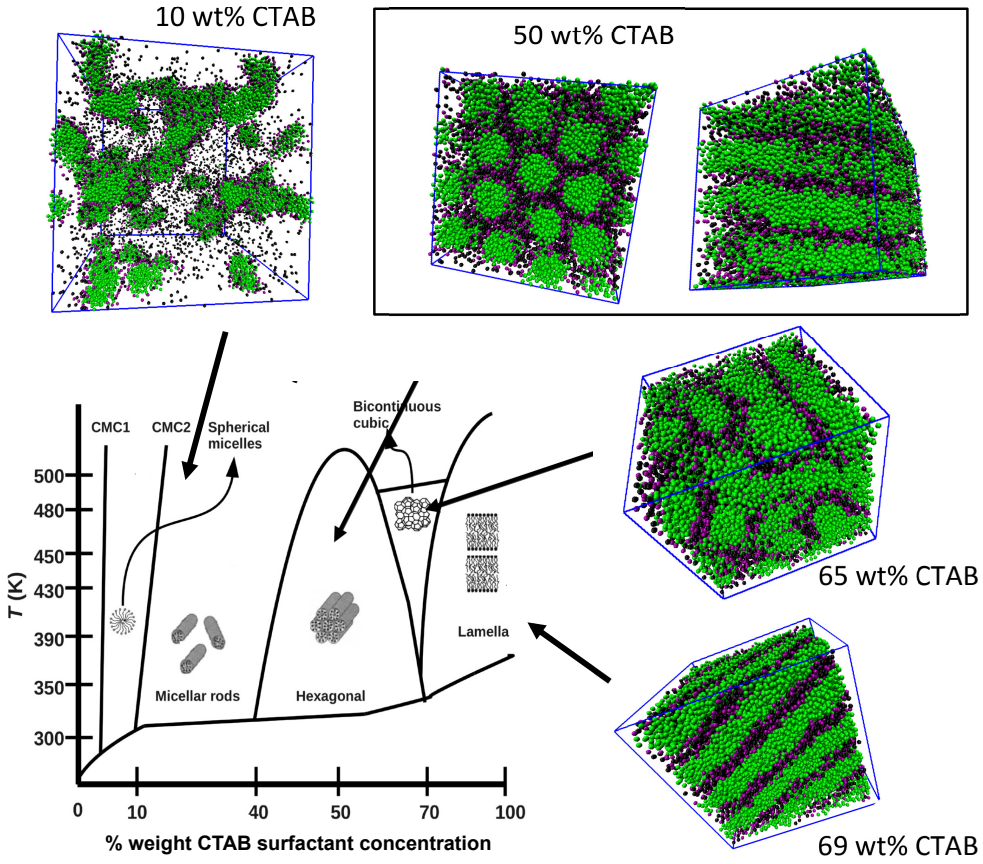

Figure 4.1. Computed graphic visualizations of phases formed in simulations obtained in this work for the CTA^+-Br^--H_2O system at 390 K. In this figure, the simulation results are directly mapped onto an experimentally determined phase diagram (adapted from Ref [19, 111]). Excellent agreement between simulations and experiments has been achieved. Color code: green for surfactant tail groups; purple for surfactant head groups; black for bromide ions (water molecules have been removed for clarity).

Phase behavior studies at lower temperatures of 300 K and 350 K were also performed. We note that 300 K is in the surfactant crystallization region of the phase diagram, and no liquid crystal phase was found from our simulation. Spherical micelles formed in a low CTAB concentration of ∼10 wt%. Whereas the simulations

at a temperature of 350 K, hexagonal structure and lamellar phase can be obtained after a longer simulation time compared to the same system at 390 K (see Figure 4.2), suggesting that systems equilibrate and reach the equilibrium states faster at a higher temperature.

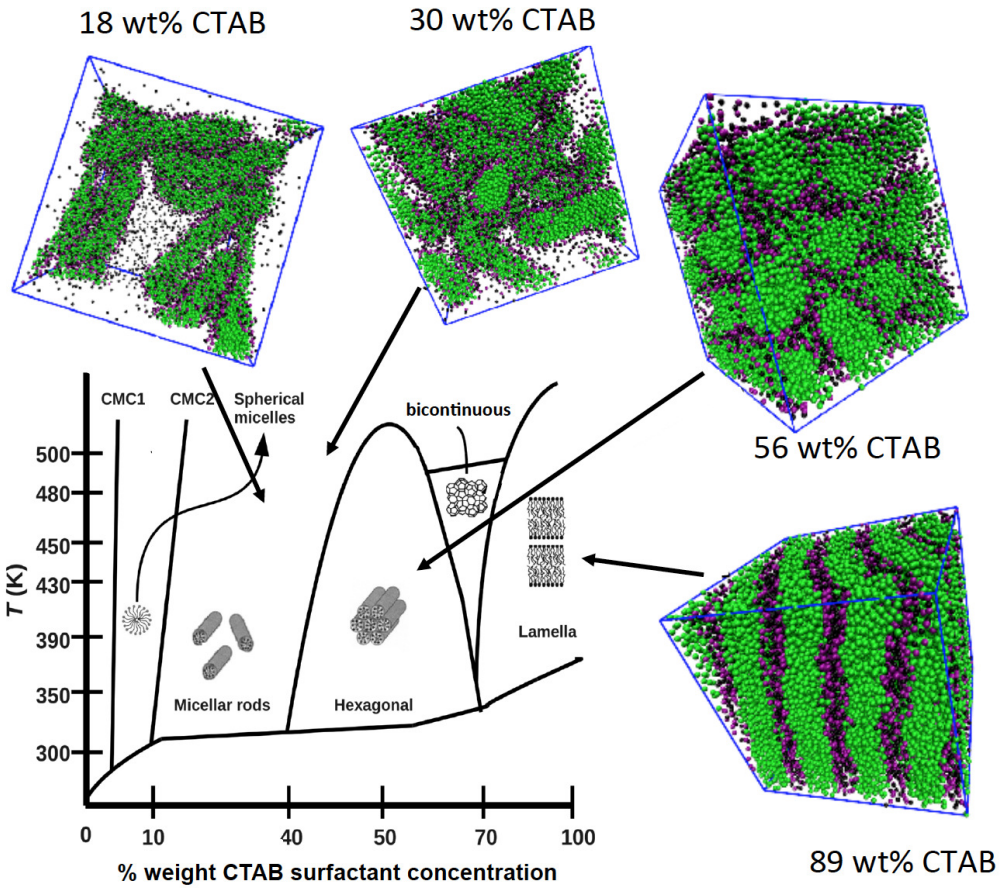

Figure 4.2. Computed graphic visualizations of phases formed in simulations obtained in this work for the CTA^+-Br^--H_2O system at 350 K. In this figure, the simulation results are directly mapped onto an experimentally determined phase diagram (adapted from Ref [19, 111]). Color code: see Figure 4.1.

Furthermore, the phase diagram at a higher temperature (i.e., 430K) was also calculated using the adopted model. As shown in Figure 4.3, a consistency in the phase behavior between simulations and experiments is observed.

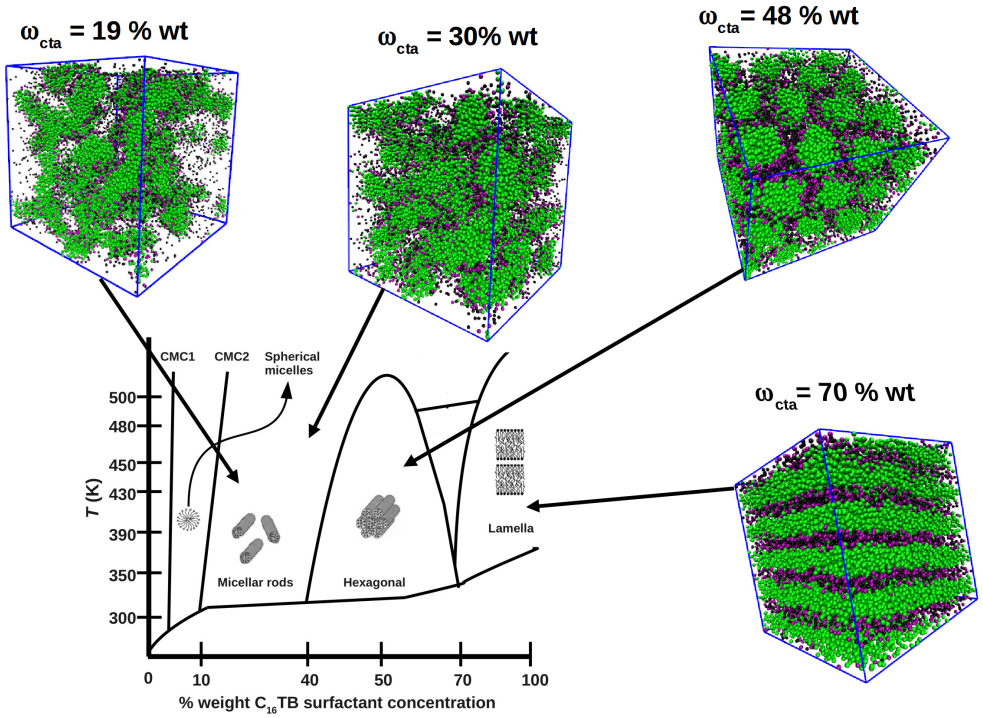

Figure 4.3. Computed graphic visualizations of phases formed in simulations obtained in this work for the CTA^+-Br^--H_2O system at 430 K. In this figure, the simulation results are directly mapped onto an experimentally determined phase diagram (adapted from Ref [19, 111]). Color code: see Figure 4.1.

At this point, it is interesting to investigate the bicontinuous phase obtained from our model. As seen in the phase diagram by Brinker and co-workers,[19] the bicontinuous phase exists between the region of hexagonal structure and lamellar structure at a high temperature. Simulated annealing was performed to investigate the phase transition of bicontinuous structure to the other two phases. Two different initial configurations—hexagonal structure and lamellar structure—were taken from the final configurations in our previous studied simulations that generated hexagonal phase and lamellar phase, respectively: (1) 52 wt% CTAB (hexagonal) using simulated annealing from 390 K to 500 K with a step change of 20 K or 30 K every 0.4 μs; and (2) 67 wt% CTAB (lamellar) with temperature increasing from 450 K to 500 K with a

step change of 10 K every 12 μs. The phase transition arises at around 460 K after 1 μs of simulation time in case of 52 wt% CTAB whereas the phase transition is at 480 K in the case of 67 wt% CTAB after 1.4 μs of simulation time. Figure 4.4 shows how the initial ordered phases gradually yield to a compact porous bicontinuous phase. It is noted that the concentration of the surfactant for forming lamellar phase slightly shifts to the lower concentration, from 70 wt% in experiments to 67 wt% in our model. This coarse-grained model has well captured the essential behavior of the interested CTA^+-Br^--H_2O system.

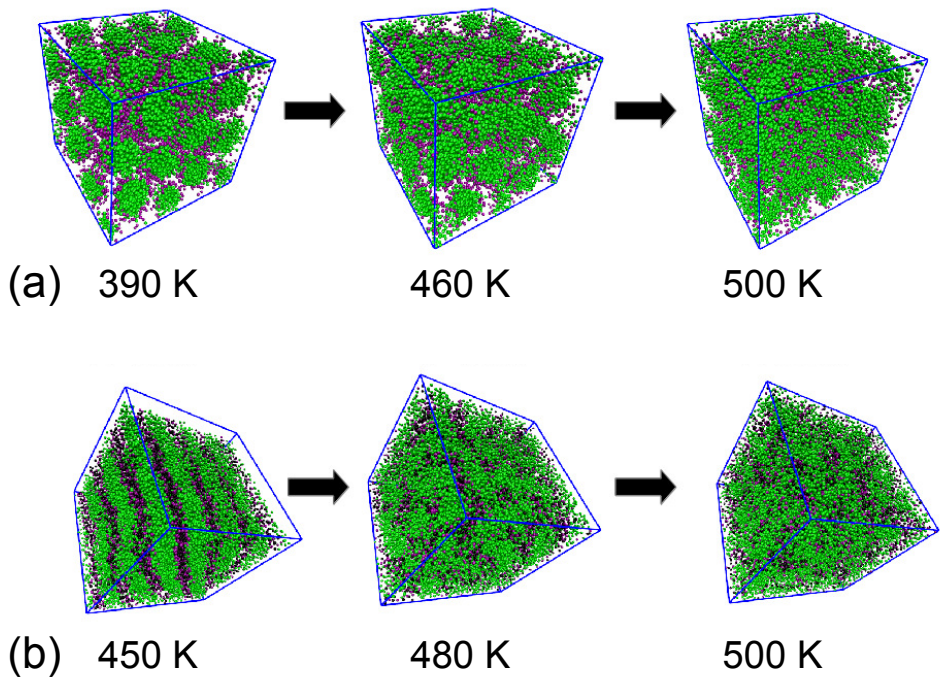

Figure 4.4. Visualizations of system configurations for the phase change from a initial ordered phase to a porous bicontinuous phase with concentrations of CTAB to be (a) 52 wt% and (b) 67 wt%.[19] Color code: see Figure 4.1.

The above results indicate that this CG MARTINI model can capture essential behavior of the CTA^+-Br^--H_2O system in forming different liquid-crystal structures. The reliability of the model and the CG parameters used our simulations allows us

to further study a more complex system in which the inorganic species, silicates, are considered.

4.3.2 Parameterization of Silicate Oligomers

The CG parameters for silicate dimers were obtained through the comparison of AA and CG density profiles of a preformed spherical micelle in a surfactant-dimer-water system. A detailed process can be found in the previous work.[108] As a Q_{SI} particle for each silica monomer (i.e., silicate-tail interaction of 3.5 kJ/mol and the silicate-solvent interaction of 4.5 kJ/mol) was reported previously to yield good agreement in density profiles between AA and CG simulations,[108] we first used two Q_{SI} particles to represent a silica dimer in the CG simulations. In both AA and CG simulations, a spherical micelle was obtained after 20 ns of simulation time, which is sufficiently long to generate a dimer-surrounded micelle. The Hoshen-Kopelman cluster counting algorithm[57] was used to identify the micellar clusters in the system. The density profiles of a micelle for revealing dimers distribution at micelle surface from the two models was then obtained. The density profiles, as shown in the upper part of Figure 4.5, indicate that the peak of the CG Q_{SI} silicate dimer ranges between surfactant head groups and surfactant tail groups. However, AA simulation shows that the silica dimers preferably located outside the micelle.

Charged Q_{da} CG particles included in the MARTINI force field were then considered to represent dimers. The subscript of Q_{da} type, da, stands for donor-acceptor hydrogen-bond character[93, 94, 108]. The ionized silicate dimer was represented by two Q_{da} CG particles. This CG parameter has silicate-tail interaction of 2.0 kJ/mol and the silicate-water interaction of 5.6 kJ/mol. The silicate-tail interaction is weaker than that of Q_{SI} particles, whereas silicate-head interaction is stronger than that of Q_{SI} particles. Interestingly we found very good agreement between AA and CG simulations by using two Q_{da} particles for a dimer. The lower part of Figure 4.5 shows

the comparison between AA simulation and CG simulation with Q_{da} particles. It is evident that the use of two Q_{da} particles[93, 94] for dimers well capture the behavior predicted using the AA simulation, and the Q_{da} type was therefore chosen for representing silicate dimers.

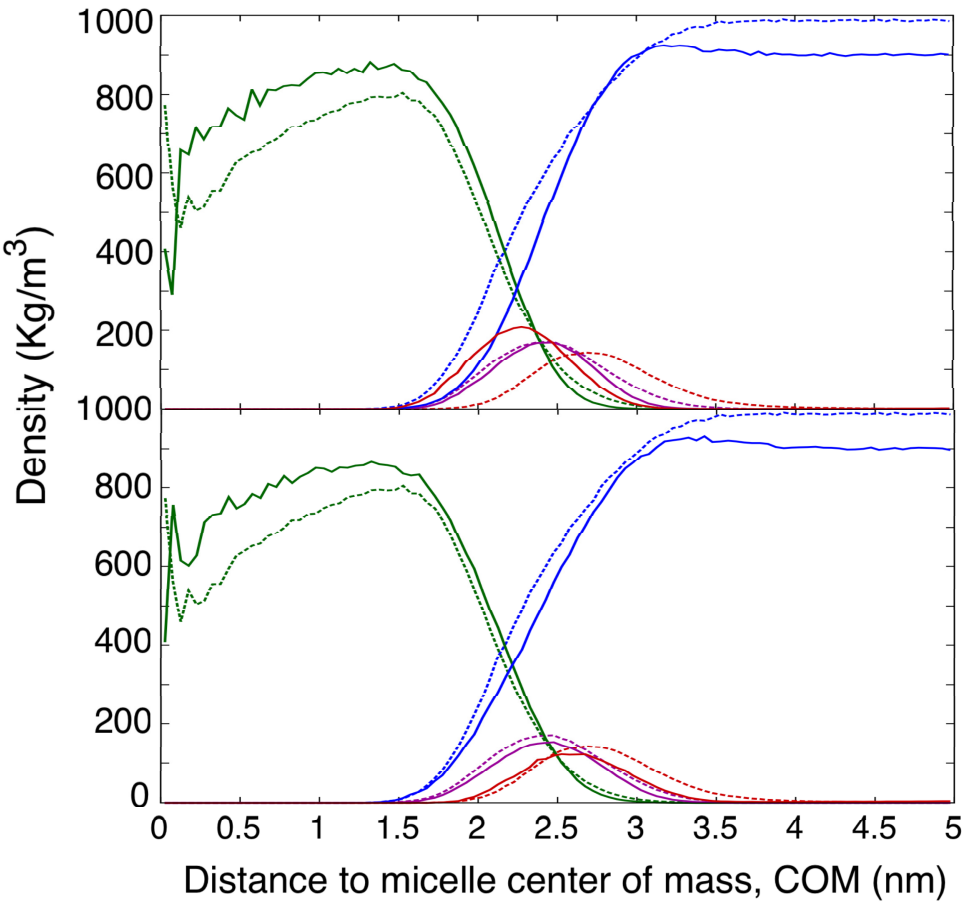

Figure 4.5. Density profiles of a spherical micelle for silica dimers obtained from AA (dashed lines) and CG simulations (solid lines) using Q_{SI} (top) and Q_{da} (bottom) particles. Tail atoms are shown in green, head atoms in purple, water in blue, and silicates in red.

Similar procedures were followed to obtain CG parameters for different oligomers, cyclic trimers (charge of 3^-), cyclic tetramers (charge of 4^-), and double-four-ring species (D4R, with charges of 4^-, 6^-, or 8^-). In the case of cyclic molecules, the use

of prefixed S beads is suggested by Marrink *et al.*[93, 94] Figure 4.6 shows the density profile of a micelle with cyclic trimers, and consistent behavior can be found while using SQ_{da} CG particles for cyclic trimers. Both AA and CG simulations show that the peak of trimers locates outside the micelle. Beside cyclic trimer, SQ_{da} particles for the aforementioned silicate oligomers were also found to yield good agreement between AA and CG results, and they were therefore chosen to represent the cyclic silica oligomers.

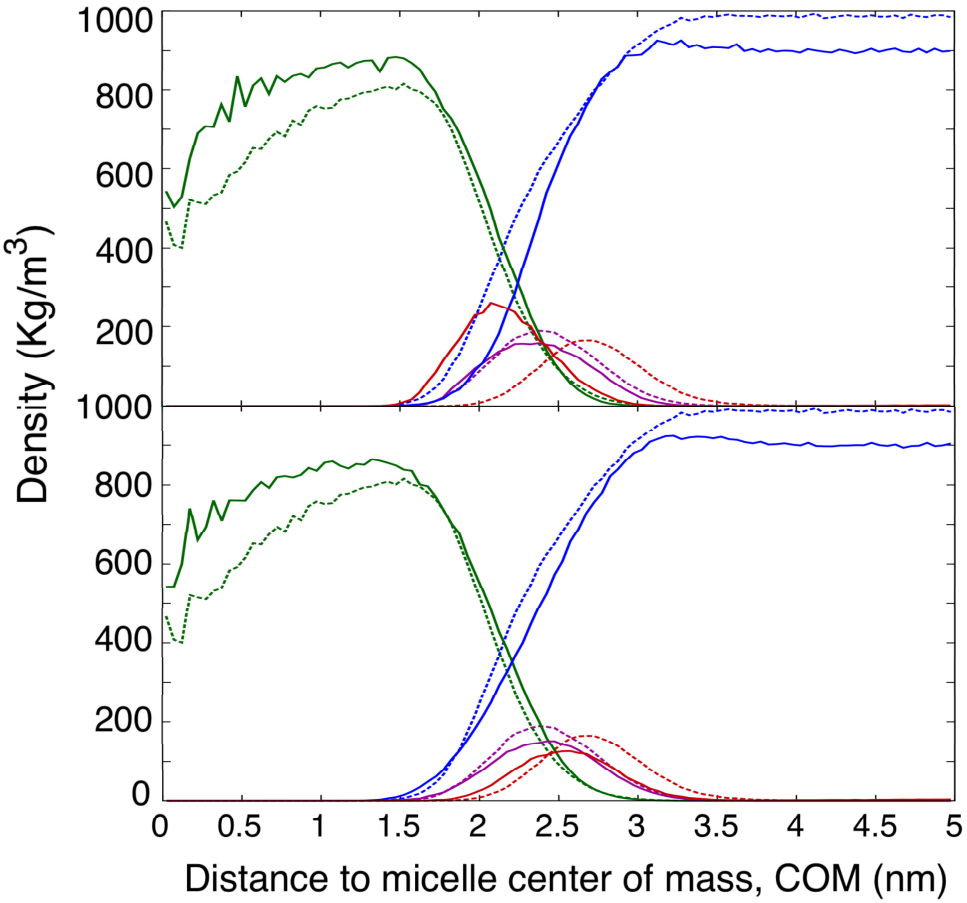

Figure 4.6. Density profiles of a spherical micelle for cyclic trimers obtained from AA (dashed lines) and CG simulations (solid lines) using Q_{SI} (top) and SQ_{da} (bottom) particles. Color code: see Figure 4.5.

4.3.3 Surfactant-Silicate Dimers-Water System

With the validated potential parameters, the CTA^+-silicate dimer-H_2O system was studied. A phase separation was found from the studied system with silica dimers represented by Q_{da} particles. Figure 4.7 shows the visualization of phase behavior as a function of the CTA^+ concentration. The hexagonal array formation in dimers system differs from the hexagonal array formation in the CTA^+-Br^--water system; in the latter case the hexagonal structures fills the entire box.

The latter system is recognized as in the weak-screening limit, where the electrostatic repulsion predominates the system and results in one single lyotropic liquid crystals (LLC) hexagonal phase that fill the entire system box.[50] Interestingly a phase separation was found in the CTA^+-silicate dimers-water system. The phase diagram shows the hexagonal phase forms at the surfactant concentrations ranging form 20 wt% to 47 wt%. The double charges on silicate dimers drive the formation of the phase separation and result in a locally high density of surfactants and silicates for generating hexagonal array structures.

The obtained hexagonal array is the featured structure of MCM-41 materials. The radius of the rod is about 37 Å, consistent to the experimental findings on MCM-41 pores using CTAB as a SDA.[12, 78] The wall thickness obtained from this work ranges from 5 Å to 10 Å.

Inspired by the work of Chmelka and co-workers[50], in which the authors studied a very low surfactant concentration system of different silicate oligomers and discovered a phase separation of species in solutions driven by multiple charges on silicates and surfactant head species, we have also performed simulations under such a low concentration system. Figure 4.8(a) shows the visualization of phase separation found in the CTA^+-dimers-water system with concentration of CTA^+ to be only about 6 wt%. In such a low concentration, phase separation was still observed. A reversible transition was found with the exchange of silicate monomers and silicate dimers. In

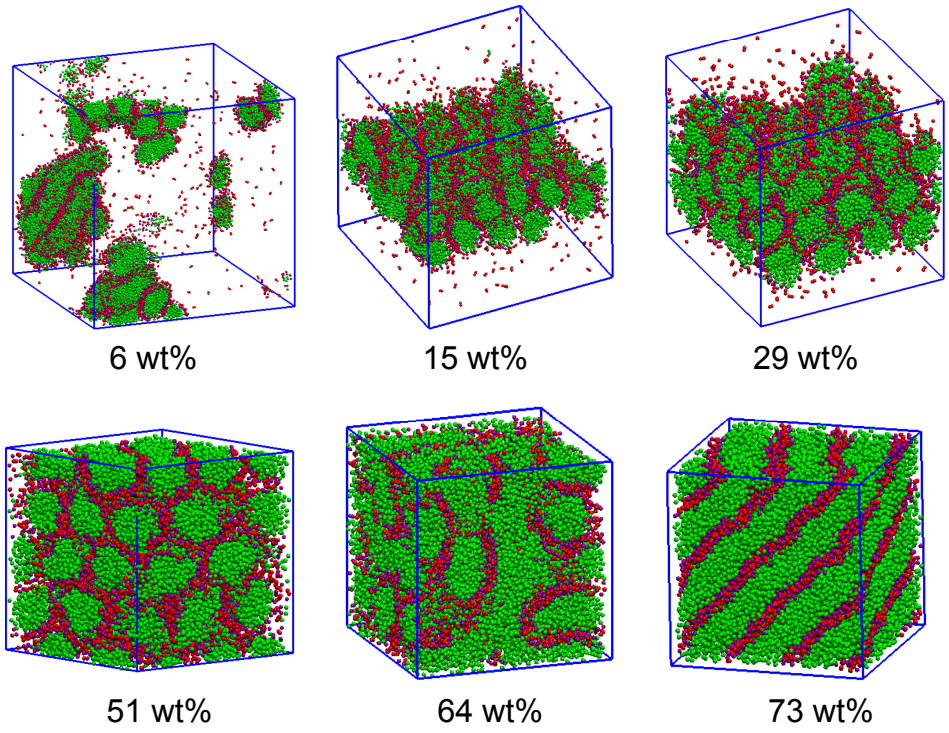

Figure 4.7. Simulations results obtained in this work for the CTA^+-silicate dimer-H_2O system with different concentrations at 390 K. Color code: green for surfactant tail groups; purple for surfactant head groups; red for anionic silicate dimers (water molecules have been removed for clarity).

our simulations, no hexagonal structure was found in the surfactant-silica monomer-water system (see Figure 4.8(b)).

To study the different behavior between silicate monomers and silicate dimers, two simulations were performed. The first simulation started with a previous simulation from 100 % of dimers followed by replacing dimers by monomers. A configuration was taken from a surfactant-silicate monomers-water system, in which the phase separation was observed, followed by replacing dimers with monomers. Same MD procedures were followed: energy minimization steps, NVT, and NpT simulations. A phase transition from close-packed micellar rods to branched rods was observed.

The second simulation on the other hand started with using the final configuration of a silicate monomer system, followed by replacing monomers with dimers. On the contrary, a phase transition from branched rods that filled the entire box to hexagonal aggregates with phase separation was observed. Figure 4.8(a) to Figure 4.8(d) and Figure 4.8(b) to Figure 4.8(e) show the first simulation and the second simulation, respectively.

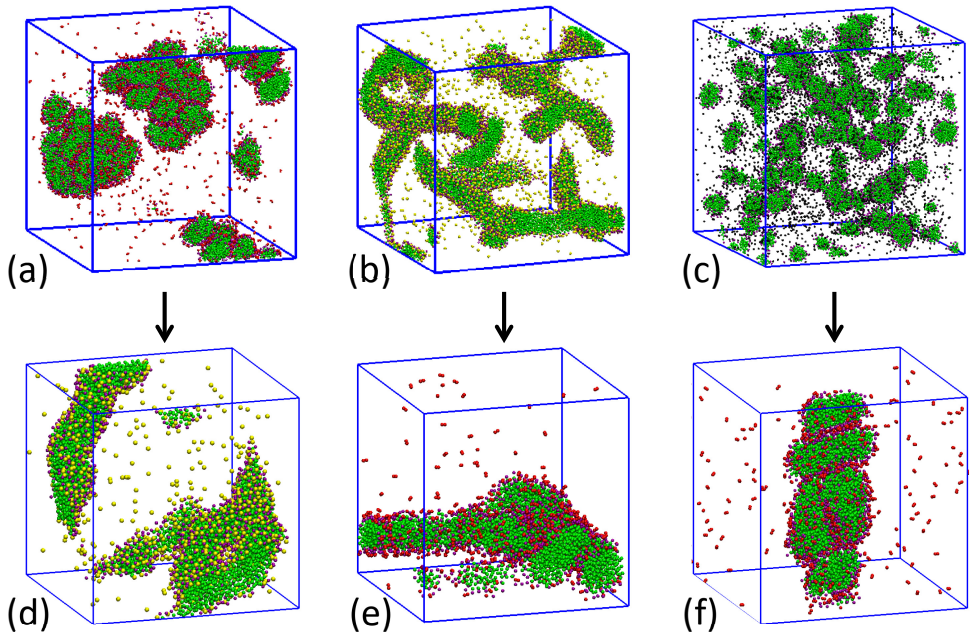

Figure 4.8. Visualizations of phase transition obtained in a low concentration of CTA^+ (6 wt%) by: (a)-(d) replacing dimers by monomers; (b)-(e) replacing monomers by dimers; and (c)-(f) replacing bromide ions by dimers at 300 K. Color code: green for surfactant tail groups; purple for surfactant head groups; yellow for anionic monomers; and red for anionic dimers (water molecules have been removed for clarity).

A simulation of bromide ions replaced by silicate dimers was also performed. Spherical micelles were obtained from a CTA^+-Br^--water system, and the bromide ions were then substituted by silicate dimers. A phase separation and aggregates of surfactants were obtained, and the phase transition can be seen in Figure 4.8 (c) to Figure 4.8(f). All simulations here suggest that the formation of different

mesophases depends on the species in the solution and nearly independent of the initial configurations suggesting that these CG MD simulations are able to represent the thermodynamically stable states of the system under study.

We also note that, to facilitate the formation of mesophases, a rectangular box [63] with an elongated side is a better choice than a cubic box. The rectangular box can largely enhance the likelihood for the formation of ordered hexagonal array along the "non-elongated" direction of the box. In particular, at a low concentration of surfactants, we found that a rectangular box is essential.

To better understand the self-assembly mechanism of MCM-41 materials, it remains of utmost importance to investigate the role of silicate monomers and silicate dimers while the self-assembly process occurs to form MCM-41 materials. To accelerate the simulations, we carried out simulations on studied systems with fewer particles. Each simulation contains 1,000 CTA^+ and 13,000 CG water particles, yielding the concentration of CTAB in water-surfactant system to be about 26 wt%. It was noted that branched rods form in the system of silicate monomers whereas in the system of dimers, a hexagonal array forms. This may result from the double charges on each silicate dimer which can interact with adjacent micellar rods, generating close packing rods, and subsequently lead the ordered arrangement of the micellar rods. In addition, silicate dimers were found to preferably locate at the micelles surface and therefore can pull the micellar rods together.

Figure 4.9(a) shows the mesostructure obtained from a system of $\sim$26 wt% of CTA^+ with the silicate contribution of 40% monomers and 60% dimers at 300 K, hexagonal structure was observed. Compared to the system with all monomers and dimers in Figure 4.9(b) and Figure 4.9(c), respectively, no similar structure like branched rod was found in the system. The simulations have shown that once the number of dimers reaches the critical fraction of the contribution of silica source, the branched rods created by monomers was not observed.

To explore how mesostructures form while the silica polymerization proceeds, we further performed a series of simulations with different molar ratios of monomer to dimer. Figure 4.9(d) shows the silica contribution with fewer dimers. Equal silicate contribution of monomers and dimers are found to be a critical ratio for hexagonal array formation. A phase separation with partially ordered micellar rod array is shown in Figure 4.9(d). Minimum 60 % of silicate contribution from dimers is needed to generate hexagonal structures. (The silicate source consists of 400 monomers and 300 dimers.) The results have shown that during the MCM-41 formation, silicate polymerization for generating oligomers is a key step to the formation of mesostructures. A substantial amount of silicate dimers is necessary. As the ratio of dimer to monomer increases, the hexagonal array gradually forms due to the sufficient amount of dimers can help pull micellar together.

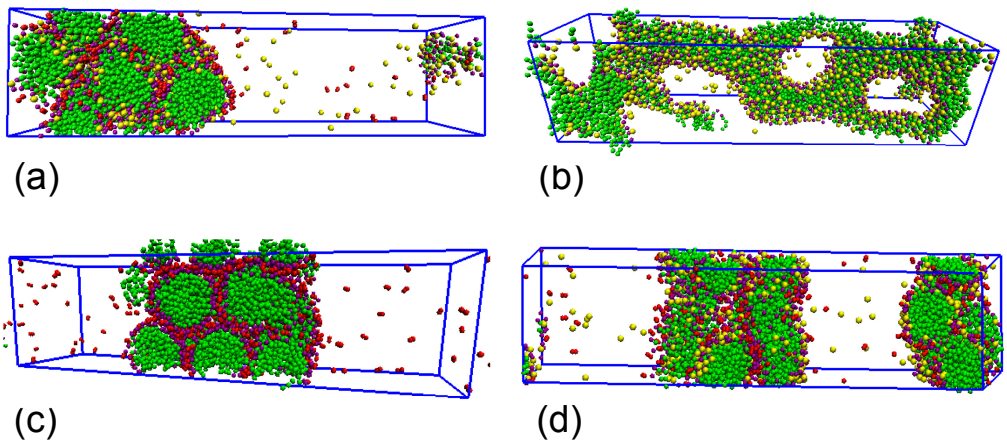

Figure 4.9. Visualizations of simulations at a CTA^+ concentration of 26 wt% in (a) 40% monomers/ 60% dimers of silicates contribution (400 monomers and 300 dimers); (b) monomers only; (c) dimers only; and (d) 50% monomers/ 50% dimers of silicate contribution (500 monomers and 250 dimers). Color code: see Figure 4.8.

We have further investigated the mesostructure obtained from a system consists of monomers and dimers. In a system of silicate contribution of 50% monomers and 50% dimers (i.e., positive charges were contributed equally from monomer and dimers), a

Silicates	Number of silicate	Number of CTA^+
dimer	500	1,000
trimer	333	999
tetramer	250	1,000
D4R	125	1,000

Table 4.1. The number of silica oligomers and surfactants used in simulations corresponding to Figure 4.11.

hexagonal structure with ordered arrangement was not found. In this case, Figure 4.10 (a) and (b) show side/front views of the micellar rods obtained from the simulation. It can be seen from the picture that silicate monomers are mostly located between the alkyl chain and surfactant head groups, whereas the silicate dimers preferably locate at the surface of micellar rods.

4.3.4 Water-CTA^+-Silicate Oligomers System

We have also studied different silicate oligomers system. The total number of silica in silicate oligomers was keeping constant to explore the effect of the degree of condensation of the formation of mesostructures in different studied systems. Table 4.1 summarizes the number of silicates oligomers and surfactants in the studied simulations. Figure 4.11 shows the visualizations of mesophases obtained from different oligomers with the almost the same number of water and CTA^+ in a rectangular box (13,000 CG water and 1,000 surfactants). At least 6 μs simulation time was performed in all simulations to ensure properly equilibrated mesostructures were achieved. Visualizations show that the hexagonal arrays can be found in the systems of silicate dimers, cyclic trimers, and cyclic tetramers. Interestingly, the hexagonal structure formed in the silicate oligomers system is flattened. The rod shape is found to change with degree of condensation from circular rod to ellipse-shaped rod. On the other hand, a lamellar phase with a phase separation is found in D4R system.

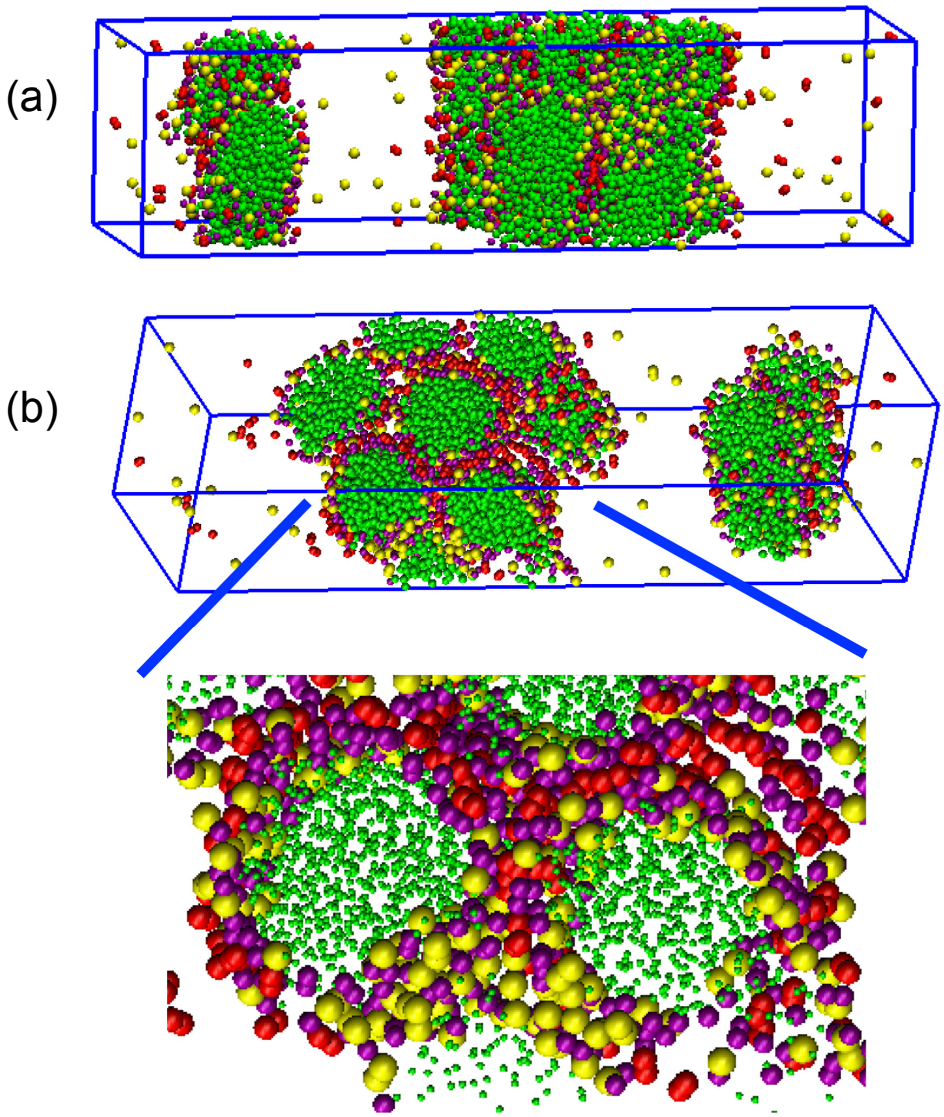

Figure 4.10. (a) Side view and (b) front view of distribution of monomers and dimers on micellar rod obtained from a system with 50 % monomers and 50% dimers of charge distribution in silicate source (the system consists of 500 monomers and 250 dimers). Color code: Yellow for monomers; red for dimers; purple for surfactant head groups; and green for surfactant tail groups.

Previous study on surfactant-silica monomer-water system has shown that the silicate monomer promotes the fusion of micelles to micellar rods.[108]. We have used the model to study the phase behavior the surfactant-silicate monomer-water system

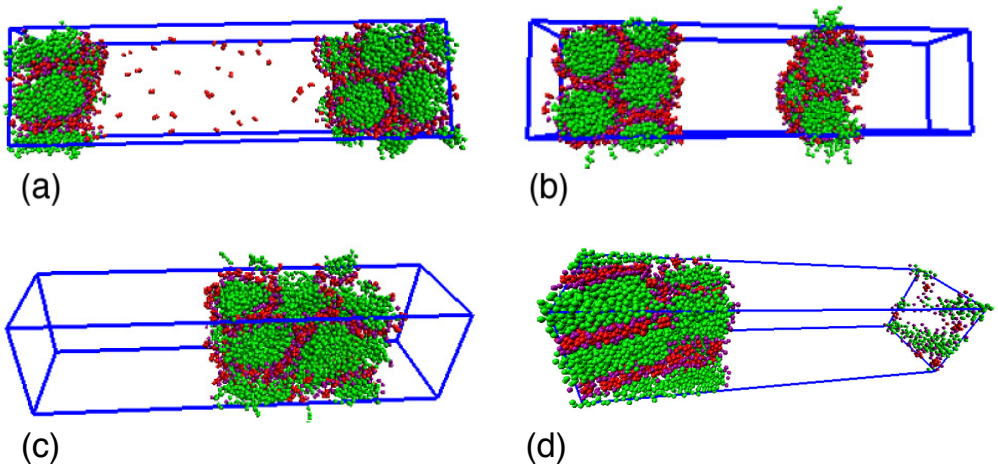

Figure 4.11. Visualizations of simulation results obtained in this work for the CTA^+-H_2O-silicate (a) dimers, (b) cyclic trimers, (c) cyclic tetramers, and (d) D4R systems at 300 K in rectangular boxes. Color code: green for surfactant tail groups; purple for surfactant head groups; red for silicate oligomers (water molecules have been removed for clarity).

and found that no hexagonal arrays form as changing the surfactant concentration. However, from the study of silicate oligomers, a hexagonal array was found. The oligomers contain higher charges shown hexagonal phase at a surfactant concentration of $\sim$ 26 wt%. Based on the results obtained from our simulations, the branch rods form in the monomer system whereas the hexagonal array forms in the dimer system. The results indicate that multiple charges on the silicate oligomers may result in hexagonal and lamellar phases. The electrostatic attraction between counterions (negatively charged silicate and surfactant head group) with the shorter distances of charges on silicate oligomers is the key to the formation of a hexagonal array. The high charge density of silicate oligomers might play an important role in facilitating the assembly of micellar rods to form an array with ordered arrangement.

Our simulation results show that D4R silicates with charge of 8^- in at surfactant concentration of about 26 wt% form lamellar phase. Simulations with D4R silicate of

charges of 6^- and 4^- were also performed. From the simulations, we found that in the systems of D4R silicates with 6^- and 4^-, a hexagonal phase can be observed. A phase separation was also found with a silica-surfactant-rich region and a solvent-rich region. All the obtained mesophases were found in the silica-surfactant-rich region. Compared to the experimental results reported by Chmelka and co-workers[50], in which the authors shown that the hexagonal array can be obtained in the system of surfactant-D4R-water at a low surfactant concentration of ~ 6 wt%. A phase separation was also observed. The experimental condition was fixed at pH of 13, sufficiently high enough to form multiple charges on silicate D4R. The authors estimated a maximum charge of 6^- on each D4R. Our simulation shows a good agreement with the experimental observations. The D4R is likely possess charges of 6^- or even 4^-.

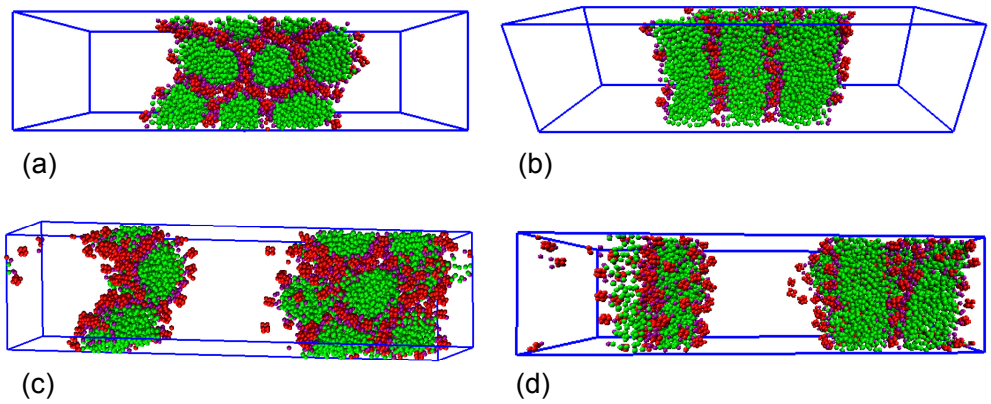

Figure 4.12. Font and side view of the final configuration obtained from the system of CTAB + H_2O + D4R with charge of (a) and (b) 6^-, and (c) and (d) 4^-. Color code: green for surfactant tail atoms; purple for surfactant heads; red for silicate oligomers (water molecules have been removed for clarity).

4.3.5 Addition of Benzene

Furthermore, Chmelka and co-workers have studied the effect of co-solutes in the mesophase, and they found that the addition of trimethylbenzene results in hexagonal array-lamellar phase transition.[50] A CG benzene molecule is represented as three

SC_4 particles, and no charge is assigned on any of them (see Figure 4.13).[94] This SC_4 particle, C stands for apolar molecules and the prefix S denotes a class of CG model for rings. A similar result is found in our simulations that add/remove of benzene results in a reversible phase transition (see Figure 4.14). Our simulations started with a hexagonal phase obtained from the final configuration of CTA^+-silicate dimers-water system with the addition benzene with a benzene to silicate ratio of 0.75. Simulations show the transformation of hexagonal arrays to lamellar phase after few nanoseconds. Most benzene molecules penetrate into micellar rods and gradually result in a phase transition. The incorporation between benzene and surfactants as well as the penetration of benzene to micelles may result in phase transition and the change of the packing parameter of the surfactants.

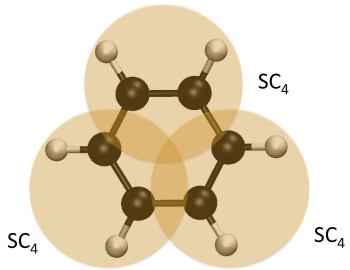

Figure 4.13. Schematic diagrams of the coarse-graining model employed for a benzene molecule: a benzene is represented by three SC_4 particles.

It is instructive to investigate whether if this planar benzene molecule has a preferential orientation that results in the phase transition. Therefore, an order parameter was proposed to investigate the orientation of the benzene molecule. The parameter is calculated by averaging the normal vectors of all benzene molecules:

$$order\ parameter = \|\frac{1}{k}\sum_{k}\hat{n}\| \tag{4.1}$$

where $\hat{n}$ is the normal vector of a benzene molecule and k is the total number of benzene molecules. The absolute value of this order parameter locates between 0 and

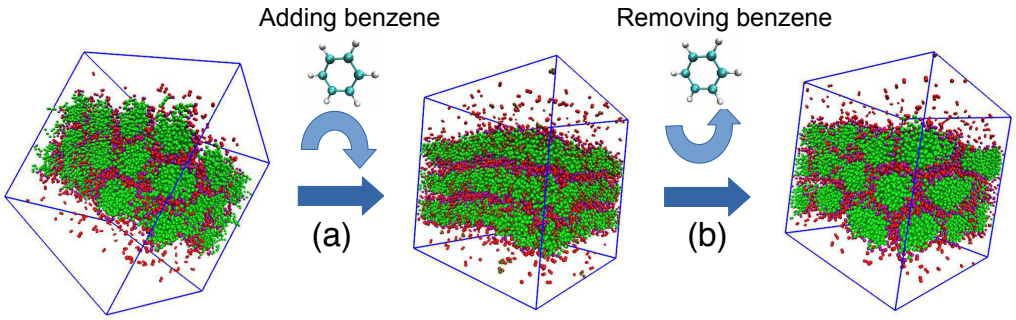

Figure 4.14. Reversible phase transition between hexagonal and lamellar phase with the (a) addition and (b) removal of CG benzene molecules.

1, corresponding to no preferential orientation of benzene to all benzene have united direction, respectively.

The calculated order parameter is about 10^{-2} while the phase transition proceeds from hexagonal phase and lamellar phase, which indicates this phase transition is independent of the planar structure of benzene molecules.

4.4 Conclusions

In the presented chapter, we have shown that MARTINI CG model predicts the phase diagram of CTAB-H_2O system well. Different mesophases such as micellar rods, hexagonal, bicontinuous and lamellar phases of CTAB-H_2O system were obtained. Phase transition between hexagonal, lamellar, and bicontinuous phases can be also obtained via changing the temperature. This model has shown good qualitative agreement with experimental observation in the phase behavior. Thus it makes the study of such large and complicated systems feasible. The development of the simulations is also important to the further study on the formation of mesoporous materials.

In this work, we have developed CG parameters for different silicate oligomers by comparing the density profiles in a spherical micelle obtained from AA and CG

simulations. From the study of different silicate oligomers, we have found that a substantial amount of silicate dimers is crucial for generating the ordered hexagonal arrays due to the double charges on the silicates may interact strongly with two adjacent micellar rods. A phase transition from branched rods to hexagonal phase with a phase separation can be observed as the degree of condensation of silicate increases. From our simulations, multiple charges on silicate oligomers were found to generate a phase separation that was also observed experimentally.[50] Different charges on D4R result in the formation of different mesophases. Lamellar phase is observed in the system of D4R with charge of 8^-, whereas D4R with mild charges (4^- and 6^-) results in hexagonal phase. This observation indicates that the D4R existed in solution are most likely remain averaged charges of no more than 6^- in the solutions.

Our simulations have shown that the CG model can capture the behavior of species in solutions while different mesostructures form. The simulations can be carried out with an assigned number of oligomers and charges, which cannot be directly accessed by experiments. The model can predict the formation of different mesostructures, leading to a powerful tool for tailoring silica mesoporous materials. With a precise control of silicates source in solutions, different materials can be achieved. Our simulations also show evidence that the incorporation of the silica anions and cationic surfactant heads results in different mesostructures, consistent with the cooperative templating mechanism.[51, 59, 60, 101]

CHAPTER 5

STUDYING THE FORMATION OF MCM-41 USING HYBRID MD/MC SIMULATIONS

In this chapter, we propose a hybrid molecular dynamics/Monte Carlo (MD/MC) approach to study the later stages of MCM-41 formation. This hybrid approach can capture the physical interaction among solvents, inorganic, and organic species by MD simulations while the reaction events are also explicitly considered by REMC simulations. The study shows that the silica surfactant ratio of 4 may be essential to form the MCM-41 materials. The preliminary study of this work also reveals several crucial elements that need to be considered to enhance the approach. First, a more consistent CG model in both MD and MC simulations is necessary. Second, the fluctuation between silica and surfactant in MC simulations may generate more realistic MCM-41 structure.

5.1 Introduction

MCM-41 is usually obtained via the synthesis starting from a solution containing alkyltrimethylammonium surfactants $C_nH_{2n+1}(CH_3)_3NBr$ as structure directing agents, together with a tetramethylammonium silicate solution, followed by a calcination.[78] Though this material has been widely studied experimentally, the nature and insights of silica polymerization during the formation of MCM-41, such as the relative roles of silica monomers and small oligomers, vs. larger oligomers and rings formation, remains unclear.

Different simulation approaches were also proposed to study the formation mechanism and atomic structures of MCM-41.[63, 68, 69, 108, 123] As introduced in the

previous chapter, due to the large length- and time-scale of the formation process, it remains a great challenge to computationally describe later stages of MCM-41 formation. Given current computer capabilities, some extent of coarse-graining is thus needed to help better understand the interplay between silica polymerization and mesoscale surfactant assembly and identify the most likely mechanism for cooperative structure formation MCM-41, involving simultaneous fluctuations and structure-formation of both surfactant and silica species in solution.

We continue the previous work described in Chapter 4 on studying the formation of different mesophases using molecular dynamics (MD) simulations. The previous study shows that the multiple charges on silicate oligomers lead the formation of the hexagonal array (MCM-41 structure). The dominant reaction, silica polymerization, however was not investigated. Thus in this work we combine the off-lattice model of silica polymerization and a coarse-grained (CG) model of the surfactant to elucidate the formation mechanism of silica mesoporous materials. In particular, we integrate our silica polymerization model and coarse-grain model of unpolymerized silica built by Jorge *et al.*[108] to study the later stages of silica polymerization. In the proposed approach, molecular dynamics can describe the behavior of surfactants in the solution, and on the other hand, our silica polymerization model with a reaction ensemble Monte Carlo (REMC) approach can sample the silica polymerization.

This chapter will present the preliminary results for the proposed hybrid MD/MC approach. To examine the feasibility of this idea, we start our simulations by generating the MCM-41 structure using MD simulations, followed by a reaction ensemble Monte Carlo simulation (REMC) for the sampling of silica polymerization to simulate the MCM-41 formation.

5.2 Model and Simulation Methodology

Seaton and co-workers[123] have used kinetic Monte Carlo simulations to study the formation of silica mesoporous materials. The silica condensation reaction was sampled on a preformed mesostructure. The ring-size distribution was obtained; however, the cooperativity between silica and the surfactant in determining the mesoscale structure is missing, such as: How does silica polymerize during formation of mesostructure? Does larger silicate oligomers form before the formation of the MCM-41 (hexagonal arrays) structure? Similar to the work of Seaton and co-workers, we prepared a preformed mesostructure from our study of silica-surfactant-water system using a MD simulation, followed by a silica condensation simulated by a REMC simulation. Using the MD simulations together with the MARTINI model can prove a more realistic mesostructure by simulating motions of particles in the solutions compared to generating the structure geometrically. The mesostructure was taken as a template for the following silica condensation. A REMC approach was later performed to take the silica polymerization into account with the aim to obtain a completed MCM-41 structure, leading to a better understanding of the formation mechanism.

The MARTINI 2.2 force field was implemented to represent molecules in the system.[35, 93, 94] The force field has been shown to represent the essential characteristics of several different molecules well. The simulation procedure follows the work of Pérez-Sánchez *et al.*[108] and our previous study on the formation of mesostructures of water-surfactant-silicate systems in Chapter 4.

The CTA^+ molecule is described by five beads with four tail beads corresponding to alkyl groups, and the last bead represents the hydrophilic head groups.[108] A C_1 (nonpolar) type CG particle was chosen to represent the surfactant tail bead, and Q_0 (charged) type particle was chosen for the surfactant head bead. The bromide CG bead is represented by Q_a type which is implicitly solvated by six water molecules. For silica monomer and silica dimer, the CG representations are deter-

mined by a comparison between AA and CG simulation results of the density profile in a preformed micelle with the same size. Each silicate monomer is represented by a single CG bead, Q_{SI} type, and each silicate dimer is represented by two Q_{da} type CG beads. The Lennard-Jones potential is used to describe the interaction between CG beads with different potential well depths, ϵ, and different σ value, the finite distance at which the inter-particle potential is zero. The depths of the potential well for different coarse-grained particles can be found in literature[108] and Chapter 4. In addition to the Lennard-Jones potential, each charged particle (type Q) bears a full charge and interacts via the Coulombic potential with a relative dielectric constant of 15. Figure 5.1 shows the schematic representations of molecules by our CG model.

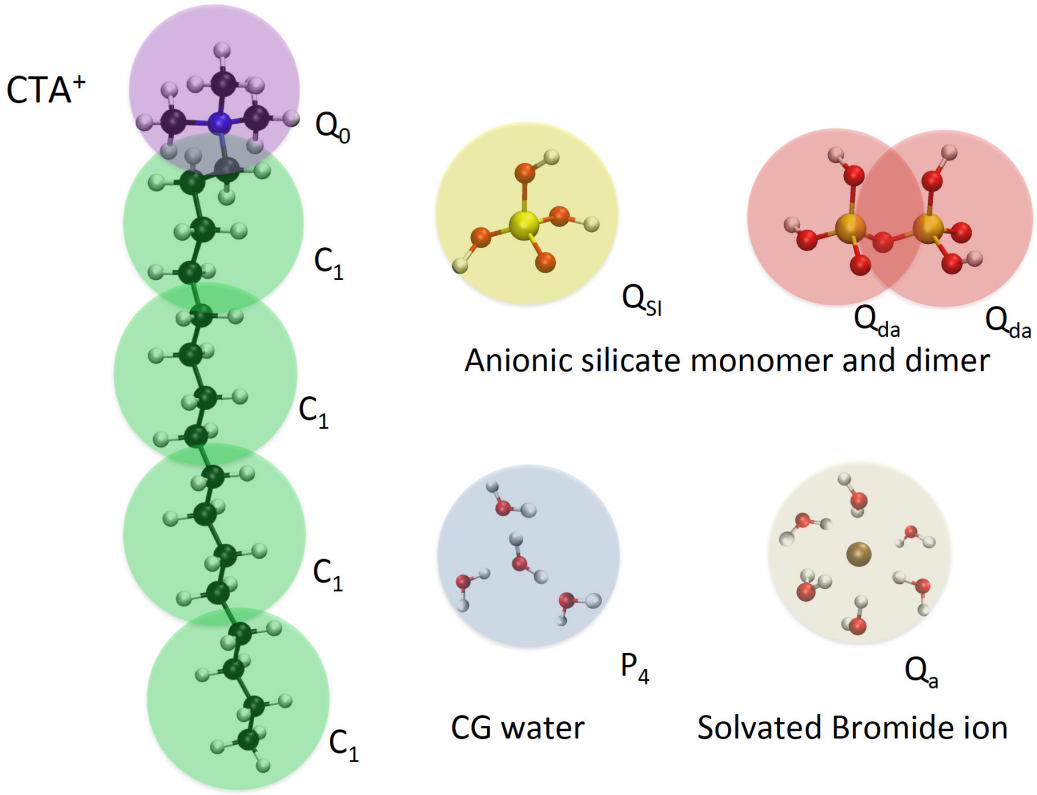

Figure 5.1. Schematic representations of the coarse-graining procedure employed in this work for the CTA^+ surfactant; neutral and anionic silicate monomers; solvated bromide ion (solvated by six water molecules), and water (representing four real water molecules). The labels correspond to MARTINI bead types (except for the new silicate beads).

Simulations for silica polymerization were carried out by an off-lattice REMC simulation, which has been implemented for studying microporous materials as shown in Chapters 2 and 3. In this model, as introduced in Chapter 2, each silica tetrahedron is represented as a hard-sphere core in the center of each tetrahedron with four corners occupied by one of three possible oxygenic species: (*i*) hydroxyl groups (OH) represented as single particles, (*ii*) one oxide atom in the case of anionic silicate, and/or (*iii*) bridging oxygen atoms (BO) for condensed silica.[27, 91, 92] The structure of each flexible tetrahedron is maintained via harmonic springs between the various kind of possible oxygen atoms according to:

$$U_1 = \sum_{i=1}^{3} \sum_{j=i+1}^{4} \frac{k_S}{2}(|r_i - r_j| - r_0)^2, \tag{5.1}$$

where U_1 is the internal potential energy of a tetrahedron, r_i is the position of the i^{th} BO/OH/O^- vertex, k_S is a spring constant, and r_0 is the equilibrium distance between two vertices (i.e., oxygen-oxygen distance). The value of k_S was determined in the previous work to be 851 kJ mol^{-1}Å^{-2},[3] while r_0 is set at 2.61 Å based on the geometry of silica tetrahedra (Si-O bond length = 1.6 Å and O-Si-O angle = 109.47°).[91, 92]

The silica polymerization process is thus viewed as the assembly of $Si(OH)_4$ and $Si(OH)_3O^-$ tetrahedra via condensation reactions. Two tetrahedra are connected via a bridging oxygen (Si-O-Si) after a condensation reaction occurs. We have modeled the Si-O-Si angle formed by the bridging oxygen in our present work using the following harmonic potential:

$$U_2 = \frac{k_A}{2}(\cos\theta - \cos\theta_0)^2, \tag{5.2}$$

where θ is the Si-O-Si angle formed by the bridging oxygen, θ_0 is a reference angle, and k_A is an angular force constant. The value of 155° was used for the reference Si-O-Si angle, and the value 226.74 kJ mol^{-1} was used for k_A. Those values were

determined by optimizing infinite silica chains using periodic DFT calculations,[3] and were found to reproduce bulk moduli of silica polymorphs.[4] We note that the value of the reference angle falls roughly midway in the range of commonly observed Si-O-Si angles in silica materials (i.e., 130-180°).[44, 70]

All MD simulations are carried out with Gromacs 4.6.1 package[13, 55, 88, 142] with the leapfrog algorithm[56] for integration of equations of motions. The temperature is fixed at 300 K and controlled by an Berendsen thermostat, and the pressure is fixed at 1 atm by an Berendsen barostat[13]. The Coulomb potential is shifted smoothly to zero between 0 and 12 Å, and van der Waals interaction is shifted to zero between 0.9 and 1.2 nm to achieve high simulation speeds. The time step for the simulations is 30 fs.

The initial configuration was built by randomly placing all particles in a rectangular system box of 79 Å × 79 Å × 279 Å using PACKMOL package,[96] followed by energy minimization and quick NVT and NpT equilibration runs. Periodic boundary conditions were applied on the X, Y, Z directions. 10 % fraction of CG water are antifreeze particles[93] to avoid unphysical freezing of the CG water. Hexagonal arrays were obtained after 6 μs with 500 silica dimers, 1,000 CTA^+ and 8,120 CG water. The obtained mesostructure of surfactants was taken as a template for followed silica condensation using REMC that was implemented in our in-house code.

In the REMC simulations, more than 50,000 MC steps were performed to allow sufficiently complete structural assemblies. MC moves including random translations and rotations for all silicate species in the canonical (NVT) ensemble are carried out to sample all possible spatial configurations. Furthermore, to sample reaction events in our simulations, the reaction ensemble MC (REMC) technique[65, 128] was used to simulate silica polymerization. Our choice for the REMC technique is further supported by the recent simulation study of the formation of silica gels and silica nanoparticles.[27, 91, 92] In general our attempt probabilities for moves were chosen

as 0.79 for translations on all species, 0.20 for tetrahedron rotations, and 0.01 for REMC moves.

5.3 Results and Discussion

In Chapter 4, we found that the multiple charges on silicate oligomers are important to the formation of hexagonal phases. To further explore the formation of MCM-41 (silica with a hexagonal array in an ordered arrangement), we have combined the MD simulation with REMC simulation to consider the silica polymerization in the simulations of MCM-41 formation. Our previous study has shown that the addition of silicate dimers promotes the formation of the hexagonal structure. This structure was obtained by the MD simulation began with a random position of 1,000 CTA^+, 500 silicate dimers, and 8,120 CG water particles after a simulation duration of 6 μs. The final configuration, the hexagonal array, was taken as a template for the following sampling on silica polymerization using the REMC simulation.

Figure 5.2 shows the hexagonal structure obtained from the MD simulation. Water molecules were removed for a clearer visualization. Front and side views show that few micellar rods form and self-assemble in partially ordered arrangement. The obtained hexagonal phase exhibited the micellar rods with radius $\sim$ 37 Å, which is corresponding to the MCM-41 pore size reported by Beck and co-workers.[12, 78]

To perform REMC for sampling the silica polymerization using the flexible corner-sharing tetrahedral model[3], we removed all water molecules from the initial configuration given that our REMC method uses an effective force-field to consider water implicitly. In addition, in order to mimic the final stage of MCM-41 formation in which most of the silica posses no charge within the MCM-41 material, each spherical silicate dimer anion was replaced by two neutral silica monomers. Due to the different CG levels in MD and MC simulations (e.g., explicit solvents vs. implicit solvents), the force-field applied in MC simulations needs to be adjusted. Hard sphere

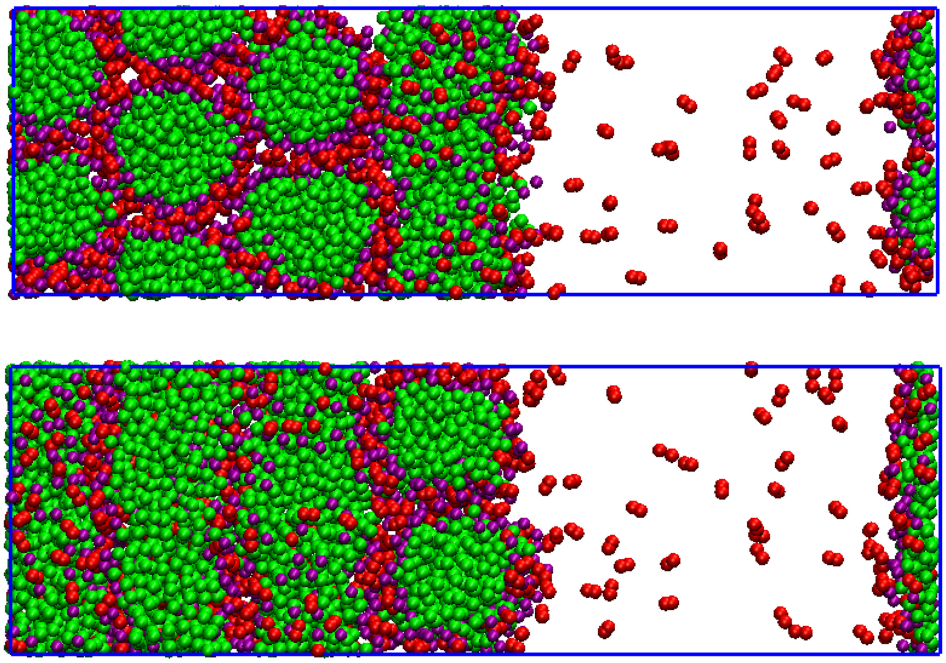

Figure 5.2. Schematic visualizations of (a) front and (b) side views of a hexagonal phase obtained for surfactant-silicate dimers-water system by the MD simulation. Color code: green for surfactant tail groups; purple for surfactant head groups; red for anionic silicate dimers (water molecules have been removed for clarity).

interaction between silicon and silicon was applied. The Lennard-Jones potential was assigned between a silica tetrahedron and a surfactant head particle. Due to the strong attraction between surfactant head groups and silicates (i.e., Coulombic potential), relatively strong potential well (2 kJ/mol) for surfactant heads to silicates was implemented. After carrying out 30,000 MC steps, few oligomers formed. Visualization is shown in Figure 5.3. Voids were found between the micellar rods. We note that the number of silica is not enough to cover the surface of all micellar rods.

The Q_n distribution, which is defined as the fraction of silicon atoms connected to n bridging oxygens, was calculated as well as the degree of condensation. The evolution of the Q_n distribution and degree of condensation of MC steps is shown in Figure 5.4. The degree of condensation reached a plateau to a value around 0.19. The

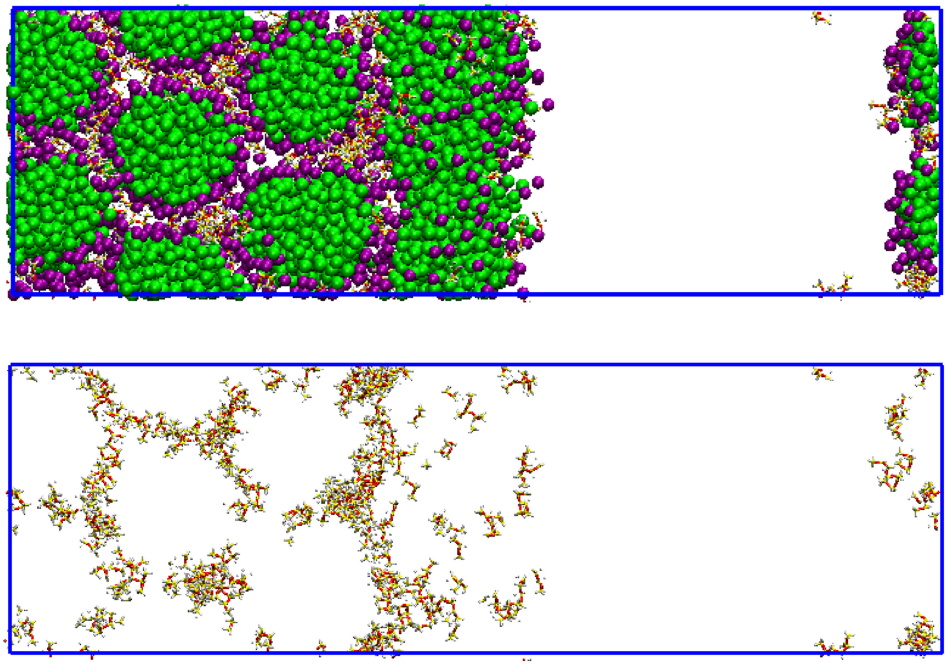

Figure 5.3. Visualization of MCM-41 structure with (a) surfactants and silicates, (b) silicates only. Color code: green for surfactant tail groups; purple for surfactant head groups; yellow for silicons; white for hydroxyl groups; and red for oxygens.

low degree of condensation and the visualization clearly suggests that more silicates are necessary to cover the micellar rods and polymerize to form a realistic structure of MCM-41.

This initial study for the hybrid MD/MC approach reveals that the ratio of silica to surfactant is not high enough to cover the surfactant of micellar rods in the hexagonal arrays. As a result, another approach to study the feasibility of the simulation is proposed: inserting more silica species to study the evolution of formation process of MCM-41.

In order to mimic the final stage of MCM-41 formation to obtain connected silica with porous structure, we removed the doubly charged dimers in the system and inserted neutral silica monomers randomly until reaching a silica to surfactant ratio of 4. Therefore 4,000 neutral silica monomers were added into the surfactant-rich region.

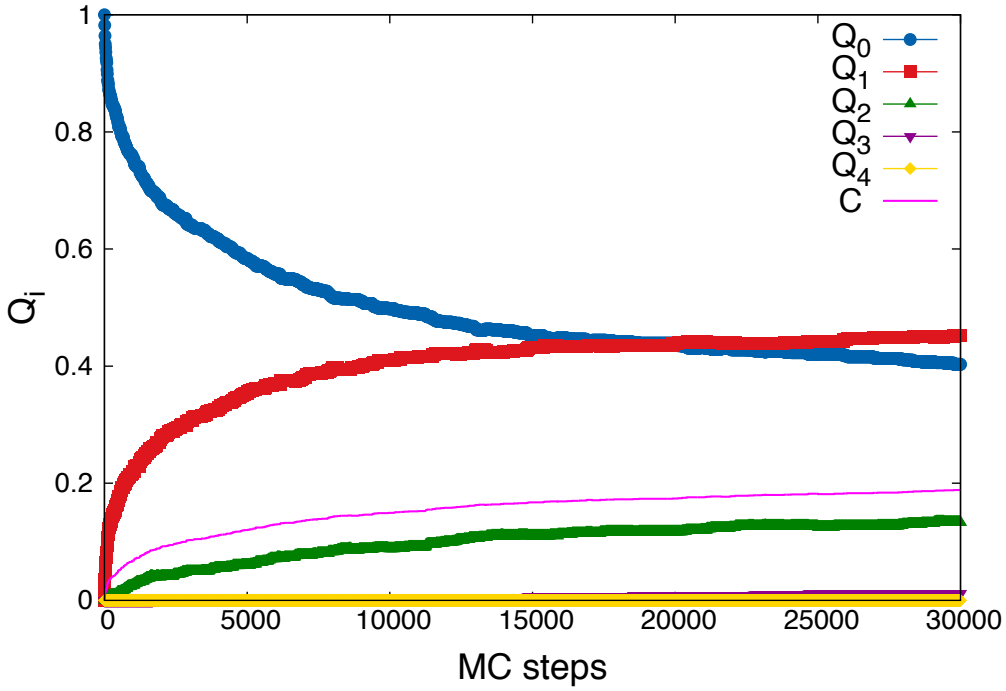

Figure 5.4. Evolution of the Q_n distribution during polymerization.

Figure 5.5 shows the visualizations of the final configuration of the simulation after REMC simulation was performed. Silicate-encapsulated hexagonal array is found.

The Q_n distribution is shown in Figure 5.6. A MCM-41 structure was obtained with a higher degree of condensation of silicates. However, we also found that the degree of condensation reached a plateau. Therefore, two systems with larger silica to surfactant ratios were further tested (silica to surfactant ratios of 5 and 6), and similar results were obtained: the degree of condensation is around 0.31 after performing 3,000 MC steps, and it remains constant as the simulation proceeds. This low degree of condensation suggests that collective fluctuations of both surfactant location and silica polymerization are necessary to reach higher, experimentally relevant, degrees of condensation. According to the findings from the simulations, the future work of this hybrid MD/MC approach should involve a flexible template, in which the

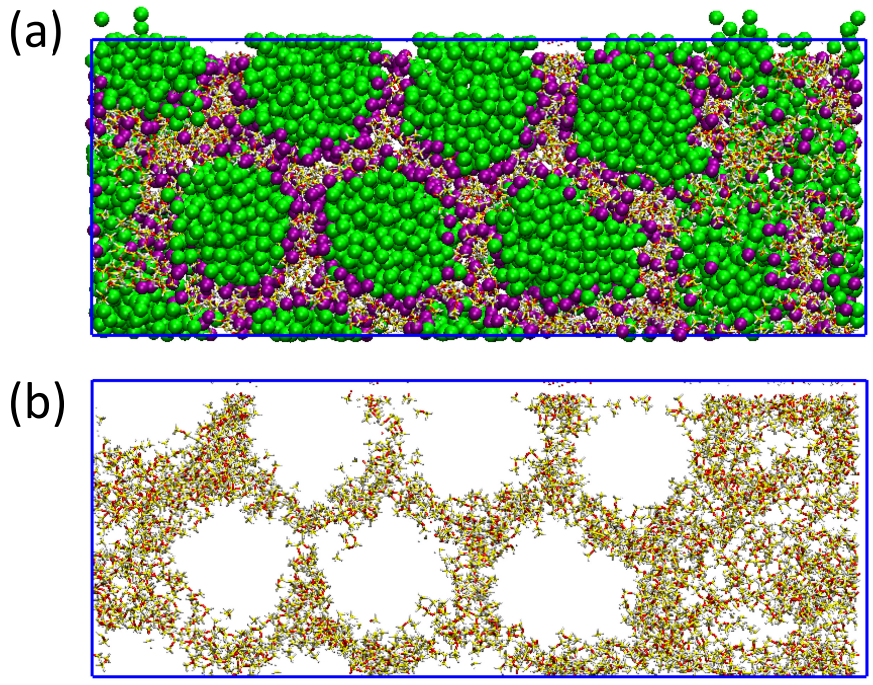

Figure 5.5. Visualizations of resulting MCM-41 structure obtained from a system consists of 1,000 surfactants and 4,000 silicate monomers: figures show (a) surfactants and (b) silicates only.

silicates-surfactant fluctuation can be well simulated, allowing more accurate results to be obtained.

Wakihara and co-workers[147] performed the reverse Monte Carlo simulations to calculate the ring-size distribution from the neutron and X-ray diffraction data, and larger fractions of 3-membered rings and 4-membered rings and broader ring-size are found in MCM-41 and SBA-15 than that in the bulk amorphous silica. We have also computed the ring-size distribution of the MCM-41 structure obtained from our simulations. Interestingly we found a prominent 3-membered ring in the obtained MCM-41, which differs from the study on silica-OSDA core-shell nanoparticles that have dominant 5-membered rings.[27] There are, however, only a total of approximately 20 rings formed in this simulated structure, and a larger number of rings is

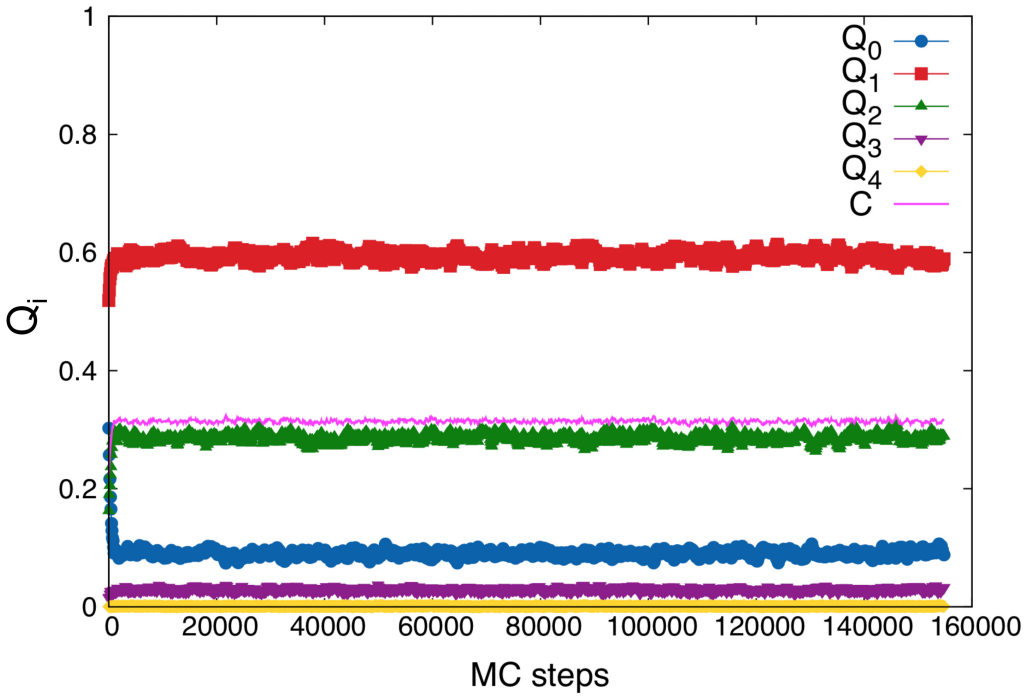

Figure 5.6. Evolution of the Q_n distribution during silica polymerization for MCM-41 formation with 1,000 surfactants and 4,000 neutral silicate monomers.

necessary to carry out a detailed comparison between experiments and our simulations.

Due to the different nature of the two models (MD uses spherical CG particles to represent all molecules whereas the REMC simulation adapts the silica tetrahedral model with implicit water), it is difficult to correctly simulate. Therefore future work should address on how to accommodate the two models with a better consistency for simulating the MCM-41 formation in the later stages.

5.4 Conclusions

In this chapter, we show the preliminary results of studying the formation mechanism of MCM-41 using a hybrid MD/MC approach. We aim to unravel the formation

mechanism of MCM-41 using the proposed approach in which the MD simulations can capture the complex interplay of physical interactions between different species whereas the MC simulations can sample the chemical reaction events of silica polymerization. A more realistic mesophase with detailed information of the atomic-level structure can be obtained from this work. Our preliminary study has shown that there are several elements that are essential for carrying out this study.

First of all, a compatible level of coarse-graining of the models is necessary. In MD simulations, the MARTINI model is applied, in which on average a group of four heavy atoms are represented as a spherical particle: a CTA^+ is viewed as a linear chain of five beads with a charge on the first one, four water molecules are represented as one polar CG bead, and every silicate is represented as a CG bead. On the other hand, in our MC model, the water molecule is implicitly considered using an effective force-field, and a flexible, corner-sharing silica tetrahedron model is used to represent the silicates. Because of the difference between the two models, while switching the simulations between MD and MC simulations, the system fluctuates greatly. Due to the solvent is the majority in our simulation system, a MD simulation with the implicit water model is considered as a future research subject.

Our simulation results showed that the same amount of silicates as surfactants is not enough to cover the micellar rods in the preformed hexagonal array. A higher silicate to surfactant ratio of 4 was therefore performed, and higher degree of condensation of silica was obtained. Experiments also showed that silica to surfactant ratio higher than 1 is essential for forming MCM-41.[25, 145] However, we also found that the degree of condensation reaches a plateau of about 0.32. The value is nearly constant while increasing the silica to surfactant ratio. Given that low value of the degree of condensation, it suggests that the high connectivity of silica networks corresponding to MCM-41 may not be reached. This may result from the frozen template that the fluctuation between micelles and silica cannot be considered for generating

reasonable space for silica to undergo the condensation reaction in MC simulations. As a result, the fluctuation between silica and surfactants may need to be included in MC simulations.

However, to consider the fluctuations involving silica and surfactant in MC simulations, the computations may not be feasible due to the system size. Therefore a different computing methodology, such as parallel computing, may possibly be applicable to save the computation time.

In this work we note that this study is indeed a challenging work due to the complexity and its large scale, therefore, more effort is needed in the further study. At this stage, we have not obtained conclusive results from this work yet. We expect to, however, get more detailed information from this MD/MC work in the near future to unravel the formation mechanism of these mesoporous materials.

CHAPTER 6

CONCLUSION AND RECOMMENDATIONS FOR THE FUTURE WORK

6.1 Conclusions

We have presented detailed studies on the formation of silica microporous and mesoporous materials using different molecular modeling techniques. Having a better understanding of the formation mechanism is crucial to the tailoring of materials,[110, 121] however, it is still incomplete. In this study, we have used reaction ensemble Monte Carlo (REMC) based on a silica tetrahedron model to study the formation of different silica nanoporous materials. We have investigated the self-assembly of silica-template nanoparticles which were found prior to the formation of silicalite-1 crystals. In addition, a replica-exchange reaction ensemble Monte Carlo (RE-REMC) simulation technique was developed to study crystallization of different silica polymorphs. In addition, the formation of mesoporous materials was also studied using molecular dynamics (MD) simulation techniques. Different mesostructures were obtained from this work. Moreover, to eliminate the limitation of pure MC and MD simulations, we combined the off-lattice REMC and coarse-grained MD to push the study of mesoporous material formation mechanism forward. Our study shows that with this coarse-grained model (silica tetrahedron, and MARTINI force-filed) can capture the interplay of physical interactions in the system during the formation of silica mesoporous materials.

6.1.1 Self-Assembly of OSDA-Silica Nanoparticles

We have applied a flexible, corner-sharing silica tetrahedron model to study the self-assembly of silica-OSDA nanoparticles during the formation of silica microporous materials. This silica tetrahedron model was proposed by Astala *et al.* for modeling the mechanical properties of crystalline silica solids.[4] Malani *et al.* also applied this model to study the formation of silica gels and the results are shown good agreement with experimental observation.[91, 92] From our simulation, a two-step formation mechanism, which comprises non-reactive preassociation, followed by silica polymerization simulated by the REMC technique, was found to be crucial to the formation of core-shell nanoparticles which was observed experimentally.[48, 49] Excellent agreement of the calculated nanoparticle density with the experimental observation is obtained. A detailed investigation of the simulated nanoparticles shows a plurality of five-membered rings, a key component of the silicalite-1 framework structure. However, no evidence for the presence of pentasil units, higher-order building units of the silicalite-1 structure involving chains of five-membered rings, was found. This work represents the first atomic-level model of the self-assembly of precursor silica-OSDA nanoparticles, providing opportunities to obtain unprecedented insights into the formation of ordered microporous materials.

6.1.2 Searching for Ground State Structures of Silica Microporous Materials using RE-REMC Simulations

We have shown that, from the study of the off-lattice silica tetrahedron REMC, the amorphous silica such as silica gels and silica nanoparticles can be obtained. However, it remains a great challenge to simulate the formation of crystalline zeolites by building connections between amorphous silica nanoparticles and ordered microporous materials. An advanced sampling technique, replica-exchange reaction ensemble Monte Carlo (RE-REMC), was thus developed and applied to model the

ground state structures of crystalline silica polymorphs and silica microporous materials. The study makes use of a model of silica polymerization based on the reactive assembly of semi-flexible tetrahedral units. This RE-REMC provides an effective and efficient sampling on the crystallization of different silica polymorphs. Crystals of dense silica polymorphs α-cristobalite, β-cristobalite, and keatite, as well as crystals of open-framework materials including SOD, EDI, DFT, and ATT structures were successfully produced by the model. Crystals that have not been observed experimentally were also obtained from the technique. This work represents an important precursor to a full study of zeolite formation by reactive assembly of silica in the presence of OSDAs.

6.1.3 Study of Self-Assembly of Periodic Mesoporous Silicas

As in the case of the formation of microporous materials, various formation mechanisms have been proposed to describe the surfactant-silica interaction in the synthesis of mesoporous materials.[12, 78, 24] The complexity and large scale of the mesophase make the study of formation mechanisms very challenging. The molecular dynamic simulation technique with the MARTINI coarse-grained model was used in our research to investigate the formation of silica mesoporous materials. We have found the multiple charges on silicate oligomers intrigue the phase separation in the solutions, promoting the formation of mesophases. Furthermore, we also observed a reversible phase transition between hexagonal arrays and lamellar phase as we add/remove benzene molecules into solutions.

The CG model used in MD simulations greatly reduces the complexity of the studied system, however, the dominant reaction during the formation of mesoporous materials, silica polymerization, is ignored. Therefore a hybrid MD/MC simulation was proposed to further combine the MC simulation for sampling reaction events with MD.

This hybrid MD/MC simulation provides an opportunity to study the formation MCM-41 materials in an accessible computational resource. We have explored the feasibility of the model and found that the inconsistency between the nature of two different methodologies makes the task extremely difficult. The obtained hexagonal arrays of surfactants exhibit the similar dimensions of the MCM-41 structure. The silica polymerization in a frozen surfactant with hexagonal arrays shows that the fluctuation between the surfactant and silicates is a key for the formation of MCM-41. A high silicate to surfactant ratio such as 4 is necessary to cover the surface of the micellar rods in the hexagonal array in agreement with typical experimental synthesis compositions.

6.2 Suggestions for Future Research

In addition to the completed work in this study, there are several topics may contribute greatly to this research field.

6.2.1 Finer Representation of OSDAs

Our initial study on the formation of silica-OSDA nanoparticles leaves scope for further refinements to the model, allows future investigation into the role of OSDA molecular structure on nanoparticle formation. Several studies have shown that the nature of OSDAs and pH value have great effects on the formation mechanism and associated energy barrier while forming the microporous materials.[146, 154, 155, 156] Therefore refinements on the currently oversimplified representations of OSDAs (i.e., viewed as a sphere) is necessary for getting a better and more accurate knowledge of silica-OSDA interaction. Studies such as how more accurate molecular representations of OSDAs influence ring-size distributions in the formation of silica-OSDA nanoparticles can be investigated.

As an example, a coarse-graining model for OSDA using TPAOH is proposed: the four propyl groups are represented by four beads, and the nitrogen is by a bead in the center of the four beads (See Figure 6.1). With a more realistic representation of OSDAs, their steric effects on the formation of nanoparticles can be studied. As a future work, which a better representation of OSDA, it is of utmost importance to first obtain the evolution of Q_n distribution over simulation steps and compare the results with the experimental data. Next, a further analysis and characterizations with this finer model can be carried out.

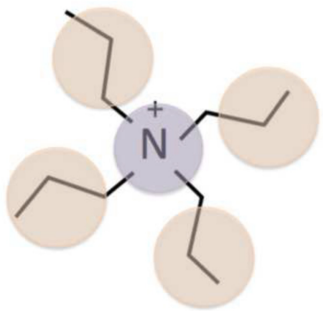

Figure 6.1. A schematic representation of the coarse-graining procedure employed on TPAOH for a finer molecular model.

6.2.2 Experimental Investigation of Silica Preassociation

From our study, we have suggested a two-step formation mechanism, in which the first step: silica preassociation, and the second step: silica polymerization, is important to generate core-shell silica nanoparticles. The first step, silica preassociation, is crucial for generating silica-OSDA nanoparticles. The rationale behind this proposed mechanism is that Pereira et al. found that silica species tend to cluster in aqueous solutions using molecular dynamics.[107] To test the predictions of this model, we propose the following experiment to characterize the silica preassociation phenomena.

The silica polymerization at the isoelectric point is slow enough to be observed and monitored by the various characterization techniques.[40, 62] Devreux et al. use ^{29}Si NMR and small-angle X-ray scattering (SAXS) to analyze the kinetics of silica polymerization at pH of around 2.5.[40] With these two approaches at our disposal, there is a chance to monitor the preassociation process experimentally. Small-angle scattering can be used to study the inhomogeneities in solutions to identify the occurrence of the aggregates of silica. Meanwhile the ^{29}Si NMR can be used to monitor the emergence of the Q_1 silicon, indicating when silica starts to polymerize.

If these experiments show silica aggregates form before ^{29}Si NMR shows the emergence of Q_1 silicon, this confirms the proposed two-step mechanism. In contrast, if no silica aggregates are observed using small-angle scattering but NMR shows the existence of Q_1 silicon or even higher connectivity of silicon, this then suggests that silica polymerization occurs first. We note that it may be that the time-scale difference in the silica preassociation and polymerization is too small to be probed experimentally.

6.2.3 New Sampling Technique for Studying the Crystalline Zeolites

In our study on searching the ground state structure of silica polymorphs and zeolite materials, we developed and applied a replica-exchange reaction ensemble Monte Carlo technique to cross the energy barrier between amorphous silica and ordered microporous silica lead to the crystalline silica. This method provides an effective and efficient sampling compared to the normal REMC method, however, the simulations are largely constrained by the system size. The largest system size of zeolites our simulation has approached is α-cristobalite with four unit cells, in which the simulation box contained 16 silica. As a result, a further development on the sampling method is needed to push this study forward.

Furthermore, in the current study, the system dimension fixed which may also impose a constraint on the simulation. The introduction of NpT ensemble may be

helpful for generating different silica polymorphs, which can shed light on the transition of different structures.

6.2.4 Simulating Ground States of Zeolitic Materials with the Existence of OSDAs

In our RE-REMC study, simulations start with random initial configurations with silicic acids only. The density and system size are determined by the unit cell of the zeolitic frameworks. Studies have shown the OSDAs lead to the formation of different crystalline structures and morphologies. It is also well-known that OSDAs change the energy barrier while condensation occurs between silica.[98, 144, 156] Therefore, it is important to introduce OSDAs into the system to study the ground state structure with the existence of OSDAs. We have built a RE-REMC model with the involvement of OSDAs. In this model, the OSDA is represented as a sphere with only hard sphere interaction between other particles.

Sodalite (SOD)[8], a porous zeolite with ultra-small cages ($\sim$ 6 Å) and windows accessible only to small molecules such as water, was also simulated by this RE-REMC technique. Tetramethylammonium (TMA) is usually used as an OSDA for SOD fabrication.[9, 33]

A fully condensed crystal with the SOD framework structure was obtained after 20 million RE-REMC steps. The simulation is about 7 times longer that simulating SOD formation using RE-REMC without the involvement of an OSDA. The final configuration of SOD is shown in Figure 6.2(a). The OSDA sphere was found to be within a cage as shown in Figure 6.2(b). Small sodalite cages and windows can also be seen in the 3×3×3 periodic extension of the final configuration in Figure 6.2(c).

A LTA zeolite framework – a zeolite that has a cubic unit cell with a dimension of 11.9 Å consisting of twenty-four TO_2 (T = Al or Si) units.[8, 28] LTA framework is built by spherical 1.1 nm cages, and the structure shows three dimensional pores

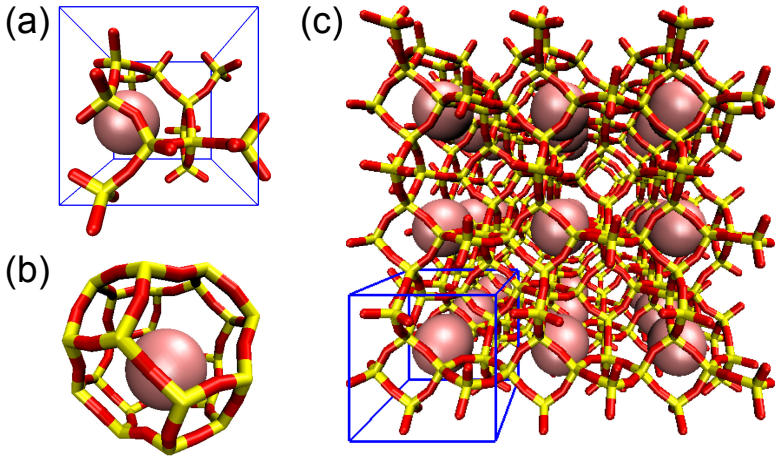

Figure 6.2. Final structure obtained from simulating the SOD zeolite framework using RE-REMC with the existence of a spherical OSDA. The hard sphere radius of OSDAs is 3.0 Å. The figure shows (a) a final unit cell structure, (b) a SOD cage obtained from this work, and (c) the obtained SOD structure with 3×3×3 extension. Color code: Si (yellow), Bridging Oxygen (red), and OSDA (pink).

with a pore diameter of 0.4 nm. The high hydrophobicity of pure-silica LTA has been fabricated.[30] We have applied the RE-REMC approach to study the LTA zeolites, and crystalline LTA has not been found yet. As a result, we herein applied the RE-REMC simulation with OSDAs to simulate the ground state structure of pure-silica LTA and study whether the involvement of OSDA can lead the formation of crystalline LTA zeolites. Simulations have been carried out by simulating the silica polymerization with 24 silicic acids in a cubic system box with the same size of the unit cell. Figure 6.3 shows the final structure obtained from the simulation of LTA frameworks with existence of two different sizes of OSDAs. The hydroxyl groups can be seen in the figures from both simulations. No crystalline LTA framework was found in both simulations after 50 million MC steps. Although the visualization shows that a cage forms at the occupation of the OSDA, 5-membered ring that is not found

in crystalline LTA was observed. The results show that OSDAs serve not just the space-fillings but also help the formation of porous structures. A finer representation and an elaborate force-field are necessary for the model to further investigate the crystallization process.

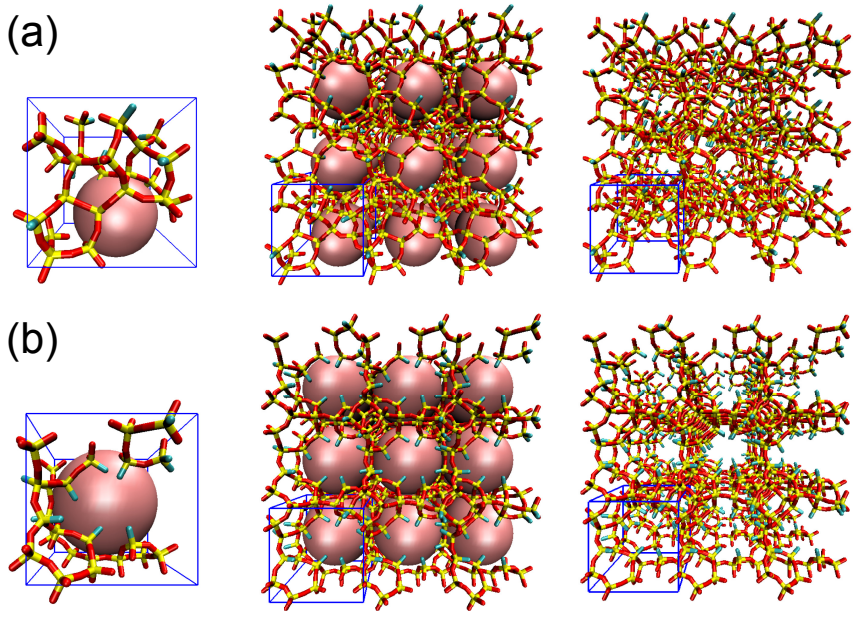

Figure 6.3. Final structure obtained from simulating with LTA parameters using RE-REMC with existence of a spherical OSDA. The hard sphere radii of OSDAs are (a) 4.0 Å and (b) 5.5 Å. No crystalline LTA was found. Color code: Si (yellow), Bridging Oxygen (red), Hydroxyl (green), and OSDA (pink).

6.2.5 Experimental Investigation of Multiple Charges on D4R Oligomers

Chemelka and co-workers showed that the hexagonal array forms with a phase separation in a system of double-four-ring (D4R). The authors also suggested that D4R possesses at most a maximum charge of 6^-.[50] They used the combination of TMAOH and CH_3OH to stabilize the anionic D4R. This was also observed from our simulations described in Chapter 4: a system of D4R with charges of 6^- yields the hexagonal array. Besides, simulations of D4R with charges of 7^- or 8^- result in the

formation of lamellar structure. The results support the experimental findings that D4R possesses at most a maximum charge of 6^- for generating the hexagonal array.

To further test the predictions of our model on D4R, an experiment of D4R with charges of 8^- is proposed. The experiment can be carried out by following the procedure described in the work by Chmelka and co-workers.[50] To maintain the higher number of charges on the D4R, raising the pH value of TMAOH and CH_3OH system may help stabilize the charges at 8^-. The final mesostructure can be identified using the deuterium NMR spectra. However, we note that it remains uncertain to know whether if the D4R can be stabilized at a higher pH system even in a system with the combination of TMAOH and CH_3OH.

6.2.6 Hybrid MD/MC Approach with Implicit Water in both MD and MC Simulations

The model we have built to study the formation of MCM-41 was hampered by the different assumption between MD and MC simulations. The developed MD model has explicit water molecules whereas in our REMC simulation has implicit water. Therefore, developing MD simulations on the interested system with implicit solvents is essential to achieve a consistent model. Recently, Marrink and co-workers have developed a "dry MARTINI coarse-graining method" to study lipids in solutions.[2] The authors developed a potential matrix of various level of interaction for different molecules without explicit water molecules.

With this implicit water model, the MD simulation and MC simulation will be more consistent. The force-field of the surfactant can be taken from the literature.[2] An effective force-field is therefore obtained. As for the parameterization of the CG model for silicate species, the similar procedure (i.e., comparing density profiles of spherical micelles obtained from AA and CG simulations) will be carried out. This

water-free model can decrease the complexity of building the interface between MD and MC simulations. In addition, it will greatly reduce the simulation time.

APPENDIX

DERIVATION OF PARALLEL-TEMPERING REACTION ENSEMBLE MONTE CARLO METHOD

The reaction canonical ensemble Monte Carlo was developed in 1994 to study the properties of chemical reactions.[65, 128, 137]

The partition function of grand canonical ensemble for a mixture of S species is

$$\Xi = \sum_{N_1=0}^{\infty} \cdots \sum_{N_S=0}^{\infty} Q(N_1, \cdots, N_S, V, T) exp\left(-\beta \sum_{i=1}^{S} N_i \mu_i\right), \tag{6.1}$$

where Ξ is the reaction-ensemble partition function, N_i is the number of molecules of type i, V is the volume of the system, β=$1/k_BT$, T is the temperature, k_B is Boltzmann's constant, Q is canonical partition function for the mixture, μ_i is the chemical potential for molecule i in the mixture, and S is the number of species.[137]

Consider a reaction in a single phase with a fix temperature and volume with the mass conservation and equilibrium criteria of the system, the probability of finding a state k with the configurational energy U_k is shown as below[137]:

$$P_k = \frac{1}{\Xi} exp\left[\beta \sum_{i=1}^{S} N_i \mu_i - \sum_{i=1}^{S} \ln(N_i!) + \sum_{i=1}^{S} N_i \ln \frac{V q_i}{\Lambda_i^3} - \beta U_k\right], \tag{6.2}$$

where q_i= $q_{i,r} \times q_{i,v} \times q_{i,e} \times q_{i,n}$ is the internal contributions (rotational, vibrational, electronic, nuclear, respectively) to the partition function for isolated molecule i, and Λ_i is the de Broglie thermal wavelength of molecule i.[137]

By further introducing the ideal gas equilibrium constant, a more general form of the transition probability from a state m to state l with extent of reaction of ξ can be written as below:

$$P_{kl}^{\xi} = min\left\{1,\ (\beta P^0 V)^{\bar{\nu}\xi} K^{\xi} \prod_{i=1}^{S} \left[\frac{(N_i^0)!}{(N_i^0 + \nu_i^0 \xi)!}\right] exp(-\beta U_{kl})\right\}, \tag{6.3}$$

where $\bar{\nu} = \sum_{i=1}^{s} \nu_i$ is the net change in the total number of molecules for the reaction, ν_i is the stoichiometric number of species i, and K is the ideal gas equilibrium constant.

To develop a exchange probability of replicas in reaction ensemble using K as an alternative parameter, a general detailed balance condition is considered:

$$N(o) \times \pi(o \to n) = N(n) \times \pi(n \to o) \tag{6.4}$$

where π is the transition matrix.

The transition probability can be further written as:

$$\pi(o \to n) = \alpha(n \to o) \times acc(n \to o) \tag{6.5}$$

where $\alpha(n \to o)$ is the probability of trial moves performed, and acc(n $\to$ o) is the probability of accepting or rejecting a trial move.

If $\alpha(n \to o)$ is chosen as a symmetric matrix, then $\alpha(n \to o) = \alpha(o \to n)$. Therefore,

$$N(o) \times acc(o \to n) = N(n) \times acc(n \to o) \tag{6.6}$$

The Metropolis acceptance probability can be therefore chosen as follow

$$\begin{aligned} acc(o \to n) &= \frac{N(n)}{N(o)} && if \quad N(n) <= N(o) \\ &= 1 && if \quad N(n) > N(o) \end{aligned} \tag{6.7}$$

Therefore, the acceptance probability of the exchange of configuration k in replica m and configuration l in replica n, P_{mn}, becomes:

$$acc[(m,k),(n,l)\rightarrow(m,l),(n,k)]=P_{mn}=min\left\{1,\frac{N(m,l)N(n,k)}{N(m,k)N(n,l)}\right\}. \quad (6.8)$$

To determine the acceptance probability of replica exchange, we start from the configurational probability in the reaction ensemble.[65, 128, 137] The probability, P_{km}, of finding a configuration k in replica m is given by:

$$P_{km}=\frac{1}{\Xi}exp\left[\beta\sum_{i=1}^{S}(N_i+\nu_i)_{km}\mu_i-\sum_{i=1}^{S}\ln\left[(N_i+\nu_i)!\right]_{km}+\sum_{i=1}^{S}(N_i+\nu_i)_{km}\ln\frac{Vq_i}{\Lambda_i^3}-\beta U_{km}\right] \quad (6.9)$$

The probabilities of finding a configuration k in replica n, a configuration l in replica m, and a configuration l in replica n may similarly be obtained:

$$P_{ln}=\frac{1}{\Xi}exp\left[\beta\sum_{i=1}^{S}(N_i+\nu_i)_{ln}\mu_i-\sum_{i=1}^{S}\ln\left[(N_i+\nu_i)!\right]_{ln}+\sum_{i=1}^{S}(N_i+\nu_i)_{ln}\ln\frac{Vq_i}{\Lambda_i^3}-\beta U_{ln}\right] \quad (6.10)$$

$$P_{lm}=\frac{1}{\Xi}exp\left[\beta\sum_{i=1}^{S}(N_i+\nu_i)_{lm}\mu_i-\sum_{i=1}^{S}\ln\left[(N_i+\nu_i)!\right]_{lm}+\sum_{i=1}^{S}(N_i+\nu_i)_{lm}\ln\frac{Vq_i}{\Lambda_i^3}-\beta U_{lm}\right] \quad (6.11)$$

$$P_{kn}=\frac{1}{\Xi}exp\left[\beta\sum_{i=1}^{S}(N_i+\nu_i)_{kn}\mu_i-\sum_{i=1}^{S}\ln\left[(N_i+\nu_i)!\right]_{kn}+\sum_{i=1}^{S}(N_i+\nu_i)_{kn}\ln\frac{Vq_i}{\Lambda_i^3}-\beta U_{kn}\right] \quad (6.12)$$

Based on the detailed balance condition, the probability of swapping adjacent replicas, m and n, with the corresponding configurations k and l, is given by:

$$
\begin{aligned}
P_{mn} &= min\left\{1,\ \frac{P_{kn}\cdot P_{lm}}{P_{km}\cdot P_{ln}}\right\} \\
&= exp\left\{\beta\sum_{i=1}^{S}\left[(N_i+\nu_i)_{kn}\,\mu_i+(N_i+\nu_i)_{lm}\,\mu_i-(N_i+\nu_i)_{km}\,\mu_i-(N_i+\nu_i)_{ln}\,\mu_i\right]\right\} \\
&\times exp\left\{\sum_{i=1}^{S}\left[(N_i+\nu_i)_{kn}\ln\frac{Vq_i}{\Lambda_i^3}+(N_i+\nu_i)_{lm}\ln\frac{Vq_i}{\Lambda_i^3}-(N_i+\nu_i)_{km}\ln\frac{Vq_i}{\Lambda_i^3}-(N_i+\nu_i)_{ln}\ln\frac{Vq_i}{\Lambda_i^3}\right]\right\} \\
&\div exp\left\{\sum_{i=1}^{S}\left(\ln\left[(N_i+\nu_i)!\right]_{kn}+\ln\left[(N_i+\nu_i)!\right]_{lm}-\ln\left[(N_i+\nu_i)!\right]_{km}-\ln\left[(N_i+\nu_i)!\right]_{ln}\right)\right\}.
\end{aligned}
\tag{6.13}
$$

At chemical equilibrium the chemical potentials satisfy $\sum_i \nu_i\mu_i = 0$; four such sums vanish in Eq. (6.13) In addition, conservation of mass provides that $(N_i)_{kn}$ = $(N_i)_{km}$ and $(N_i)_{lm} = (N_i)_{ln}$. Taking chemical equilibrium and mass conservation together causes the second and fourth lines in Eq. (6.13) to vanish, yielding the following replica exchange probability:

$$
P_{mn} = min\left\{1,\ exp\left[\sum_{i=1}^{S}\left(\Delta\left(N_i+\nu_i\right)_n\ln\frac{Vq_i}{\Lambda_i^3}+\Delta\left(N_i+\nu_i\right)_m\ln\frac{Vq_i}{\Lambda_i^3}\right)\right]\right\}. \tag{6.14}
$$

By introducing the following ideal gas equilibrium constant relationships:

$$
K = exp\left(-\frac{\sum_{i=1}^{S}\nu_i\mu_i^0}{RT}\right), \tag{6.15}
$$

where μ_i^0 is the ideal gas chemical potential for component i, given by:

$$
\frac{\mu_i^0}{RT} = -\ln\left(\frac{q_i}{\beta P^0\Lambda_i^3}\right), \tag{6.16}
$$

in addition, inverse equilibrium constant, K_{inv} (K_{inv}=$1/K$), is used, the probability thus becomes:

$$
P_{mn} = min\left\{1,\ \left(\beta P^0 V\right)_m^{\bar{\nu}(\xi_n-\xi_m)}K_{inv,m}^{\xi_m-\xi_n}\cdot\left(\beta P^0 V\right)_n^{\bar{\nu}(\xi_m-\xi_n)}K_{inv,n}^{\xi_n-\xi_m}\right\}. \tag{6.17}
$$

In Eq. (6.17), $\bar{\nu} = \sum_i \nu_i$ is the net change in the total number of molecules; ξ_m and ξ_n are extents of reaction before performing a swapping move in replica m and n, respectively.

In the reaction system studied herein, $A + B \rightarrow C + D$, the value of the net stoichiometry $\bar{\nu}$ equals zero. Accordingly, the acceptance probability provided in Eq. (6.17) becomes

$$P_{mn} = min\left\{1,\ K_{inv,m}^{\xi_m - \xi_n} \cdot K_{inv,n}^{\xi_n - \xi_m}\right\}. \tag{6.18}$$

Furthermore, the quantities, ξ_n-$\xi_m = N_{BOn} - N_{BOm}$, in which N_{BOm} and N_{BOn} are the numbers of bridging oxygens in replica m and n, respectively. Accordingly, the final form of the RE-REMC probability with K_{inv} (K_{inv}=$1/K_{eq}$) can be used herein:

$$P_{mn} = min\left\{1,\ \left(\frac{K_{inv,n}}{K_{inv,m}}\right)^{\xi_n - \xi_m}\right\} = min\left\{1,\ \left(\frac{K_{inv,n}}{K_{inv,m}}\right)^{N_{BOn} - N_{BOm}}\right\}. \tag{6.19}$$

In Eq. (6.19), $K_{inv,m}$ is the inverse reaction equilibrium constant ($K_{inv} = 1/K_{eq}$) in replica m; $K_{inv,n}$ is the inverse reaction equilibrium constants in replica n; $\bar{\nu} = \sum_i \nu_i$ is the net change in the total number of molecules; V is volume and P^0 is the reference pressure that connects an equilibrium constant to a reference free energy; ξ_m and ξ_n are the extent of reaction in the current configuration (before performing a swapping move) in replica m and n, respectively.

BIBLIOGRAPHY

[1] Aerts, A., Haouas, M., Caremans, T. P., Follens, L. R. A., van Erp, T. S., Taulelle, F., Vermant, J., Martens, J. A., and Kirschhock, C. E. A. Investigation of the mechanism of colloidal silicalite-1 crystallization by using DLS, SAXS, and ^{29}Si NMR spectroscopy. *Chem. Eur. J. 16*, 9 (2010), 2764–74.

[2] Arnarez, C., Uusitalo, J. J., Masman, M. F., Ingolfsson, H. I., de Jong, D. H., Melo, M. N., Periole, X., de Vries, A. H., and Marrink, S. J. Dry martini, a coarse-grained force field for lipid membrane simulations with implicit solvent. *J. Chem. Theory Comput. 11*, 1 (2015), 260–275.

[3] Astala, R., Auerbach, S. M., and Monson, P. A. Density functional theory study of silica zeolite structures: stabilities and mechanical properties of SOD, LTA, CHA, MOR, and MFI. *J. Phys. Chem. B 108*, 26 (2004), 9208–9215.

[4] Astala, R., Auerbach, S. M., and Monson, P. A. Normal mode approach for predicting the mechanical properties of solids from first principles: Application to compressibility and thermal expansion of zeolites. *Phys. Rev. B 71* (2005), 014112.

[5] Auerbach, S. M., Carrado, K. A., and Dutta, P. K. *Handbook of Zeolite Science and Technology*. Marcel Dekker Inc., New York, New York, 2003.

[6] Auerbach, S. M., Fan, W., and Monson, P. A. Modelling the assembly of nanoporous silica materials. *Int. Rev. Phys. Chem. 34*, 1 (2015), 35–70.

[7] Auerbach, S. M., Ford, M. H., and Monson, P. A. New insights into zeolite formation from molecular modeling. *Curr. Opin. Colloid Interface Sci. 10*, 56 (2005), 220–225.

[8] Baerlocher, C., McCusker, L. B., and Olson, D. H. *Atlas of Zeolite Framework Types*, 6 ed. Elsevier, 2007.

[9] Baerlocher, C., and Meier, W. M. Synthese und kristallstruktur von tetramethylammonium-sodalith. *Helv. Chim. Acta. 52*, 7 (1969), 1853–1860.

[10] Barton, T. J., Bull, L. M., Klemperer, W. G., Loy, D. A., McEnaney, B., Misono, M., Monson, P. A., Pez, G., Scherer, G. W., Vartuli, J. C., and Yaghi, O. M. Tailored porous materials. *Chem. Mater 11*, 10 (1999), 2633–2656.

[11] Beck, J. S., Vartuli, J. C., Kennedy, G. J., Roth, W. J., and Schramm, S. E. Molecular or supramolecular templating: Defining the role of surfactant chemistry in the formation of microporous and mesoporous molecular sieves. *Chem. Mater. 6* (1994), 1816–1821.

[12] Beck, J. S., Vartuli, J. C., Roth, W. J., Leonowicz, M. E., Kresge, C. T., Schmitt, K. D., Chu, C. T.-W., Olson, D. H., Sheppard, E. W., McCullen, S. B., Higgins, J. B., and Schlenker, J. L. A new family of mesoporous molecular sieves prepared with liquid crystal templates. *J. Am. Chem. Soc. 114* (1992), 10834–10843.

[13] Berendsen, H., van der Spoel, D., and van Drunen, R. Gromacs: A message-passing parallel molecular dynamics implementation. *Comput. Phys. Commun. 91*, 13 (1995), 43 – 56.

[14] Beurroies, I., Ågren, P., Büchel, G., Rosenholm, J. B., Amenitsch, H., Denoyel, R., and Lindén, M. Detailed in situ xrd and calorimetric study of the formation

of silicate/mixed surfactant mesophases under alkaline conditions. influence of surfactant chain length and synthesis temperature. *J. Phys. Chem. B 110*, 33 (2006), 16254–16260.

[15] Bibby, D. M., and Dale, M. P. Synthesis of silica-sodalite from non-aqueous systems. *Nature 317*, 6033 (Sept. 1985), 157–158.

[16] Bnown, G. E., Gibbs, G. V., and Ribbe, P. H. The nature and the variation in length of the Si-O-Si and Al-O bonds in framework of silicates. *Am. Mineral. 54* (Aug 1969), 1044–1061.

[17] Bonilla, G., Diaz, I., Tsapatsis, M., Jeong, H.-K., Lee, Y., and Vlachos, D. G. Zeolite MFI crystal morphology control using organic structure-directing agents. *Chem. Mater. 16*, 26 (2004), 5697–5705.

[18] Botella, P., Corma, A., and Quesada, M. Synthesis of ordered mesoporous silica templated with biocompatible surfactants and applications in controlled release of drugs. *J. Mater. Chem. 22* (2012), 6394–6401.

[19] Brinker, C. J. Porous inorganic materials. *Curr. Opin. Colloid Interface Sci. 1*, 6 (1996), 798 – 805.

[20] Burkett, S. L., and Davis, M. E. Mechanisms of structure direction in the synthesis of pure-silica zeolites. 1. synthesis of TPA/Si-ZSM-5. *Chem. Mater. 7*, 5 (1995), 920–928.

[21] Bussi, G., Donadio, D., and Parrinello, M. Canonical sampling through velocity rescaling. *J. Chem. Phys. 126*, 1 (2007), 1–7.

[22] Caratzoulas, S., Vlachos, D. G., and Tsapatsis, M. Potential of Mean Force for Tetramethylammonium Binding to Cagelike Oligosilicates in Aqueous Solution. *J. Am. Chem. Soc. 128* (2006), 16138–16147.

[23] Catlow, C. R. A., Ackermann, L., Bell, R. G., Cora, F., Gay, C.-D. H., Nygren, M. A., Pereira, C. J., Sastre, G., Slater, C.-B., and Sinclair, E. P. Introductory lecture computer modelling as a technique in solid state chemistry. *Faraday Discuss. 106* (1997), 1–40.

[24] Chen, C.-Y., Burkett, S. L., Li, H.-X., and Davis, M. E. Studies on mesoporous materials ii. synthesis mechanism of MCM-41. *Microporous Mater. 2*, 1 (1993), 27–34.

[25] Chen, C.-Y., Li, H.-X., and Davis, M. E. Studies on mesoporous materials: I. synthesis and characterization of MCM-41. *Microporous Mater. 2*, 1 (1993), 17 – 26.

[26] Chen, J., Natarajan, S., Thomas, J. M., Jones, R. H., and Hursthouse, M. B. A Novel Open-Framework Cobalt Phosphate Containing a Tetrahedrally Coordinated Cobalt(II) Center: $CoPO_4 \cdot 0.5C_2H_{10}N_2$. *Angew. Chem. Int. Ed. 33*, 6 (1994), 639–640.

[27] Chien, S.-C., Auerbach, S. M., and Monson, P. A. Modeling the self-assembly of silica-templated nanoparticles in the initial stages of zeolite formation. *Langmuir 31*, 17 (2015), 4940–4949.

[28] Cho, K., Cho, H. S., de Ménorval, L.-C., and Ryoo, R. Generation of mesoporosity in lta zeolites by organosilane surfactant for rapid molecular transport in catalytic application. *Chem. Mater. 21*, 23 (2009), 5664–5673.

[29] Corma, A. From microporous to mesoporous molecular sieve materials and their use in catalysis. *Chem. Rev. 97*, 6 (1997), 2373–2420.

[30] Corma, A., Rey, F., Rius, J., Sabater, M. J., and Valencia, S. Supramolecular self-assembled molecules as organic directing agent for synthesis of zeolites. *Nature 431* (2004), 287–290.

[31] Coronas, J. Present and future synthesis challenges for zeolites. *Chem. Eng. J. 156*, 2 (2010), 236–242.

[32] Davis, M. E. Zeolites from a materials chemistry perspective. *Chem. Mater. 26*, 1 (2014), 239–245.

[33] Davis, M. E., and Lobo, R. F. Zeolite and molecular sieve synthesis. *Chem. Mater. 4*, 4 (1992), 756–768.

[34] Davis, T. M., Drews, T. O., Ramanan, H., He, C., Dong, J., Schnablegger, H., Katsoulakis, M. A., Kokkoli, E., McCormick, A. V., Penn, R. L., and Tsapatsis, M. Mechanistic principles of nanoparticle evolution to zeolite crystals. *Nat. Mater. 5* (2006), 400–408.

[35] de Jong, D. H., Singh, G., Bennett, W. F. D., Arnarez, C., Wassenaar, T. A., Schäfer, L. V., Periole, X., Tieleman, D. P., and Marrink, S. J. Improved parameters for the martini coarse-grained protein force field. *J. Chem. Theory Comput. 9*, 1 (2013), 687–697.

[36] de Moor, P. E. A., Beelen, T. P. M., Komanschek, B. U., Beck, L. W., Wagner, P., Davis, M. E., and van Santen, R. A. Imaging the assembly process of the organic-mediated synthesis of a zeolite. *Chem. Eur. J. 5*, 7 (1999), 2083–2088.

[37] de Moor, P.-P. E. A., Beelen, T. P. M., and van Santen, R. A. In situ observation of nucleation and crystal growth in zeolite synthesis. a small-angle X-ray scattering investigation on Si-TPA-MFI. *J. Phys. Chem. B 103*, 10 (1999), 1639–1650.

[38] de Moor, P.-P. E. A., Beelen, T. P. M., van Santen, R. A., Tsuji, K., and Davis, M. E. SAXS and USAXS investigation on nanometer-scaled precursors in organic-mediated zeolite crystallization from gelating systems. *Chem. Mater. 11*, 1 (1999), 36–43.

[39] Deem, M. W., Pophale, R., Cheeseman, P. A., and Earl, D. J. Computational discovery of new zeolite-like materials. *J. Phys. Chem. C 113*, 51 (2009), 21353–21360.

[40] Devreux, F., Boilot, J. P., Chaput, F., and Lecomte, A. Sol-gel condensation of rapidly hydrolyzed silicon alkoxides: A joint ^{29}Si NMR and small-angle X-ray scattering study. *Phys. Rev. A 41* (1990), 6901–6909.

[41] Díaz, J., and Jr, K. J. B. Enzyme immobilization in mcm-41 molecular sieve. *J. Mol. Catal. B: Enzym. 2*, 2-3 (1996), 115 – 126.

[42] Doadrio, A., Sousa, E., Doadrio, J., Pariente, J. P., Izquierdo-Barba, I., and Vallet-Reg, M. Mesoporous sba-15 {HPLC} evaluation for controlled gentamicin drug delivery. *J. Control. Release 97*, 1 (2004), 125 – 132.

[43] Downs, R., and Hall-Wallace, M. The american mineralogist crystal structure database. *Am. Mineral. 88* (2003), 247–250.

[44] Dupree, E., and Pettifer, R. F. Determination of the Si-O-Si bond angle distribution in vitreous silica by magic angle spinning NMR. *Nature 308* (1984), 523–525.

[45] Earl, D. J., and Deem, M. W. Parallel tempering: Theory, applications, and new perspectives. *Phys. Chem. Chem. Phys. 7* (2005), 3910–3916.

[46] Earl, D. J., and Deem, M. W. Toward a database of hypothetical zeolite structures. *Ind. Eng. Chem. Res. 45*, 16 (2006), 5449–5454.

[47] Falcioni, M., and Deem, M. W. A biased Monte Carlo scheme for zeolite structure solution. *J. Chem. Phys. 110*, 3 (1999), 1754–1766.

[48] Fedeyko, J. M., Rimer, J. D., Lobo, R. F., and Vlachos, D. G. Spontaneous formation of silica nanoparticles in basic solutions of small tetraalkylammonium cations. *J. Phys. Chem. B 108*, 33 (2004), 12271–12275.

[49] Fedeyko, J. M., Vlachos, D. G., and Lobo, R. F. Formation and structure of self-assembled silica nanoparticles in basic solutions of organic and inorganic cations. *Langmuir 21*, 11 (2005), 5197–5206.

[50] Firouzi, A., Atef, F., Oertli, A. G., Stucky, G. D., and Chmelka, B. F. Alkaline lyotropic silicatesurfactant liquid crystals. *J. Am. Chem. Soc. 119*, 15 (1997), 3596–3610.

[51] Firouzi, A., Kumar, D., Bull, L. M., Besier, T., Sieger, P., Huo, Q., Walker, S. A., Zasadzinski, J. A., Glinka, C., Nicol, J., Margolese, D., Stucky, G. D., and Chmelka, B. F. Cooperative organization of inorganic-surfactant and biomimetic assemblies. *Science 267* (1995), 1138–1143.

[52] Hammonds, K. D., Heine, V., and Dove, M. T. Rigid-unit modes and the quantitative determination of the flexibility possessed by zeolite frameworks. *J. Phys. Chem. B 102*, 10 (1998), 1759–1767.

[53] Hartmann, M. Ordered mesoporous materials for bioadsorption and biocatalysis. *Chem. Mater. 17*, 18 (2005), 4577–4593.

[54] Hatton, B., Landskron, K., Whitnall, W., Perovic, D., and Ozin, G. A. Past, present, and future of periodic mesoporous organosilicasthe pmos. *Acc. Chem. Res. 38*, 4 (2005), 305–312. PMID: 15835877.

[55] Hess, B., Kutzner, C., van der Spoel, D., and Lindahl, E. Gromacs 4: Algorithms for highly efficient, load-balanced, and scalable molecular simulation. *J. Chem. Theory Comput. 4*, 3 (2008), 435–447.

[56] Hockney, R., Goel, S., and Eastwood, J. Quiet high-resolution computer models of a plasma. *J. Comput. Phys. 14*, 2 (1974), 148 – 158.

[57] Hoshen, J., and Kopelman, R. Percolation and cluster distribution. i. cluster multiple labeling technique and critical concentration algorithm. *Phys. Rev. B 14* (Oct 1976), 3438–3445.

[58] Houssin, C. J. Y., Kirschhock, C. E. A., Magusin, P. C. M. M., Mojet, B. L., Grobet, P. J., Jacobs, P. A., Martens, J. A., and van Santen, R. A. Combined in situ ^{29} Si NMR and small-angle X-ray scattering study of precursors in MFI zeolite formation from silicic acid in TPAOH solutions. *Phys. Chem. Chem. Phys. 5* (2003), 3518–3524.

[59] Huo, Q., Leon, R., Petroff, P. M., and Stucky, G. D. Mesostructure design with gemini surfactants: Supercage formation in a three-dimensional hexagonal array. *Science 2* (1995), 1324–1327.

[60] Huo, Q., Margolese, D. I., Ciesla, U., Feng, P., Gier, T. E., Sieger, P., Leon, R., Petroff, P. M., Schth, F., and Stucky, G. D. Generalized syntheses of periodic surfactant/inorganic composite materials. *Nature 368* (1994), 317–321.

[61] Iler, R. K. *The Chemistry of Silica: Solubility, Polymerization, Colloid and Surface Properties, and Biochemistry.* Wiley, New York, 1979.

[62] Jin, L., Auerbach, S. M., and Monson, P. A. Modeling nanoparticle formation during early stages of zeolite growth: A low-coordination lattice model of template penetration. *J. Phys. Chem. C 114*, 34 (2010), 14393–14401.

[63] Jin, L., Auerbach, S. M., and Monson, P. A. Simulating the formation of surfactant-templated mesoporous silica materials: a model with both surfactant self-assembly and silica polymerization. *Langmuir 29*, 2 (2013), 766–780.

[64] Jin, L., Auerbach, S. M., and Monson, P. A. Emergence of zeolite analogs and other microporous crystals in an atomic lattice model of silica and related materials. *J. Phys. Chem. Lett. 3*, 6 (Mar. 2012), 761–765.

[65] Johnson, J. K., Panagiotopoulos, A. Z., and Gubbins, K. E. Reactive canonical monte carlo a new simulation technique for reacting or associating fluids. *Mol. Phys. 81*, 3 (1994), 717–733.

[66] Jorge, M. Molecular dynamics simulation of self-assembly of n-decyltrimethylammonium bromide micelles. *Langmuir 24*, 11 (2008), 5714–5725.

[67] Jorge, M., Auerbach, S. M., and Monson, P. A. Modeling spontaneous formation of precursor nanoparticles in clear-solution zeolite synthesis. *J. Am. Chem. Soc. 127* (2005), 14388–14400.

[68] Jorge, M., Gomes, J. R. B., Cordeiro, M. N. D. S., and Seaton, N. A. Molecular simulation of silica/surfactant self-assembly in the synthesis of periodic mesoporous silicas. *J. Am. Chem. Soc. 129*, 50 (2007), 15414–15415.

[69] Jorge, M., Gomes, J. R. B., Cordeiro, M. N. D. S., and Seaton, N. A. Molecular dynamics simulation of the early stages of the synthesis of periodic mesoporous silica. *J. Phys. Chem. B 113* (2009), 708–718.

[70] Keskar, N. R., and Chelikowsky, J. R. Structural properties of nine silica polymorphs. *Phys. Rev. B 46* (1992), 1–13.

[71] Kirschhock, C. E. A., Ravishankar, R., Jacobs, P. A., and Martens, J. A. Aggregation mechanism of nanoslabs with zeolite MFI-type structure. *J. Phys. Chem. B 103*, 50 (1999), 11021–11027.

[72] Kirschhock, C. E. A., Ravishankar, R., Looveren, L. V., Jacobs, P. A., and Martens, J. A. Mechanism of transformation of precursors into nanoslabs in the early stages of MFI and MEL zeolite formation from TPAOH-TEOS-H2O and TBAOH-TEOS-H2O mixtures. *J. Phys. Chem. B 103*, 24 (1999), 4972–4978.

[73] Kirschhock, C. E. A., Ravishankar, R., Verspeurt, F., Grobet, P. J., Jacobs, P. A., and Martens, J. A. Identification of precursor species in the formation of MFI zeolite in the TPAOH-TEOS-H2O system. *J. Phys. Chem. B 103*, 24 (1999), 4965–4971.

[74] Knops-Gerrits, P., De Vos, D. E., Feijen, E. J. P., and Jacobs, P. A. Raman spectroscopy on zeolites. *Microporous Mater. 8*, 1-2 (1997), 3–17.

[75] Kofke, D. A. On the acceptance probability of replica-exchange monte carlo trials. *J. Chem. Phys. 117* (2002), 6911–6914.

[76] Kone, A., and Kofke, D. A. Selection of temperature intervals for parallel-tempering simulations. *J. Chem. Phys. 122* (2005), 206101.

[77] Kragten, D. D., Fedeyko, J. M., Sawant, K. R., Rimer, J. D., Vlachos, D. G., Lobo, R. F., and Tsapatsis, M. Structure of the silica phase extracted from Silica/(TPA)OH solutions containing nanoparticles. *J. Phys. Chem. B 107*, 37 (2003), 10006–10016.

[78] Kresge, C. T., Leonowicz, M. E., Roth, W. J., Vartuli, J. C., and Beck, J. S. Ordered mesoporous molecular sieves synthesized by liquid-crystal templates mechanism. *Nature 359* (1992), 710–712.

[79] Kresge, C. T., and Roth, W. J. The discovery of mesoporous molecular sieves from the twenty year perspective. *Chem. Soc. Rev. 42* (2013), 3663–3670.

[80] Kruk, M., Jaroniec, M., Shin, H. J., and Ryoo, R. Optimization of silica/surfactant ratio in MCM-41 synthesis. In *Nanoporous Materials IV Proceedings of the 4th International Symposium on Nanoporous Materials*, Abdelhamid Sayari and Mietek Jaroniec, Eds., vol. 156 of *Studies in Surface Science and Catalysis*. Elsevier, 2005, pp. 55 – 62.

[81] Kumar, D., Schumacher, K., du Fresne von Hohenesche, C., Grn, M., and Unger, K. MCM-41, MCM-48 and related mesoporous adsorbents: their synthesis and characterisation. *Colloids Surf., A 187-188*, 0 (2001), 109 – 116.

[82] Kumar, S., Penn, R. L., and Tsapatsis, M. On the nucleation and crystallization of silicalite-1 from a dilute clear sol. *Microporous Mesoporous Mater. 144*, 13 (2011), 74–81.

[83] Kumar, S., Wang, Z., Penn, R. L., and Tsapatsis, M. A structural resolution cryo-TEM study of the early stages of MFI growth. *J. Am. Chem. Soc. 130*, 51 (2008), 17284–17286.

[84] L. Popović, D. d. W., and Boeyens, J. C. A. Correlation between raman wavenumbers and p-o bond lengths in crystalline inorganic phosphates. *J. Raman Spectrosc. 36*, 1 (2005), 2–11.

[85] Larson, R. G. Self-assembly of surfactant liquid crystalline phases by monte carlo simulation. *J. Chem. Phys. 91*, 4 (1989), 2479–2488.

[86] Le Bail, A. Inorganic structure prediction with *GRINSP*. *J. Appl. Crystallogr. 38*, 2 (Apr 2005), 389–395.

[87] Lesthaeghe, D., Vansteenkiste, P., Verstraelen, T., Ghysels, A., Kirschhock, C. E. A., Martens, J. A., Van Speybroeck, V., and Waroquier, M. MFI fingerprint: How pentasil-induced IR bands shift during zeolite nanogrowth. *J. Phys. Chem. C 112*, 25 (2008), 9186–9191.

[88] Lindahl, E., Hess, B., and van der Spoel, D. Gromacs 3.0: a package for molecular simulation and trajectory analysis. *Molecular modeling annual 7*, 8 (2001), 306–317.

[89] Liu, X., Tian, B., Yu, C., Gao, F., Xie, S., Tu, B., Che, R., Peng, L.-M., and Zhao, D. Room-temperature synthesis in acidic media of large-pore three-dimensional bicontinuous mesoporous silica with ia3d symmetry. *Angewandte Chemie International Edition 41*, 20 (2002), 3876–3878.

[90] Lupulescu, A. I., and Rimer, J. D. In situ imaging of silicalite-1 surface growth reveals the mechanism of crystallization. *Science 344*, 6185 (2014), 729–732.

[91] Malani, A., Auerbach, S. M., and Monson, P. A. Probing the mechanism of silica polymerization at ambient temperatures using Monte Carlo simulations. *J. Phys. Chem. Lett. 1*, 21 (2010), 3219–3224.

[92] Malani, A., Auerbach, S. M., and Monson, P. A. Monte Carlo simulations of silica polymerization and network formation. *J. Phys. Chem. C 115*, 32 (2011), 15988–16000.

[93] Marrink, S. J., deVries, A. H., and Mark, A. E. Coarse grained model for semiquantitative lipid simulations. *J. Phys. Chem. B 108* (2004), 750.

[94] Marrink, S. J., Risselada, H. J., Yefimov, S., Tieleman, D. P., and de Vries, A. H. The MARTINI force field: Coarse grained model for biomolecular simulations. *J. Phys. Chem. B 111* (2007), 7812.

[95] Marrink, S. J., and Tieleman, D. P. Perspective on the martini model. *Chem. Soc. Rev. 42* (2013), 6801–6822.

[96] Martnez, L., Andrade, R., Birgin, E. G., and Martnez, J. M. Packmol: A package for building initial configurations for molecular dynamics simulations. *J. Comput. Chem. 30*, 13 (2009), 2157–2164.

[97] Melde, B. J., Holland, B. T., Blanford, C. F., and Stein, A. Mesoporous sieves with unified hybrid inorganic/organic frameworks. *Chem. Mater. 11*, 11 (1999), 3302–3308.

[98] Moliner, M., Rey, F., and Corma, A. Towards the rational design of efficient organic structure-directing agents for zeolite synthesis. *Angew. Chem. Int. Ed. 52*, 52 (2013), 13880–13889.

[99] Molinero, V., and Moore, E. B. Water modeled as an intermediate element between carbon and silicon. *J. Phys. Chem. B 113*, 13 (2009), 4008–16.

[100] Moller, K., and Bein, T. Inclusion chemistry in periodic mesoporous hosts. *Chem. Mater. 10*, 10 (1998), 2950–2963.

[101] Monnier, A., Schuth, F., Huo, Q., Kumar, D., Margolese, D., Maxwell, R. S., Stucky, G. D., Krishnamurty, M., Petroff, P., Firouzi, A., Janicke, M., and Chmelka, B. F. Cooperative formation of inorganic-organic interfaces in the synthesis of silicate mesostructuresd. *Science 261* (1993), 1299–1303.

[102] Mora-Fonz, M. J., Catlow, C. R. A., and Lewis, D. W. Oligomerization and cyclization processes in the nucleation of microporous silicas. *Angew. Chem. Int. Ed. 117*, 20 (2005), 3142–3146.

[103] Mora-Fonz, M. J., Catlow, C. R. A., and Lewis, D. W. Modeling aqueous silica chemistry in alkali media. *J. Phys. Chem. C 111*, 49 (2007), 18155–18158.

[104] Moteki, T., Keoh, S. H., and Okubo, T. Synthesis of zeolites using highly amphiphilic cations as organic structure-directing agents by hydrothermal treatment of a dense silicate gel. *Chem. Commun. 50* (2014), 1330–1333.

[105] Na, K., Choi, M., and Ryoo, R. Recent advances in the synthesis of hierarchically nanoporous zeolites. *Microporous Mesoporous Mater. 166* (2013), 3–19.

[106] Parrinello, M., and Rahman, A. Polymorphic transitions in single crystals: A new molecular dynamics method. *J. Appl. Phys. 52*, 12 (1981), 7182–7190.

[107] Pereira, J. C. G., Catlow, C. R. A., and Price, G. D. Molecular dynamics simulation of methanolic and ethanolic silica-based solgel solutions at ambient temperature and pressure. *J. Phys. Chem. A 106*, 1 (2002), 130–148.

[108] Pérez-Sánchez, G., Gomes, J. R. B., and Jorge, M. Modeling self-assembly of silica/surfactant mesostructures in the templated synthesis of nanoporous solids. *Langmuir 29* (2013), 2387–2396.

[109] Pophale, R., Cheeseman, P. A., and Deem, M. W. A database of new zeolite-like materials. *Phys. Chem. Chem. Phys. 13*, 27 (2011), 12407–12412.

[110] Pophale, R., Daeyaert, F., and Deem, M. W. Computational prediction of chemically synthesizable organic structure directing agents for zeolites. *J. Mater. Chem. A 1* (2013), 6750–6760.

[111] Raman, N. K., Anderson, M. T., and Brinker, C. J. Template-based approaches to the preparation of amorphous, nanoporous silicas. *Chemistry of Materials 8*, 8 (1996), 1682–1701.

[112] Rankin, S. E., Kasehagen, L. J., McCormick, A. V., and Macosko, C. W. Dynamic Monte Carlo simulation of gelation with extensive cyclization. *Macromolecules 33*, 20 (2000), 7639–7648.

[113] Rao, N. Z., and Gelb, L. D. Molecular dynamics simulations of the polymerization of aqueous silicic acid and analysis of the effects of concentration on silica polymorph distributions, growth mechanisms, and reaction kinetics. *J. Phys. Chem. B 108*, 33 (2004), 12418–12428.

[114] Rathore, N., Chopra, M., and de Pablo, J. J. Optimal allocation of replicas in parallel tempering simulations. *J. Chem. Phys. 122* (2005), 024111.

[115] Ravishankar, R., Kirschhock, C. E. A., Knops-Gerrits, P.-P., Feijen, E. J. P., Grobet, P. J., Vanoppen, P., De Schryver, F. C., Miehe, G., Fuess, H., Schoeman, B. J., Jacobs, P. A., and Martens, J. A. Characterization of nanosized material extracted from clear suspensions for /MFI zeolite synthesis. *J. Phys. Chem. B 103*, 24 (1999), 4960–4964.

[116] Rimer, J. D., Kumar, M., Li, R., Lupulescu, A. I., and Oleksiak, M. D. Tailoring the physicochemical properties of zeolite catalysts. *Catal. Sci. Technol. 4* (2014), 3762–3771.

[117] Rimer, J. D., Trofymluk, O., Lobo, R. F., Navrotsky, A., and Vlachos, D. G. Thermodynamics of silica nanoparticle self-assembly in basic solutions of monovalent cations. *J. Phys. Chem. C 112*, 38 (2008), 14754–14761.

[118] Rimer, J. D., Lobo, R. F., and Vlachos, D. G. Physical basis for the formation and stability of silica nanoparticles in basic solutions of monovalent cations. *Langmuir 21*, 19 (2005), 8960–8971.

[119] Rivas-Cardona, A., Chovanetz, M., and Shantz, D. F. A systematic investigation of silicalite-1 precursor mixtures with varying degrees of dilution. *Microporous Mesoporous Mater. 155*, 0 (2012), 56–64.

[120] Ryoo, R., and Jun, S. Improvement of hydrothermal stability of MCM-41 using salt effects during the crystallization process. *J. Phys. Chem. B 101*, 3 (1997), 317–320.

[121] Schmidt, J. E., Deem, M. W., and Davis, M. E. Synthesis of a specified, silica molecular sieve by using computationally predicted organic structure-directing agents. *Angew. Chem. Int. Ed. 126*, 32 (2014), 8512–8514.

[122] Schoeman, B. J. Analysis of the nucleation and growth of TPA-silicalite-1 at elevated temperatures with the emphasis on colloidal stability. *Microporous Mesoporous Mater. 22* (1998), 9–22.

[123] Schumacher, C., Gonzalez, J., Wright, P. A., and Seaton, N. A. Generation of atomistic models of periodic mesoporous silica by kinetic Monte Carlo simulation of the synthesis of the material. *J. Phys. Chem. B 110* (2006), 319–333.

[124] Sefcik, J., and McCormick, A. V. Thermochemistry of aqueous silicate solution precursors to ceramics. *AIChE Journal 43*, S11A (1997), 2773–2784.

[125] Seo, Y., Lee, S., Jo, C., and Ryoo, R. Microporous aluminophosphate nanosheets and their nanomorphic zeolite analogues tailored by hierarchical structure-directing amines. *J. Am. Chem. Soc. 135*, 24 (2013), 8806–8809.

[126] Siperstein, F. R., and Gubbins, K. E. Phase separation and liquid crystal self-assembly in surfactantinorganicsolvent systems. *Langmuir 19*, 6 (2003), 2049–2057.

[127] Smith, J. V., and Bailey, S. W. Second review of Al–O and Si–O tetrahedral distances. *Acta Cryst. 16*, 8 (Aug 1963), 801–811.

[128] Smith, W. R., and Triska, B. The reaction ensemble method for the computer simulation of chemical and phase equilibria. i. theory and basic examples. *J. Chem. Phys. 100*, 4 (1994), 3019–3027.

[129] Stillinger, F. H., and Weber, T. A. Computer simulation of local order in condensed phases of silicon. *Phys. Rev. B 31* (1985), 5262–5271.

[130] Swendsen, R. H., and Wang, J.-S. Replica monte carlo simulation of spin-glasses. *Phys. Rev. Lett. 57* (Nov 1986), 2607–2609.

[131] Taguchi, A., and Schüth, F. Ordered mesoporous materials in catalysis. *Microporous Mesoporous Mater. 77*, 1 (2005), 1 – 45.

[132] Tanev, P. T., and Pinnavaia, T. J. Mesoporous silica molecular sieves prepared by ionic and neutral surfactant templating: A comparison of physical properties. *Chem. Mater. 8*, 8 (1996), 2068–2079.

[133] Tang, F., Li, L., and Chen, D. Mesoporous silica nanoparticles: Synthesis, biocompatibility and drug delivery. *Adv. Mater. 24*, 12 (2012), 1504–1534.

[134] Trinh, T. T., Jansen, A. P. J., van Santen, R. A., and Meijer, E. J. Role of water in silica oligomerization. *J. Phys. Chem. C 113*, 7 (2009), 2647–2652.

[135] Trinh, T. T., Jansen, A. P. J., van Santen, R. A., VandeVondele, J., and Meijer, E. J. Effect of counter ions on the silica oligomerization reaction. *ChemPhysChem 10*, 11 (2009), 1775–1782.

[136] Trofymluk, O., Levchenko, A. A., and Navrotsky, A. Mesoporous silica synthesis: Energetics of interaction between framework and structure directing agent. *Microporous Mesoporous Mater. 149* (2012), 119–125.

[137] Turner, C. H., Brennan, J. K., Lísal, M., Smith, W. R., Johnson, J. K., and Gubbins, K. E. Simulation of chemical reaction equilibria by the reaction ensemble Monte Carlo method: a review. *Mol. Simulat. 34*, 2 (2008), 119–146.

[138] Turner, C., Brennan, J. K., and Lisal, M. Replica exchange for reactive monte carlo simulations. *J. Phys. Chem. C 111*, 43 (2007), 15706–15715.

[139] Vallet-Regi, M., Rámila, A., del Real, R. P., and Pérez-Pariente, J. A new property of MCM-41: a drug delivery system. *Chem. Mater. 13*, 2 (2001), 308–311.

[140] Vallet-Regí, M., Balas, F., and Arcos, D. Mesoporous materials for drug delivery. *Angew. Chem. Int. Ed. 46*, 40 (2007), 7548–7558.

[141] Valtchev, V., and Tosheva, L. Porous nanosized particles: Preparation, properties, and applications. *Chem. Rev. 113*, 8 (2013), 6734–6760.

[142] van der Spoel, D., Lindahl, E., Hess, B., Groenhof, G., Mark, A. E., and Berendsen, H. J. C. Gromacs: Fast, flexible, and free. *J. Comput. Chem. 26*, 16 (2005), 1701–1718.

[143] Van Der Voort, P., Mathieu, M., Mees, F., and Vansant, E. F. Synthesis of high-quality MCM-48 and MCM-41 by means of the gemini surfactant method. *J. Phys. Chem. B 102*, 44 (1998), 8847–8851.

[144] Van Speybroeck, V., Hemelsoet, K., Joos, L., Waroquier, M., Bell, R. G., and Catlow, C. R. A. Advances in theory and their application within the field of zeolite chemistry. *Chem. Soc. Rev.* (2015).

[145] Vartuli, J. C., Schmitt, K. D., Kresge, C. T., Roth, W. J., Leonowicz, M. E., McCullen, S. B., Hellring, S. D., Beck, J. S., and Schlenker, J. L. Effect of surfactant/silica molar ratios on the formation of mesoporous molecular sieves:

Inorganic mimicry of surfactant liquid-crystal phases and mechanistic implications. *Chem. Mater. 6*, 12 (1994), 2317–2326.

[146] Verstraelen, T., Szyja, B. M., Lesthaeghe, D., Declerck, R., Van Speybroeck, V., Waroquier, M., Jansen, A. P., Aerts, A., Follens, L. R., Martens, J. A., Kirschhock, C. E., and van Santen, R. A. Multi-level modeling of silicatemplate interactions during initial stages of zeolite synthesis. *Top. Catal. 52*, 9 (2009), 1261–1271.

[147] Wakihara, T., Fan, W., Kohara, S., Ogura, M., Sankar, G., and Okubo, T. Intermediate-range order in mesoporous silicas investigated by a high-energy x-ray diffraction technique. *Chem. Lett. 37*, 1 (2008), 30–31.

[148] Wang, W., Grozea, D., Kim, A., Perovic, D. D., and Ozin, G. A. Vacuum-assisted aerosol deposition of a low-dielectric-constant periodic mesoporous organosilica film. *Adv. Mater. 22*, 1 (2010), 99–102.

[149] Wu, M. G., and Deem, M. W. Monte Carlo study of the nucleation process during zeolite synthesis. *J. Chem. Phys. 116*, 5 (2002), 2125–2137.

[150] Yang, P., Deng, T., Zhao, D., Feng, P., Pine, D., Chmelka, B. F., Whitesides, G. M., and Stucky, G. D. Hierarchically ordered oxides. *Science 282*, 5397 (1998), 2244–2246.

[151] Ying, J. Y., Mehnert, C. P., and Wong, M. S. Synthesis and applications of supramolecular-templated mesoporous materials. *Angew. Chem. Int. Ed. 38*, 1-2 (1999), 56–77.

[152] Yuan, X., and Cormack, A. N. Efficient algorithm for primitive ring statistics in topological networks. *Comput. Mater. Sci. 24*, 3 (2002), 343–360.

[153] Zhang, J., Luz, Z., and Goldfarb, D. EPR studies of the formation mechanism of the mesoporous materials MCM-41 and MCM-50. *J. Phys. Chem. B 101*, 36 (1997), 7087–7094.

[154] Zhang, X., Liu, D., Xu, D., Asahina, S., Cychosz, K. A., Agrawal, K. V., Wahedi, Y. A., Bhan, A., Hashimi, S. A., Terasaki, O., Thommes, M., and Tsapatsis, M. Synthesis of self-pillared zeolite nanosheets by repetitive branching. *Nature 336* (2012), 2125–2137.

[155] Zhang, X.-Q., Trinh, T. T., van Santen, R. A., and Jansen, A. P. J. Mechanism of the initial stage of silicate oligomerization. *J. Am. Chem. Soc. 133*, 17 (2011), 6613–6625.

[156] Zhang, X.-Q., Trinh, T. T., van Santen, R. A., and Jansen, A. P. J. Structure-directing role of counterions in the initial stage of zeolite synthesis. *J. Phys. Chem. C 115*, 19 (2011), 9561–9567.

[157] Zhao, X. S., Lu, G. Q. M., and Millar, G. J. Advances in mesoporous molecular sieve mcm-41. *Ind. Eng. Chem. Res. 35*, 7 (1996), 2075–2090.